

Interplay of LFV and slepton mass splittings at the LHC as a probe of the SUSY seesaw

A. Abada^a, A. J. R. Figueiredo^b, J. C. Romão^b and A. M. Teixeira^c

^a Laboratoire de Physique Théorique, CNRS – UMR 8627,
Université de Paris XI, F-91405 Orsay Cedex, France

^b Centro de Física Teórica de Partículas, Instituto Superior Técnico,
Av. Rovisco Pais 1, 1049-001 Lisboa, Portugal

^c Laboratoire de Physique Corpusculaire, CNRS/IN2P3 – UMR 6533,
Campus des Cézeaux, 24 Av. des Landais, F-63177 Aubière Cedex, France

Abstract

We study the impact of a type-I SUSY seesaw concerning lepton flavour violation (LFV) both at low-energies and at the LHC. The study of the di-lepton invariant mass distribution at the LHC allows to reconstruct some of the masses of the different sparticles involved in a decay chain. In particular, the combination with other observables renders feasible the reconstruction of the masses of the intermediate sleptons involved in $\chi_2^0 \rightarrow \tilde{\ell} \ell \rightarrow \ell \ell \chi_1^0$ decays. Slepton mass splittings can be either interpreted as a signal of non-universality in the SUSY soft breaking-terms (signalling a deviation from constrained scenarios as the cMSSM) or as being due to the violation of lepton flavour. In the latter case, in addition to these high-energy processes, one expects further low-energy manifestations of LFV such as radiative and three-body lepton decays. Under the assumption of a type-I seesaw as the source of neutrino masses and mixings, all these LFV observables are related. Working in the framework of the cMSSM extended by three right-handed neutrino superfields, we conduct a systematic analysis addressing the simultaneous implications of the SUSY seesaw for both high- and low-energy lepton flavour violation. We discuss how the confrontation of slepton mass splittings as observed at the LHC and low-energy LFV observables may provide important information about the underlying mechanism of LFV.

KEYWORDS: Supersymmetry, LHC, slepton mass splittings, lepton flavour violation, neutrino masses

1 Introduction

The experimental observation of non-vanishing neutrino masses and mixings [1], constitutes clear evidence for physics beyond the Standard Model (SM), and as of today, little is known about the underlying model of new physics. Since neutrinos are very weakly interacting particles and their masses lie orders of magnitude below the other fermion masses of the SM, additional experimental input will be instrumental to shed some light on the new physics model.

In extensions of the SM where ν oscillations (and hence massive neutrinos) can be naturally accommodated, many other new phenomena could in principle be expected. Among them, and given that neutrino oscillations indisputably signal lepton flavour violation (LFV) in the neutral sector, it is only natural to expect that charged lepton flavour will also be violated in these extensions (for a review, see Ref. [2]). The search for manifestations of charged LFV constitutes the goal of several experiments [3–15], exclusively dedicated to look for signals of processes such as rare radiative as well as three-body decays and lepton conversion in muonic nuclei.

In parallel to these low-energy searches, the high-energy Large Hadron Collider (LHC) has started its quest of unveiling the mechanism of electroweak (EW) symmetry breaking and of possibly providing a solution to the SM hierarchy problem. Supersymmetry (SUSY) is a well motivated solution for the hierarchy problem that also offers an elegant solution for the existence of non-baryonic dark matter (DM) in the Universe [16–18]. If the LHC indeed finds signatures of SUSY, it is then extremely appealing to consider supersymmetric models that can also accommodate neutrino oscillation phenomena. One of the most economical and elegant possibilities is perhaps to embed a seesaw mechanism [19–21] in a supersymmetric framework, the so-called SUSY seesaw.

If a type-I seesaw [19] is at work and explains the observed neutrino masses and leptonic mixings, then the neutrino Yukawa couplings could leave their imprint in the slepton mass matrices: as first shown in [22], starting from flavour diagonal soft supersymmetry breaking terms at some high energy unification scale, flavour violation appears at low-energies due to the renormalisation group (RG) evolution of the SUSY soft-breaking parameters [23, 24]. Having natural values for the neutrino Yukawa couplings implies that the seesaw scale (e.g. the right-handed neutrino mass scale in the case of a type-I seesaw) is very high, close to the Grand Unified Theory (GUT) scale ($M_{\text{GUT}} \sim 10^{16}$ GeV). Moreover, the flavour off-diagonal structure of the neutrino Yukawa couplings required to comply with the observed large mixing in the lepton sector [25, 26], can then induce potentially large lepton flavour violation in the slepton sector. Low-energy manifestations of LFV in the framework of the SUSY seesaw include sizable branching ratios (BR) for radiative decays as $l_i \rightarrow l_j \gamma$, three-body decays, $l_i \rightarrow 3l_j$ and $\mu - e$ transitions in heavy nuclei [27–49]. In the presence of CP violation, one can also have T- and P-odd asymmetries in LFV decays and contributions to lepton electric dipole moments (see for example [50–53]).

The quest for new physics is currently being pursued along different avenues: high-energy colliders like the LHC are the ideal laboratory to directly discover the particle content of the SM extension; low-energy experiments probe the new physics contributions (arising from new particles and/or interactions) to several observables (muon anomalous magnetic moment, electric dipole moments, LFV, B-physics, etc.). A successful (or even partial) reconstruction of the underlying model of new physics will necessarily rely on the complementarity of the information derived from direct and indirect searches, which can be further strengthened by data from neutrino experiments,

dark matter searches and cosmological observations.

In this work, we study the impact of a type-I SUSY seesaw concerning flavour violation both at low-energies and at the LHC. At the LHC, there are three possible signals of LFV: firstly, one can have sizable widths for LFV decay processes like $\chi_2^0 \rightarrow \ell_i^\pm \ell_j^\mp \chi_1^0$ [47, 54–57]; secondly, one can have flavoured slepton mass splittings (MS). These can be identified since under certain conditions, one can effectively reconstruct slepton masses via observables such as the kinematic end-point of the invariant mass distribution of the leptons coming from the cascade decays $\chi_2^0 \rightarrow \tilde{\ell}^\pm \ell^\mp \rightarrow \ell^\pm \ell^\mp \chi_1^0$. If the slepton in the decay chain is real, the di-lepton invariant mass spectrum has a kinematical edge that might then be measured with very high precision (up to 0.1 %) [58–60]. Together with data arising from other observables, this information allows to reconstruct the slepton masses [58–62]. Finally, one can observe multiple edges in di-lepton invariant mass distributions $\chi_2^0 \rightarrow \chi_1^0 \ell_i^\pm \ell_i^\mp$, arising from the exchange of a different flavour slepton $\tilde{\ell}_j$ (in addition to the left- and right-handed sleptons, $\tilde{\ell}_{L,R}$). Slepton mass splittings can be either interpreted as a signal of non-universality in the SUSY soft breaking-terms (hinting towards a deviation from flavour-blind scenarios of SUSY breaking such as the constrained Minimal Supersymmetric Standard Model (cMSSM)) or as being due to the violation of lepton flavour.

The potential of LHC experiments in probing the allowed seesaw parameters through measurements of masses and branching ratios of supersymmetric particles has also been discussed in Refs. [63–65]. Recently, another study of slepton mass-splittings as a probe of LFV at the LHC was performed [66] for scenarios with an effective parametrization of flavour violation. In our case, we consider the specific framework of a type-I SUSY seesaw, where the source of flavour violation for both the LHC and the low-energy observables is unique - the neutrino Yukawa couplings - implying that all these LFV observables will be correlated. Working in the framework of the cMSSM extended by three right-handed neutrino superfields, and taking into account the DM constraints [18], we conduct a systematic analysis addressing the simultaneous implications of the SUSY seesaw for both high- and low-energy LFV.

Under the assumption of a type-I SUSY seesaw, the interplay of a joint measurement of LFV branching ratios and of the Chooz angle θ_{13} has been shown to be a powerful tool to shed some light on the SUSY seesaw parameters (see for example [46]). Here we will focus on how the confrontation of slepton mass splittings (as potentially observable at the LHC) and of low-energy LFV observables may provide important information about the underlying mechanism of LFV. After having identified regions in the cMSSM parameter space, where the slepton masses could in principle be reconstructed from the kinematical edges of di-lepton mass distributions (i.e. $\chi_2^0 \rightarrow \ell_i^\pm \ell_i^\mp \chi_1^0$ can occur with a non-negligible number of events), we study the different slepton mass splittings arising in this case from small flavour-conserving radiative effects and LR slepton mixing. We then discuss the effect of implementing a type-I seesaw for the slepton mass splittings, also exploring the implications for LFV decays. We investigate several scenarios in which the SUSY seesaw can be tested and propose, in addition to two already existing LHC benchmark points, other minimal Supergravity (mSUGRA) inspired benchmarks embedded in a type-I seesaw.

As we will show in this work, if the seesaw is indeed the source of both neutrino masses and leptonic mixings and accounts for low-energy LFV observables within future sensitivity reach, interesting slepton phenomena are expected to be observed at the LHC: in addition to the mass splittings, the most striking effect will be the possible appearance of new edges in di-lepton mass distributions. From the comparison of the predictions for the two sets of observables (high and low energy) with the current experimental bounds and future sensitivities, one can either derive information about the otherwise unreachable seesaw parameters, or disfavour the type-I SUSY

seesaw as the unique source of LFV.

The paper is organised as follows. In Section 2 we discuss how lepton masses can be reconstructed from observation at the LHC, describing the mechanisms for production, the favoured decay chains and the kinematical observables. In Section 3 we define the model, providing a brief overview on the implementation of a type-I seesaw in the constrained MSSM, as well as its implications for low-energy LFV observables. We also comment on the possibility of generating the observed BAU from leptogenesis, and how complying with present observation can constrain the SUSY seesaw parameters. In Section 4 we study, both for the cMSSM and its type-I seesaw extension, the impact of LFV at the LHC. Our results are presented in Section 5 where, after briefly considering the cMSSM case, we study the different high- and low-energy observables in the seesaw case. This will also allow to draw some conclusions on the viability of a type-I seesaw as the underlying mechanism of LFV. Further discussion is presented in the concluding Section 6.

2 Slepton masses and invariant mass distributions at the LHC

In this work we are interested in the study of slepton mass differences to probe deviations from the cMSSM, and possibly derive some information about the underlying theory of flavour violation in the (s)lepton sector. We briefly outline in this section how slepton masses can be reconstructed from observation at the LHC. We describe the mechanisms for production, the favoured decay chains and finally the kinematical observables used to reconstruct the slepton masses and hence their mass splittings.

We recall that the cMSSM is defined by its superpotential,

$$\mathcal{W}^{\text{MSSM}} = \hat{U}^c Y^u \hat{Q} \hat{H}_2 + \hat{D}^c Y^l \hat{Q} \hat{H}_1 + \hat{E}^c Y^l \hat{L} \hat{H}_1 + \mu \hat{H}_1 \hat{H}_2, \quad (2.1)$$

and by the mSUGRA-inspired conditions imposed on the soft-breaking SUSY Lagrangian: universal gaugino masses ($M_1 = M_2 = M_3 = M_{1/2}$), universal scalar masses for Higgs bosons, squarks and sleptons ($m_{H_1, H_2} = m_{\tilde{Q}, \tilde{U}, \tilde{D}} = m_{\tilde{L}, \tilde{E}} = m_0$) and universal trilinear couplings ($A_{u,d,l} = A_0 Y^{u,d,l}$), the universality being imposed at some high energy scale, which we chose to be the gauge coupling unification scale. The model is further defined by the ratio of the vacuum expectation value of the Higgs fields, $\tan \beta = v_2/v_1$ and $\text{sign}(\mu)$, leading to a total of 4 continuous and one discrete parameter.

2.1 Slepton production at the LHC

If R-parity is preserved, SUSY particles are produced in pairs, and decay to the lightest SUSY particle (LSP), which is stable. The usually complex decay cascades lead to signatures involving in general multiple jets and/or missing transverse energy from the LSPs escaping the detector. Several reconstruction methods have been proposed (see, e.g. [58–60] and references therein) allowing to extract very precise combinations of masses and branching ratios from several experimental measurements. In particular, the analysis of endpoints in kinematical distributions for specific final states allows to determine fundamental parameters of the model, especially in the case of simple SUSY realisations as the cMSSM. In favourable cases, where one expects to observe a large number of events, and if the signal to background ratio is large, the cMSSM parameters are likely to be measured with very good accuracy [61, 62].

Provided the SUSY breaking scale is not too high, supersymmetric particles are expected to be abundantly produced at the LHC, operating at a centre of mass (c.o.m.) energy $\sqrt{s} = 7 \text{ TeV} - 14 \text{ TeV}$. The production of coloured SUSY particles will dominantly occur from quark-antiquark

annihilation and gluon-gluon fusion, and possibly also via (strong) quark-quark scattering and quark-gluon fusion. QCD-singlet particles as sleptons can be directly produced via Drell-Yan processes (s -channel Z - or γ -exchange) or arise from gaugino-like neutralino decays. However, in the first case the associated production cross sections are in general small and detection is compromised due to the large SM backgrounds. The second process is more favourable, since neutralinos can be produced directly, or arise from cascade decays of squarks; if kinematically allowed, squark decays lead to a large number of chains with intermediate slepton states (like for instance $\tilde{q}_L \rightarrow q_L \chi_2^0 \rightarrow q_L \tilde{\ell} \ell \rightarrow q_L \ell \ell \chi_1^0$).

At the LHC, squarks might be pair produced $pp \rightarrow \tilde{q}\tilde{q}^*$, $\tilde{q}\tilde{q}$ and single produced $pp \rightarrow \tilde{q}\tilde{g}$ [67]. Squarks can then decay to a $\chi_i^0 q$ pair, while the gluino preferably decays to $\tilde{q}_R q, \tilde{t}_1 t$. Direct neutralino production goes either through pure electroweak interactions ($pp \rightarrow \chi_2^0 \chi_i^0, \chi_2^0 \chi_i^\pm$) or mixed EW-strong ($pp \rightarrow \chi_2^0 \tilde{q}_{L,R}^i, \chi_2^0 \tilde{g}$, with \tilde{q} possibly decaying into $\chi_2^0 q$).

Here we will distinguish between three primary production modes: “direct” neutralino production ($pp \rightarrow \chi_2^0 X$), squark-decay ($pp \rightarrow \tilde{q}_L Y$) and gluino-gluino mode ($\tilde{g}\tilde{g}$). In the cMSSM framework, the process $pp \rightarrow \tilde{g}\tilde{g}$ is in general kinematically suppressed ($m_{\tilde{g}} > m_{\tilde{q}}$). We also consider separately the prospects for at least one- and exactly two- χ_2^0 production.

2.2 Di-lepton invariant mass distributions

As extensively discussed in the literature, in scenarios where the χ_2^0 is sufficiently heavy to decay via a real (on-shell) slepton, the process $\chi_2^0 \rightarrow \ell'^\pm \ell^\mp \chi_1^0$ is greatly enhanced while providing a very distinctive signal [58–60, 62]: same-flavour opposite-charged leptons with missing energy. Moreover, the momentum of the leptons is expected to be easily reconstructed (accounting for smearing effects in τ 's), thus allowing to extract indirect information on the mass spectrum of the involved sparticles.

As previously mentioned, the best approach to reconstruct the intermediate particle masses in a decay chain is the construction of invariant kinematical quantities, which are comparatively easy to measure (even in the presence of large amounts of missing energy). In particular, the di-lepton invariant mass distribution presents kinematical edges (di-particle or tri-particle), which allow to derive information on the mass of the exchanged sparticles.

In order to reduce the SM background, several cuts have to be applied in the reconstruction of the events. It has been shown [59, 60] that one of those was having two isolated leptons with large transverse momentum, $p_T > 10$ GeV. We will therefore always require hard outgoing leptons in our analysis. From the SUSY decay chain, $\tilde{q}_L \rightarrow \chi_2^0 q \rightarrow \tilde{\ell}_{L,R} \ell q \rightarrow \chi_1^0 \ell \ell q$, one can construct several invariant quantities:

- (i) 3 di-particle invariant masses

$$m_{\ell\ell}^{\max} = M(m_{\chi_2^0}, m_{\tilde{\ell}_{L,R}}, m_{\chi_1^0}), \quad (2.2)$$

$$m_{\ell\text{near}q}^{\max} = M(m_{\tilde{q}_L}, m_{\chi_2^0}, m_{\tilde{\ell}_{L,R}}), \quad (2.3)$$

$$m_{\ell\text{far}q}^{\max} = M'(m_{\tilde{q}_L}, m_{\chi_2^0}, m_{\tilde{\ell}_{L,R}}, m_{\chi_1^0}), \quad (2.4)$$

where

$$M(x, y, z) = 1/y \sqrt{(x^2 - y^2)(y^2 - z^2)}, \quad M'(x, y, z, w) = 1/w \sqrt{(x^2 - y^2)(w^2 - z^2)},$$

and whose end-points have a common structure;

(ii) tri-particle invariant mass

$$m_{\ell\ell q}^{\max} = M(m_{\tilde{q}_L}, m_{\chi_2^0}, m_{\chi_1^0}). \quad (2.5)$$

Here, we shall focus on di-lepton invariant mass distributions [60, 68]:

$$m_{\ell\ell} \equiv \sqrt{(p_{\ell'} + p_{\ell})^2} = m_{\ell\ell}^{(\max)} \cos \frac{\theta}{2}, \quad m_{\ell\ell}^{(\max)} = \frac{1}{m_{\tilde{\ell}}} \sqrt{(m_{\chi_2^0}^2 - m_{\tilde{\ell}}^2)(m_{\tilde{\ell}}^2 - m_{\chi_1^0}^2)}, \quad (2.6)$$

where $\pi - \theta$ is the angle between the two leptons in the slepton's rest frame. In general terms, the $\chi_2^0 \rightarrow \chi_1^0 \ell'^{\pm} \ell^{\mp}$ decay process occurs via: t - and u -channel with charged slepton exchange; exchange of the lightest Higgs boson¹, h ; or via a Z boson.

Considering the complete decay process, i.e., via on-shell and off-shell intermediate states, the di-lepton invariant mass distribution has “true” start- and end-points given by

$$\overline{m}_{\ell\ell}^{\min} = m_{\ell'} + m_{\ell}, \quad \overline{m}_{\ell\ell}^{\max} = m_{\chi_2^0} - m_{\chi_1^0}, \quad (2.7)$$

respectively. It can be easily verified that the $\overline{m}_{\ell\ell}$ end-point matches the on-shell end-point for a slepton of mass $m_{\tilde{\ell}} = \sqrt{m_{\chi_2^0} m_{\chi_1^0}}$, in which case no decreasing event rate is expected to be observed beyond $\overline{m}_{\ell\ell}^{\max}$.

The invariant mass distributions can also be used to extract the mass splittings of the intermediate sleptons by looking at distinctive two-edge distributions which are expected to emerge whenever two different sleptons $\tilde{\ell}_{1,2}$ have sufficiently high rates for $\chi_2^0 \rightarrow \tilde{\ell}_{1,2} \ell_1 \rightarrow \chi_1^0 \ell_2 \ell_1$. In our analysis we will study the di-muon and di-electron invariant mass distributions, looking for edges that correspond to the exchanged selectron and smuon states, thus allowing to reconstruct the \tilde{e}_L and $\tilde{\mu}_L$ masses (and in some cases, \tilde{e}_R and $\tilde{\mu}_R$ as well). Hard outgoing taus can decay hadronically and can also be identified, however the background will be much larger in this case. Nevertheless, we also address $\tilde{\mu} - \tilde{\tau}$ mass differences.

As we will discuss in detail in the following section, the mass differences of sleptons of the first two generations are expected to be extremely small. However, if slepton universality is broken (e.g. via diagonal, but non-universal soft-breaking slepton masses), or if lepton flavour is violated in the (s)lepton sector, distinct two-edge distributions can be observable provided there is sufficient resolution to be sensitive to a certain amount of mass splitting [69]. The kinematical edge is expected to be measurable at LHC with a precision up to 0.1% [58–62]. The relative slepton mass splittings, which are defined as

$$\frac{\Delta m_{\tilde{\ell}}}{m_{\tilde{\ell}}}(\tilde{\ell}_i, \tilde{\ell}_j) = \frac{|m_{\tilde{\ell}_i} - m_{\tilde{\ell}_j}|}{\langle m_{\tilde{\ell}_{i,j}} \rangle}, \quad (2.8)$$

can then be inferred from the kinematical edges with a sensitivity of $\mathcal{O}(0.1\%)$ [70] for $\tilde{e}_L - \tilde{\mu}_L$ and $\mathcal{O}(1\%)$ for $\tilde{\mu}_L - \tilde{\tau}_2$. Even if already impressive, the edge splitting can be further enhanced by considering the so-called fractional shift of the kinematical edge in the di-lepton invariant mass distribution:

$$\frac{\Delta m_{\ell\ell}}{m_{\ell\ell}} = \frac{\Delta m_{\tilde{\ell}}}{m_{\tilde{\ell}}} \left[\frac{m_{\chi_2^0}^2 m_{\chi_1^0}^2 - m_{\tilde{\ell}}^4}{(m_{\chi_2^0}^2 - m_{\tilde{\ell}}^2)(m_{\tilde{\ell}}^2 - m_{\chi_1^0}^2)} \right]. \quad (2.9)$$

Even though this will be discussed in greater detail in Section 5, it is clear from the above discussion that certain conditions must be fulfilled in order to render feasible the study of slepton

¹In mSUGRA scenarios the exchange of the heaviest CP-even (H) or of the CP-odd (A) Higgs bosons are off-shell suppressed.

mass splittings. Firstly, sleptons must be produced in non-negligible amounts: this translates into having a not excessively heavy SUSY spectrum (to allow for abundant squark and χ_2^0 production), and in a neutralino-slepton hierarchy such that the decays of χ_2^0 into real sleptons are kinematically viable. As already noticed in [66], in the regions of the cMSSM where the latter decays are allowed, the $\text{BR}(\chi_2^0 \rightarrow \chi_1^0 \ell \ell)$ is in general enhanced when compared to the case of virtual intermediate sleptons. Secondly, an efficient tagging/event selection requires “hard” - highly energetic - outgoing leptons, implying the following requirement for the phase space: $m_{\chi_2^0} - m_{\tilde{e}_L, \tilde{\mu}_L, \tilde{\tau}_2} \geq 10 \text{ GeV}$. In summary, the experimental study of slepton mass differences at the LHC will only be possible if the specific realisation of the SUSY model meets the above requirements.

3 Lepton flavour violation in the SUSY seesaw

Extensions of the SM by heavy states such as fermionic singlets [19] or fermionic triplets [21] or scalar triplets [20], allow to explain the smallness of the neutrino masses via seesaw-like mechanisms. In these realisations, the violation of lepton flavour number can be easily accommodated in the neutral lepton sector and parametrized by a leptonic mixing matrix. One may also have lepton flavour violation in the charged sector through four-fermion dimension-six effective operators (see for example [71], where several lepton violation processes were studied in the three different seesaw types). In this study, we will consider a type-I seesaw (heavy fermionic singlets with masses at a sufficiently high scale to have large enough Yukawa couplings: $10^{10} \text{ GeV} - 10^{15} \text{ GeV}$) embedded in the framework of supersymmetric theories as a source of lepton flavour violation in the charged lepton sector. Within the so-called SUSY seesaw, flavour violation in the neutrino sector is transmitted to the charged leptons via radiative effects involving the neutrino Yukawa couplings Y^ν . Even under GUT scale universality conditions, the RGE-induced flavour violation is sufficiently large to account for sizable rates of LFV observables such as radiative ($\ell_i \rightarrow \ell_j \gamma$) and three-body ($\ell_i \rightarrow \ell_j \ell_k \ell_k$) decays, and $\mu - e$ conversion in nuclei. It may also account for potentially large mass splittings for the slepton masses (in addition to the usual LR -mixing) and, in the presence of complex Y^ν , for CPV observables, such as T- and P-odd asymmetries in radiative and three-body decays as well as contributions to the lepton electric dipole moments (EDMs). Remarkably, having a unique source of flavour violation in the lepton sector implies that all the above mentioned observables will be strongly related.

In this section, we briefly overview the implementation of a type-I seesaw in the constrained MSSM, as well as its implications for low-energy LFV observables. We also comment on the possibility of generating the observed baryon asymmetry of the Universe (BAU) from leptogenesis, and how complying with present observation on the baryon asymmetry can constrain the SUSY seesaw parameters. The impact of LFV for high-energy experiments, manifest in observables such as slepton mass splittings or direct flavour violation in sparticle decays, will be discussed in Section 4.

3.1 Type-I SUSY seesaw

We consider an extension of the MSSM to which three right-handed neutrino superfields are added. Each supermultiplet \hat{N}^c contains the right-handed neutrinos ν_R and their superpartners $\tilde{\nu}_R$. The SUSY type-I seesaw is defined by the superpotential \mathcal{W} of the MSSM extended by two additional terms involving \hat{N}^c . The leptonic part of \mathcal{W} is then given by:

$$\mathcal{W}^{\text{lepton}} = \hat{N}^c Y^\nu \hat{L} \hat{H}_2 + \hat{E}^c Y^l \hat{L} \hat{H}_1 + \frac{1}{2} \hat{N}^c M_N \hat{N}^c. \quad (3.1)$$

The lepton Yukawa couplings $Y^{l,\nu}$ and the Majorana mass M_N are 3×3 matrices in lepton flavour space. Hereafter we will always assume, without loss of generality, that we are in a basis where both Y^l and M_N are diagonal:

$$Y^l = \text{diag}(Y^e, Y^\mu, Y^\tau), \quad M_N = \text{diag}(M_{N_1}, M_{N_2}, M_{N_3}). \quad (3.2)$$

The slepton part of the soft-SUSY breaking Lagrangian is specified by

$$\begin{aligned} \mathcal{V}_{\text{soft}}^{\text{slepton}} = -\mathcal{L}^{\text{slepton}} = & m_{\tilde{L}}^2 \tilde{l}_L \tilde{l}_L^* + m_{\tilde{E}}^2 \tilde{l}_R \tilde{l}_R^* + m_{\tilde{\nu}_R}^2 \tilde{\nu}_R \tilde{\nu}_R^* + \\ & + \left(A_l H_1 \tilde{l}_L \tilde{l}_R^* + A_\nu H_2 \tilde{\nu}_L \tilde{\nu}_R^* + B_\nu \tilde{\nu}_R \tilde{\nu}_R + \text{H.c.} \right). \end{aligned} \quad (3.3)$$

Motivated by SUSY breaking schemes mediated by flavour-blind gravitational interactions (minimal supergravity inspired), we work within the framework of the constrained MSSM, where the soft-SUSY breaking parameters are assumed to be universal at some high-energy scale M_X , which we choose to be the gauge coupling unification scale $M_{\text{GUT}} \sim 10^{16}$ GeV. Thus, at M_X , the additional parameters in $\mathcal{L}^{\text{slepton}}$ also obey the following universality conditions:

$$\begin{aligned} (m_{\tilde{L}})_{ij}^2 &= (m_{\tilde{E}})_{ij}^2 = (m_{\tilde{\nu}_R})_{ij}^2 = m_0^2 \delta_{ij}, \\ (A_l)_{ij} &= A_0 (Y^l)_{ij}, \quad (A_\nu)_{ij} = A_0 (Y^\nu)_{ij}, \end{aligned} \quad (3.4)$$

where m_0 and A_0 are the universal scalar soft-breaking mass and trilinear coupling of the cMSSM, and i, j denote lepton flavour indices ($i, j = 1, 2, 3$).

After electroweak symmetry breaking (EWSB), the Dirac mass terms for the charged leptons and neutrinos are

$$m_l = Y^l v_1, \quad m_D^\nu = Y^\nu v_2, \quad (3.5)$$

where v_i are the vacuum expectation values (VEVs) of the neutral Higgs scalars, $v_{1(2)} = v \cos(\sin)\beta$ with $v = 174$ GeV. Assuming Y^l diagonal in flavour space, one has $m_l = \text{diag}(m_e, m_\mu, m_\tau)$, while the masses of the physical Majorana neutrinos are given by the eigenvalues of the 6×6 neutrino mass matrix,

$$M^\nu = \begin{pmatrix} 0 & m_D^{\nu T} \\ m_D^\nu & M_N \end{pmatrix}. \quad (3.6)$$

In the seesaw limit (i.e. $M_{N_i} \gg v$), and at lowest order in the $(m_D^\nu/M_N)^n$ expansion, the above matrix can be block-diagonalized, leading to the usual seesaw equation for the light neutrino mass matrix,

$$m_\nu = -m_D^{\nu T} M_N^{-1} m_D^\nu, \quad (3.7)$$

while the masses of the heavy eigenstates are simply given by M_{N_i} .

The light neutrino mass matrix m_ν is diagonalized by the Maki-Nakagawa-Sakata unitary matrix U^{MNS} [72],

$$m_\nu^{\text{diag}} = U^{\text{MNS}T} m_\nu U^{\text{MNS}} = \text{diag}(m_{\nu_1}, m_{\nu_2}, m_{\nu_3}), \quad (3.8)$$

where under the standard parameterisation U^{MNS} is given by

$$U^{\text{MNS}} = \begin{pmatrix} c_{12} c_{13} & s_{12} c_{13} & s_{13} e^{-i\delta} \\ -s_{12} c_{23} - c_{12} s_{23} s_{13} e^{i\delta} & c_{12} c_{23} - s_{12} s_{23} s_{13} e^{i\delta} & s_{23} c_{13} \\ s_{12} s_{23} - c_{12} c_{23} s_{13} e^{i\delta} & -c_{12} s_{23} - s_{12} c_{23} s_{13} e^{i\delta} & c_{23} c_{13} \end{pmatrix} \cdot V, \quad (3.9)$$

with

$$V = \text{diag}(e^{-i\frac{\varphi_1}{2}}, e^{-i\frac{\varphi_2}{2}}, 1), \quad (3.10)$$

and $c_{ij} \equiv \cos \theta_{ij}$, $s_{ij} \equiv \sin \theta_{ij}$. θ_{ij} are the leptonic mixing angles, δ is the Dirac CPV phase and $\varphi_{1,2}$ the Majorana CPV phases.

Current (best-fit) analyses of the low-energy neutrino data favour the following intervals for the mixing angles [26]

$$\theta_{12} = (34.4 \pm 1.0)^\circ, \quad \theta_{23} = (42.8^{+4.7}_{-2.9})^\circ, \quad \theta_{13} = (5.6^{+3.0}_{-2.7})^\circ (\leq 12.5^\circ), \quad (3.11)$$

while for the mass-squared differences one has

$$\Delta m_{12}^2 = (7.6 \pm 0.2) \times 10^{-5} \text{ eV}^2, \quad \Delta m_{13}^2 = \begin{cases} (-2.36 \pm 0.11) \times 10^{-3} \text{ eV}^2 \\ (+2.46 \pm 0.12) \times 10^{-3} \text{ eV}^2 \end{cases}, \quad (3.12)$$

where the two ranges for Δm_{13}^2 correspond to normal and inverted neutrino spectrum.

A convenient means of parametrizing the neutrino Yukawa couplings, while at the same time allowing to accommodate the experimental data, is given by the Casas-Ibarra parametrization [32], which reads at the seesaw scale M_N

$$Y^\nu v_2 = m_D^\nu = i\sqrt{M_N^{\text{diag}}} R \sqrt{m_\nu^{\text{diag}}} U^{\text{MNS}\dagger}. \quad (3.13)$$

In the above R is a complex orthogonal 3×3 matrix that encodes the possible mixings involving the right-handed neutrinos, in addition to those of the low-energy sector (i.e. U^{MNS}). R can be parameterized in terms of three complex angles θ_i ($i = 1, 2, 3$) as

$$R = \begin{pmatrix} c_2 c_3 & -c_1 s_3 - s_1 s_2 c_3 & s_1 s_3 - c_1 s_2 c_3 \\ c_2 s_3 & c_1 c_3 - s_1 s_2 s_3 & -s_1 c_3 - c_1 s_2 s_3 \\ s_2 & s_1 c_2 & c_1 c_2 \end{pmatrix}, \quad (3.14)$$

with $c_i \equiv \cos \theta_i$, $s_i \equiv \sin \theta_i$. Before advancing, it is worth commenting that out of the 18 parameters involved in the seesaw (as readily verified from either side of Eq. (3.13)), in practice only the degrees of freedom related to the light neutrinos (masses, leptonic mixings angles, and potentially 2 of the 3 CPV phases) can be effectively reconstructed from low-energy data and cosmological observations. Unless the seesaw scale is very low, in which case Y^ν is very small, this implies that the dynamics of the right-handed neutrino sector is unreachable, and may only be indirectly probed.

3.2 Radiative LFV in the slepton sector

In the presence of mixings in the lepton sector, Y^ν is clearly non-diagonal in flavour space. At the seesaw scale Y^ν satisfies Eq. (3.13), and the running from M_X down to the seesaw scale will induce flavour mixing in the otherwise (approximately) flavour conserving SUSY breaking terms. The low-energy parameters are obtained by solving the full set of renormalisation group equations (RGEs), which include additional terms and equations due to the extended neutrino and sneutrino sectors. In our work, the running is carried in several steps: the full set of equations is first run down from M_X to the seesaw scales; below the seesaw threshold, after the right-handed neutrinos (and sneutrinos) decouple, the new RGEs are then run down to EW scale, where the low-energy mass matrices and couplings are finally computed.

Due to the mixing induced by the RGE running in the slepton mass matrices, at low energies, the charged slepton squared mass matrix, M_l^2 , can be decomposed in four blocks (LL , RR , LR and RL) whose elements are given by (see, e.g. [73])

$$\begin{aligned} M_{LL}^{ij2} &= m_{L,ij}^2 + v_1^2 \left(Y^{l\dagger} Y^l \right)_{ij} + M_Z^2 \cos 2\beta \left(-\frac{1}{2} + \sin^2 \theta_W \right) \delta_{ij}, \\ M_{RR}^{ij2} &= m_{E,ij}^2 + v_1^2 \left(Y^l Y^{l\dagger} \right)_{ij} - M_Z^2 \cos 2\beta \sin^2 \theta_W \delta_{ij}, \\ M_{LR}^{ij2} &= v_1 \left(A_l^\dagger \right)_{ij} - v_2 \mu Y_{ij}^{l\dagger}, \\ M_{RL}^{ij2} &= \left(M_{LR}^{ji2} \right)^*, \end{aligned} \quad (3.15)$$

where M_Z is the Z -boson mass and θ_W the weak mixing angle. The low-energy sneutrino mass eigenstates are dominated by the $\tilde{\nu}_L$ components [74] (the right-handed sneutrinos having decoupled at the seesaw scale), and are described by the following mass matrix:

$$(M_{\tilde{\nu}}^2)_{ij} = m_{L,ij}^2 + \frac{1}{2} M_Z^2 \cos 2\beta \delta_{ij}. \quad (3.16)$$

Although in the numerical studies of Section 5 a full 2-loop RGE evaluation is conducted, a useful analytical estimation of the amount of flavour violation induced from RGE running on the slepton mixing matrices can be obtained using the leading logarithmic approximation (LLog). At leading order, one has the following radiative corrections to the soft slepton mass matrices entering in Eqs. (3.15, 3.16):

$$\begin{aligned} (m_{\tilde{L}}^2)_{ij} &= \left(m_0^2 + 0.5 M_{1/2}^2 - m_0^2 |y| (Y^l)_{ij}^2 \right) \delta_{ij} + (\Delta m_{\tilde{L}}^2)_{ij}, \\ (m_{\tilde{E}}^2)_{ij} &= \left(m_0^2 + 0.15 M_{1/2}^2 - 2 m_0^2 |y| (Y^l)_{ij}^2 \right) \delta_{ij} + (\Delta m_{\tilde{E}}^2)_{ij}, \end{aligned} \quad (3.17)$$

with

$$|y| \approx \frac{1}{8\pi^2} \left(3 + \frac{A_0^2}{m_0^2} \right) \log\left(\frac{M_X}{m_{\text{SUSY}}}\right) \quad (3.18)$$

where m_{SUSY} represents a generic (average) SUSY mass, and where the terms Δm^2 and also the correction to the trilinear coupling, ΔA_l , are only present for non-vanishing neutrino Yukawa couplings:

$$\begin{aligned} (\Delta m_{\tilde{L}}^2)_{ij} &= -\frac{1}{8\pi^2} (3m_0^2 + A_0^2) (Y^{\nu\dagger} L Y^\nu)_{ij}, \\ (\Delta A_l)_{ij} &= -\frac{3}{16\pi^2} A_0 Y_{ij}^l (Y^{\nu\dagger} L Y^\nu)_{ij}, \\ (\Delta m_{\tilde{E}}^2)_{ij} &= 0; \quad L_{kl} \equiv \log\left(\frac{M_X}{M_{N_k}}\right) \delta_{kl}. \end{aligned} \quad (3.19)$$

These terms can give rise to flavour mixing in the slepton mass matrix, originated by the running from M_X to the right-handed threshold M_N . The amount of flavour violation is encoded in the matrix elements $(Y^{\nu\dagger} L Y^\nu)_{ij}$ of Eq. (3.19), which can be related to high- and low-energy neutrino parameters using Eq. (3.13).

As can be seen from the above equations, the RGE corrections have an impact regarding both flavour non-universality and flavour violation in the charged slepton sector: (i) the charged lepton Yukawa couplings (in particular Y^τ) induce flavour non-universality, i.e. a splitting between the

soft masses of the third and the first two slepton generations (the latter remaining approximately degenerate); (ii) the neutrino Yukawa couplings contribute to both flavour non-universality and flavour violating effects. Due to the underlying seesaw mechanism, the Y^ν can be sizable (even $\mathcal{O}(1)$), so that the associated RGE corrections can be important. From the previous equations it is also manifest that LR mixing is only significant for the third generation (τ).

The physical masses and states are obtained by diagonalizing the previous mass matrices, leading to

$$\begin{aligned} M_{\tilde{l}}^{2\text{diag}} &= R^{\tilde{l}} M_{\tilde{l}}^2 R^{\tilde{l}\dagger} = \text{diag}(m_{\tilde{l}_1}^2, \dots, m_{\tilde{l}_6}^2), \\ M_{\tilde{\nu}}^{2\text{diag}} &= R^{\tilde{\nu}} M_{\tilde{\nu}}^2 R^{\tilde{\nu}\dagger} = \text{diag}(m_{\tilde{\nu}_1}^2, m_{\tilde{\nu}_2}^2, m_{\tilde{\nu}_3}^2), \end{aligned} \quad (3.20)$$

where $R^{\tilde{l}}$ and $R^{\tilde{\nu}}$ are unitary (6×6 and 3×3 , respectively) rotation matrices.

3.3 Low energy LFV observables

The exact formulae for the branching ratios of the radiative and three-body LFV lepton decays can be found in [2], and are incorporated in the SPHENO code [75] used for the numerical analysis.

Radiative decays $\ell_i \rightarrow \ell_j \gamma$ receive contributions from sneutrino-chargino and slepton-neutralino loop. However, a simple and illustrative expression can be obtained using the LLog approximation: since the dominant contribution to the transitions stems from the RGE induced flavour violating entry $(\Delta m_{\tilde{L}}^2)_{ij}$, one has

$$\text{BR}(\ell_i \rightarrow \ell_j \gamma) = \frac{\alpha^3 \tan^2 \beta}{G_F^2 m_{\text{SUSY}}^8} \left| \frac{1}{8\pi^2} (3m_0^2 + A_0^2) (Y^{\nu\dagger} L Y^\nu)_{ij} \right|^2, \quad (3.21)$$

where G_F is the Fermi constant, α the electromagnetic coupling constant.

The full computation of the three-body decays $\ell_i \rightarrow 3\ell_j$ includes photon-, Z - and Higgs-penguins as well as box diagrams. Since the dominant contribution is found to originate from the photon-penguin diagrams as occurs in the case of the radiative decays [38, 42], the BR for the $\ell_i \rightarrow 3\ell_j$ decay can be approximately related to that of the radiative decay as follows:

$$\text{BR}(\ell_i \rightarrow 3\ell_j) = \frac{\alpha}{3\pi} \left(\log \frac{m_{\tilde{l}_i}^2}{m_{\tilde{l}_j}^2} - \frac{11}{4} \right) \times \text{BR}(\ell_i \rightarrow \ell_j \gamma). \quad (3.22)$$

From Eqs. (3.21, 3.22) it is straightforward to derive the dependence of the observables on the relevant SUSY parameters. The impact of the seesaw parameters (right-handed neutrino masses, light neutrino mass hierarchy, R -matrix angles and θ_{13}) on the BRs has been studied in [46], and can be analytically understood from explicitly writing $(Y^{\nu\dagger} L Y^\nu)_{ij}$, using Eq. (3.13).

Equally interesting LFV observables are $\mu - e$ conversions in heavy nuclei such as aluminium, gold or titanium (for detailed discussions see, e.g. [76]). In the limit of photon-penguin dominance, the conversion rate $\text{CR}(\mu - e)$ in nuclei and $\text{BR}(\mu \rightarrow e \gamma)$ are strongly correlated, since both observables are sensitive to the same leptonic mixing parameters [48]. Typically, the SUSY seesaw predictions regarding the conversion rates are smaller than $\text{BR}(\mu \rightarrow e \gamma)$ by approximately two orders of magnitude (the actual factor depending on the mSUGRA parameters and on the properties of the muonic nucleus) [44]. However, and although significant improvements are expected regarding the experimental sensitivity to $\mu \rightarrow e \gamma$ ($< 10^{-13}$ [12]), the most challenging experimental prospects arise for the $\text{CR}(\mu - e)$ in heavy nuclei such as titanium or gold. The

possibility of lowering the sensitivities to values as low as $\sim 10^{-18}$ renders this observable an extremely powerful probe of LFV in the muon-electron sector.

We summarise in Table 1 the current bounds on the above discussed LFV observables, as well as the future sensitivity of dedicated experimental facilities.

LFV process	Present bound	Future sensitivity
$\text{BR}(\mu \rightarrow e\gamma)$	1.2×10^{-11} [77]	10^{-13} [12]
$\text{BR}(\tau \rightarrow e\gamma)$	1.1×10^{-7} [4]	10^{-9} [11]
$\text{BR}(\tau \rightarrow \mu\gamma)$	4.5×10^{-8} [15]	10^{-9} [11]
$\text{BR}(\mu \rightarrow 3e)$	1.0×10^{-12} [77]	2×10^{-10} [11]
$\text{BR}(\tau \rightarrow 3e)$	3.6×10^{-8} [77]	
$\text{BR}(\tau \rightarrow 3\mu)$	3.2×10^{-8} [77]	
$\text{CR}(\mu - e, \text{Ti})$	4.3×10^{-12} [77]	$\mathcal{O}(10^{-16})$ ($\mathcal{O}(10^{-18})$) [78] ([79])
$\text{CR}(\mu - e, \text{Au})$	7×10^{-13} [77]	
$\text{CR}(\mu - e, \text{Al})$		$\mathcal{O}(10^{-16})$ [79]

Table 1: Present bounds and future sensitivities for several LFV observables discussed in the text.

3.3.1 Lepton electric dipole moments

The bounds on the LFV BRs mostly constrain the source of mixing (i.e. off-diagonal elements) while the bounds on the lepton EDMs constrain the flavour-conserving CP-violating phases. Notice that CP violation in the lepton sector is also a consequence of the seesaw. Both low and high-energy CPV phases will give rise to complex soft breaking terms, potentially contributing to charged lepton EDMs. The present upper bound on the electron (muon) EDM is 1.4×10^{-27} (7.1×10^{-19}) e cm [77] while the future experiments are expected to reach a sensitivity of 10^{-31} e cm for the electron EDM [80] and 10^{-24} e cm for the muon EDM [81].

3.4 Implications of the SUSY seesaw for thermal leptogenesis

As mentioned in the Introduction, in addition to explaining the smallness of neutrino masses, the seesaw can also provide an interesting explanation to the observed baryon asymmetry of the Universe. The minimal thermal leptogenesis scenario [82] (for a recent review, see [83]) is based on the type-I seesaw mechanism, consisting of the SM extended by 2 or 3 right-handed (RH) Majorana neutrinos with hierarchical masses, which can be easily generalized to supersymmetric extensions of the SM. In these scenarios, the lightest RH neutrino N_1 , produced in the thermal bath after inflation by inverse decays and scatterings, decays through out-of-equilibrium processes that violate lepton number, C and CP symmetries. These processes induce a dynamical production of a lepton asymmetry, which can be later converted into a BAU through (B+L)-violating sphaleron interactions. In supersymmetric scenarios, the constraint from the reheating temperature T_{RH} (arising from the so-called gravitino problem [84]) already sets an upper bound on the mass of the lightest RH neutrino. Assuming an optimal washout (efficiency) and a successful BAU leads in turn to the following interval (lower bound) on M_{N_1} , $M_{N_1} \simeq 10^9 \text{ GeV} - 10^{10} \text{ GeV}$ [85].

In order to ensure that CP is indeed violated (via interference between loop and tree level decays), the neutrino Yukawa couplings have to be complex and CP violation is encoded in the R and U^{MNS} matrices ($Y^\nu = \frac{i}{v_2} \sqrt{M_N^{\text{diag}}} R \sqrt{m_\nu^{\text{diag}}} U^{\text{MNS}\dagger}$). It has been recently shown that a

correct formulation of the lepton asymmetry should be done considering each flavour separately (the number of distinguishable lepton flavours depending on the energies at which leptogenesis occurs) [86–88]. Having flavours play an important rôle in leptogenesis also means that both low- and high-energy CPV phases contribute to the CP asymmetry; however, the flavoured BAU can be accounted for exclusively with R phases (for any value of θ_{13} , δ , φ_1 , φ_2) [85, 89] - in other words even if the U^{MNS} phases are measured, the BAU can have any value.

Of course one cannot use a successful leptogenesis requirement to derive constraints on the CP violating sources, since leptogenesis is not an observable (contrarily to EDMs and LFV widths). However, one can have an idea about the range of variation of the complex angles θ_i of the R matrix that succeed in accounting for a viable (flavoured) leptogenesis (see for instance [85], where it has been shown that although all the three complex angles enter the flavoured CP-asymmetry, the rôle of θ_1 is indirect, manifest via increasing (decreasing) the θ_2 – θ_3 parameter space associated with a BAU compatible with current observation).

The interplay of LFV (and EDMs) and leptogenesis in constraining a type-I SUSY seesaw has been addressed, for instance, in [89–93].

Although in the numerical analysis of Section 5 we will conduct general surveys of the seesaw parameter space, we will also consider the following leptogenesis inspired ranges for the R matrix complex angles: $\text{Re}(\theta_2), \text{Re}(\theta_3) \in [-\pi/4, 0[\cup]0, +\pi/4]$ (for example). Complying with the (severe) reheating temperature constraint suggests that the arguments of the latter complex angles should have modulus in the range $[\pi/16, \pi/4]$. This corresponds to a conservative choice of volume in the θ_2 – θ_3 parameter space.

4 LFV at the LHC: slepton mass splittings and flavour violating χ_2^0 decays

As mentioned in Section 2, the different experiments at the LHC have the potential to measure with high precision the kinematical edges of the di-lepton invariant mass spectrum, so that one can potentially study the slepton mass differences. In what follows we discuss the different sources of slepton mass splittings, and also derive, for some simple limiting cases, approximate relations for $\frac{\Delta m_{\tilde{\ell}}}{m_{\tilde{\ell}}}(\tilde{\ell}_i, \tilde{\ell}_j)$.

4.1 Charged slepton mass differences in the type-I SUSY seesaw

Within the cMSSM, and in the absence of flavour mixing angles, there are only two sources of non-universality for the masses of left- and right-handed sleptons: (i) RGE effects proportional to $(Y^l)_{ij}^2$ (see Eqs. (3.17)); (ii) LR mixing effects, also proportional to the lepton masses ($m_i^l \tan \beta$). The mass difference of the first generations of sleptons is thus extremely small: neglecting RGE corrections, and considering only LR mixing for the smuons, the mass splitting between the left-handed selectron and the heaviest smuon is approximately given by

$$\frac{\Delta m_{\tilde{\ell}}}{m_{\tilde{\ell}}}(\tilde{e}_L, \tilde{\mu}_L) \approx \frac{m_\mu^2}{2m_{\tilde{\ell}}^2} \left| \frac{(A_0 - \mu \tan \beta)^2}{0.35 M_{1/2}^2 + M_Z^2 \cos 2\beta (-1/2 + 2 \sin^2 \theta_W)} \right|, \quad (4.1)$$

where $m_{\tilde{\ell}}$ denotes an averaged slepton mass, in this case $m_{\tilde{\ell}} \approx 1/2(|m_{\tilde{L}}^2|_{11}|^{1/2} + |m_{\tilde{L}}^2|_{22}|^{1/2})$. The cMSSM mass differences between the first two families are thus extremely small implying that, to a large extent, the left- and right-handed selectrons and smuons are nearly degenerate, the mass splitting typically lying at the per mille level.

For the stau sector, LR mixing effects and loop contributions are more important and to a very good approximation, the mass difference of the heaviest (mostly left-handed) stau and left-handed smuon is related to that of $\tilde{e}_L - \tilde{\mu}_L$ as

$$\frac{\Delta m_{\tilde{\ell}}}{m_{\tilde{\ell}}}(\tilde{e}_L, \tilde{\mu}_L) \approx \frac{m_\mu^2}{m_\tau^2} \frac{\Delta m_{\tilde{\ell}}}{m_{\tilde{\ell}}}(\tilde{\mu}_L, \tilde{\tau}_2). \quad (4.2)$$

When mixings are present in the lepton sector, flavour violation also occurs in the slepton sector. The radiative corrections introduced by the neutrino Yukawa couplings induce both flavour conserving and flavour violating contributions to the slepton soft masses: in addition to generating LFV effects, the new terms proportional to Y^ν will also break the approximate universality of the first two generations. An augmented mixing between \tilde{e} , $\tilde{\mu}$ and $\tilde{\tau}$ translates into larger mass splittings for the mass eigenstates. In particular, as noticed in [66], large mixings involving the third generation can lead to sizable values of the mass splitting between slepton mass eigenstates, while avoiding the stringent $\text{BR}(\mu \rightarrow e\gamma)$ constraint.

In the presence of seesaw-induced contributions to the distinct $(\Delta m_L^2)_{ij}$ and $(\Delta A_l)_{ij}$, see Eqs. (3.19), an analytical approach to the problem becomes extremely complicated. Even neglecting LR mixings for the two first generations, a numerical diagonalization is required to obtain the different mass eigenstates, as given in Eqs. (3.20). However, one can consider interesting limiting cases that provide useful information (and also help in understanding the numerical analysis of Section 5). Disentangling LR - from RGE-induced mixings, one then has for the mass difference $\tilde{\ell}_i - \tilde{\ell}_j$

$$\frac{\Delta m_{\tilde{\ell}}}{m_{\tilde{\ell}}}(\tilde{\ell}_i, \tilde{\ell}_j) \approx \frac{1}{2m_{\tilde{\ell}}^2} \left| \frac{m_i^2 (A_0 - \mu \tan \beta)^2}{0.35M_{1/2}^2 + M_Z^2 \cos 2\beta (-1/2 + 2 \sin^2 \theta_W) + (\Delta m_L^2)_{ii}} \pm 2 |(\Delta m_L^2)_{ij}| \right|, \quad (4.3)$$

where m_i denotes the mass of the heaviest lepton and where we have again neglected the RGE contributions proportional to the charged lepton Yukawa coupling.

If the seesaw scale is sufficiently high, large values of the neutrino Yukawa couplings are possible, and hence large off-diagonal entries can be generated. Assuming that a particular $(\Delta m_L^2)_{ij}$ constitutes the dominant source of LFV, one can approximate Eq. (4.3) as

$$\frac{\Delta m_{\tilde{\ell}}}{m_{\tilde{\ell}}}(\tilde{\ell}_i, \tilde{\ell}_j) \approx \left| \frac{(\Delta m_L^2)_{ij}}{(m_L^2)} \right|. \quad (4.4)$$

In particular, large flavour violating entries involving the second and third generation can be easily induced. In this case, and further assuming that the stau mass eigenstates are strongly dominated by either the left- or the right-handed state, the diagonalization of the $\tilde{\mu}_L - \tilde{\tau}_2$ mixing matrix (for non-vanishing $(\Delta m_L^2)_{23}$) leads to the following approximate relation

$$\frac{\Delta m_{\tilde{\ell}}}{m_{\tilde{\ell}}}(\tilde{\mu}_L, \tilde{\tau}_2) \approx \left| \frac{(\Delta m_L^2)_{23}}{(m_L^2)_{33}} \right|, \quad (4.5)$$

where the quantities on the right-hand side can be found in Eqs. (3.17- 3.19), and where we have also neglected cMSSM-like mass differences $\sim \mathcal{O}((m_L^2)_{22} - (m_L^2)_{33})$. Rewriting the left-handed smuon mass in terms of the above mass splitting further allows to relate the $\tilde{e}_L - \tilde{\mu}_L$ and the $\tilde{\mu}_L - \tilde{\tau}_2$ mass differences in the $R = 1$ seesaw limit

$$\frac{\Delta m_{\tilde{\ell}}}{m_{\tilde{\ell}}}(\tilde{e}_L, \tilde{\mu}_L) \approx \frac{1}{2} \frac{\Delta m_{\tilde{\ell}}}{m_{\tilde{\ell}}}(\tilde{\mu}_L, \tilde{\tau}_2). \quad (4.6)$$

Although one can derive approximate relations that translate the dependence of the mass splittings on the mSUGRA parameters, it is important to stress that the conditions to ensure that the slepton masses can indeed be reconstructed (see Section 2) imply that mSUGRA parameters cannot be independently varied. Under the approximations above referred, one can nevertheless obtain a simple illustrative expression for the mass splittings, which we write below for the case of $\tilde{\mu}_L - \tilde{\tau}_2$

$$\frac{\Delta m_{\tilde{\ell}}}{m_{\tilde{\ell}}}(\tilde{\mu}_L, \tilde{\tau}_2) \approx \frac{1}{8\pi^2} \frac{L_{33} M_{N_3}}{v^2 \sin^2 \beta} \frac{3m_0^2 + A_0^2}{m_0^2 + 0.5M_{1/2}^2} \left| \sum_{ij} U_{2i}^{\text{MNS}} U_{3j}^{\text{MNS}*} R_{3i}^* R_{3j} \sqrt{m_{\nu_i} m_{\nu_j}} \right|. \quad (4.7)$$

In the above equation, we have considered a strongly hierarchical right-handed neutrino spectrum, only keeping the contribution associated with the heaviest state N_3 , in the limit where $\theta_{13} \approx 0$.

It is also interesting to investigate the relation between two flavour violating observables strongly affected by the same LFV entry. For instance, let us again consider $\tilde{\mu}_L - \tilde{\tau}_2$ mass splittings and the $\text{BR}(\tau \rightarrow \mu\gamma)$. Comparing the previous expression with Eq. (3.21), one has, in the same seesaw limit as above

$$\text{BR}(\tau \rightarrow \mu\gamma) \approx \frac{\alpha^3}{16\pi^2 G_F^2} \frac{m_0^2 + 0.5M_{1/2}^2}{v^2 \cos^2 \beta m_{\text{SUSY}}^8} (3m_0^2 + A_0^2) L_{33} M_{N_3} m_{\nu_3} \sin 2\theta_{23} \times \frac{\Delta m_{\tilde{\ell}}}{m_{\tilde{\ell}}}(\tilde{\mu}_L, \tilde{\tau}_2). \quad (4.8)$$

Finally, it is important to stress that depending on the amount of flavour violation, a type-I SUSY seesaw can lead to scenarios where two non-degenerate mass eigenstates have almost identical flavour content (maximal flavour mixing). As an example, one can have mass eigenstates whose composition is approximately given by

$$\tilde{\ell}_{i,j} \sim (\sqrt{2}/2 + \varepsilon) \tilde{\mu}_L \pm (\sqrt{2}/2 - \varepsilon) \tilde{\tau}_L + \varepsilon \tilde{\tau}_R,$$

where ε ($\varepsilon \ll 1$) accounts for the LR mixing. To correctly interpret a mass splitting between sleptons with quasi-degenerate flavour content (QDFC), one has to introduce an “effective” mass

$$m_i^{(\text{eff})} \equiv \sum_{X=\tilde{\tau}_2, \tilde{\mu}_L, \tilde{e}_L} m_{\tilde{\ell}_X} \left(|R_{XiL}^{\tilde{\ell}}|^2 + |R_{XiR}^{\tilde{\ell}}|^2 \right), \quad (4.9)$$

which in turn provides the notion of “effective” mass splitting,

$$\left(\frac{\Delta m}{m} \right)^{(\text{eff})}(\tilde{\ell}_i, \tilde{\ell}_j) \equiv \frac{2|m_i^{(\text{eff})} - m_j^{(\text{eff})}|}{m_i^{(\text{eff})} + m_j^{(\text{eff})}}. \quad (4.10)$$

For mass splittings involving QDFC and non-QDFC sleptons, one should then use the “effective” mass splittings, cf. Eq. (4.10); in the case where mass splittings involving two QDFC sleptons or two non-QDFC sleptons, the real mass splitting (see e.g. Eq. (4.3)) can be employed.

4.2 Di-lepton invariant masses from flavour violating χ_2^0 decays

In the cMSSM, the decays of the χ_2^0 into a di-lepton final state $\chi_2^0 \rightarrow \ell_i^\pm \ell_i^\mp \chi_1^0$ are flavour conserving, implying that if measurable, the kinematical edges of a di-lepton mass distribution, $m_{\ell_i \ell_i}$ necessarily lead to the reconstruction of intermediate sleptons of the same flavour, $\tilde{\ell}_{L,R}^i$.

SUSY models violating strict lepton flavour symmetry may leave distinct imprints on the di-lepton mass distribution, depending on whether the soft-breaking slepton terms are non-universal

(but flavour conserving) or truly flavour-violating. In the first case, the most significant effect will be a visible displacement of the kinematical edges in each of the di-lepton distributions: for instance, the edge corresponding to \tilde{e}_L in m_{ee} will not appear at the same values as that of $\tilde{\mu}_L$ in $m_{\mu\mu}$, thus implying that $m_{\tilde{e}_L} \neq m_{\tilde{\mu}_L}$.

The second case will lead to far richer imprints: as discussed in the previous subsection, flavour violation has the potential to induce significant mass differences for the sleptons, so that one should again observe a relative displacement of the $\tilde{\ell}_X$ in the corresponding $m_{\ell_i\ell_i}$ distributions. Nevertheless, the most striking effect is the appearance of new edges in a given di-lepton mass distribution: provided there is a large flavour mixing in the mass eigenstates (and that all the decays are kinematically viable), one can have

$$\chi_2^0 \rightarrow \left\{ \begin{array}{l} \tilde{\ell}_L^i \ell_i \\ \tilde{\ell}_R^i \ell_i \\ \tilde{\ell}_X^j \ell_i \end{array} \right\} \rightarrow \chi_1^0 \ell_i \ell_i \quad (4.11)$$

so that in addition to the two $\tilde{\ell}_{L,R}^i$ edges, an additional one would appear due to the exchange of $\tilde{\ell}_X^j$.

5 Numerical results and discussion

We start our analysis by first considering the cMSSM parameter space, looking for regions where one can fulfil the necessary conditions to have reasonably large BR for the decay $\chi_2^0 \rightarrow \chi_1^0 \ell\ell$, with sufficiently hard outgoing leptons. After identifying some representative (benchmark) points, we analyse the prospects for the LHC (production cross sections and decay rates). The second part of our analysis will be devoted to slepton mass splittings and flavour violation in the type-I SUSY seesaw: we briefly discuss the cMSSM case and then study the different high- and low-energy observables in the seesaw case. This will also allow to draw some conclusions on the viability of a type-I SUSY seesaw as the underlying mechanism of LFV.

For the numerical computation, we have used the public code SPHENO (v3.beta.47) [75] to carry out the numerical integration of the RGEs of the cMSSM (extended by three right-handed neutrino superfields). With the exception of light neutrino data (masses and mixing angles) which is set as a low-energy input, all the parameters of the model are defined at the GUT scale. The low-energy parameters are then computed by running first the full set of RGEs to the seesaw scale, where the boundary conditions of Eq. (3.13) are imposed, and at which the heavy RH neutrinos decouple at their corresponding thresholds. We notice that we do not take into account separate thresholds for right-handed neutrinos and sneutrinos, and that we also neglect B_ν - see Eq. (3.3) - which is valid, provided that one considers $B_\nu \ll M_N$. Below M_{N_1} , the cMSSM RGEs are run to the EW scale, at which the low-energy Lagrangian (masses² and couplings) is determined and the different observables (such as the LFV BRs and CR [42], as well as lepton EDMs) are computed. The dark matter relic density is evaluated using a link to MICROMEAS v2.2 [94].

The production cross sections at LHC operating at c.o.m. of 7 TeV and 14 TeV have been computed using PROSPINO2.1 [95]. To obtain the di-lepton invariant mass distributions $\frac{d\Gamma}{dm_{ij}}(\chi_2^0 \rightarrow$

²We notice that SPHENO uses the $\overline{\text{DR}}$ scheme. Also, 2-loop RGEs are used for the running of the slepton masses, while the actual pole masses are calculated at the one-loop level, with all running parameters set at the SUSY scale. We have also verified that self-energies (and associated uncertainties) provide a negligible source of slepton mass splittings.

$\chi_1^0 \ell_i \ell_j$), we have used CUBA’s DIVONNE algorithm [96] to integrate numerically over the $\ell - \chi^0$ angle in the c.o.m. frame of the two leptons.

In what concerns the experimental constraints applied to the Higgs boson and sparticle spectrum, we have imposed that all SUSY particles comply with LEP and Tevatron bounds [77]. Throughout the analysis, and except if otherwise stated, we will always be imposing the bound for a SM-like Higgs boson to the lightest scalar: $m_h \gtrsim 114$ GeV [97]. Finally, the LSP relic density is required to lie within a 3σ interval (extrapolated from WMAP 7-year data taking [18], and assuming a gaussian distribution):

$$0.0941 \lesssim \Omega h^2 \lesssim 0.1277. \quad (5.1)$$

5.1 Di-lepton final states: neutralino production and cascade decays in the cMSSM

We begin by studying the cMSSM (without implementing a type-I seesaw), looking for regions in the mSUGRA parameter space where the requirements of a “standard window” can be met:

- (i) the spectrum is such that the decay chain $\chi_2^0 \rightarrow \tilde{\ell}\ell \rightarrow \chi_1^0 \ell\ell$, with intermediate real sleptons, is allowed;
- (ii) it is possible to have sufficiently hard outgoing leptons: $m_{\chi_2^0} - m_{\tilde{\ell}_L, \tilde{\tau}_2} > 10$ GeV.

Notice that the above requirements automatically ensure that the sparticle spectrum complies with current experimental bounds. Once these regions are identified, we then impose the requirements of a correct relic density, cf. Eq. (5.1). Naturally, in order to maximise the prospects for observing the above processes at the LHC, the SUSY spectrum should not be excessively heavy (as to have a sufficiently large production cross section) and the BRs of the χ_2^0 decay into slepton-lepton pairs (neutral or charged) also have to be large (as to render these decays observable). Here we will systematically consider two centre of mass energies for the LHC, $\sqrt{s} = 7$ TeV and 14 TeV (correspondingly, we consider either $\mathcal{L} = 1$ fb $^{-1}$ or 100 fb $^{-1}$ for the integrated luminosity [98]).

Before starting the discussion, we remark that throughout the analysis, and except if otherwise stated, we will always denote the flavour corresponding to an electron or a muon by ℓ to distinguish it from the τ flavour (except in inset figure labels).

In Fig. 1 we present the $m_0 - M_{1/2}$ parameter space, for $\mu > 0$ ³ and two combinations of A_0 and $\tan\beta$. On the left we take $A_0 = -1$ TeV and $\tan\beta = 10$, while on the right $A_0 = 0$ and $\tan\beta = 40$. All the points presented are in agreement with current LEP and Tevatron constraints [77] on the sparticle and Higgs boson spectra, and the region where the LSP relic density is in agreement with WMAP observations (within a 3σ interval, Eq. (5.1)) is denoted by a black band across the parameter space. The excluded (shaded) areas correspond to a charged LSP and to kinematically disfavoured regimes, while the white region in the centre corresponds to the requirements of a “standard window”. We superimpose the contour lines for $\text{BR}(\chi_2^0 \rightarrow \chi_1^0 \ell\ell)$ and $\text{BR}(\chi_2^0 \rightarrow \chi_1^0 \tau\tau)$. Approximately horizontal lines denote different values of the production cross section of (at least) one χ_2^0 .

The left panel of Fig. 1 corresponds to a scenario of a relatively light SUSY spectrum (with slepton masses between 110 GeV and 730 GeV, and $230 \text{ GeV} \lesssim m_{\chi_2^0} \lesssim 805 \text{ GeV}$). The region compatible with the “standard window” constraints is quite large, and the correct LSP relic density can be easily obtained (the dominant channel being $\chi_1^0 - \tilde{\tau}_1$ co-annihilation). Having a

³Throughout the numerical analysis we will always be considering positive values of μ .

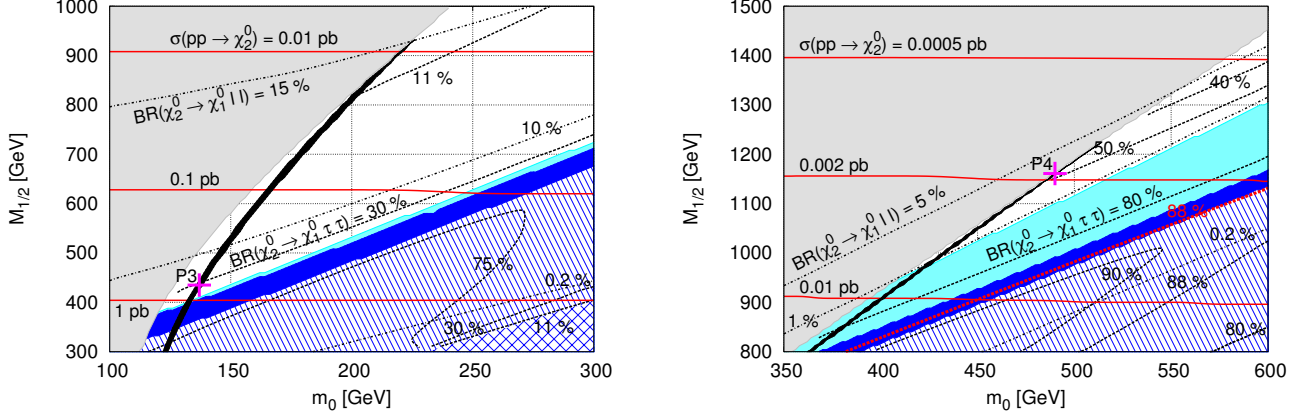


Figure 1: $m_0 - M_{1/2}$ plane (in GeV), for $A_0 = -1$ TeV and $\tan \beta = 10$ (left); the same but with $A_0 = 0$ and $\tan \beta = 40$ (right). In both figures, the shaded region on the left is excluded due to the presence of a charged LSP. The full black region corresponds to a WMAP compatible χ_1^0 relic density. Likewise, on the dashed region on the bottom, the spectrum does not fulfil the kinematical requirements described in the text: the solid regions correspond to having $m_{\chi_2^0} < m_{\tilde{\ell}_L} + 10$ GeV (cyan), $m_{\chi_2^0} < m_{\tilde{\tau}_2} + 10$ GeV (blue), $m_{\chi_2^0} < m_{\tilde{\ell}_L, \tau_2}$ (dashed blue), and $m_{\chi_2^0} < m_{\tilde{\tau}_1} + m_\tau$ (blue crosses). The centre (white) region denotes the parameter space obeying the “standard window” constraints. The dotted and dashed lines respectively denote isosurfaces for $\text{BR}(\chi_2^0 \rightarrow \chi_1^0 \ell \ell)$ and $\text{BR}(\chi_2^0 \rightarrow \chi_1^0 \tau \tau)$. Full red lines denote the contours of χ_2^0 production cross sections. Superimposed crosses (pink) correspond to benchmark points P3 and P4 (see Table 2).

light neutralino spectrum further implies that the production cross section of at least one χ_2^0 at the LHC (with $\sqrt{s} = 14$ TeV, via direct and indirect processes - see Section 2) is expected to be $0.01 \text{ pb} \lesssim \sigma(pp \rightarrow \chi_2^0) \lesssim 1 \text{ pb}$. In the “standard window”, the probability of having opposite-sign di-leptons in the final state ranges between 11% and 30% for $\tau\tau$, and between 10% and 15% for $\ell\ell$ (i.e. $ee, \mu\mu$) final states. It is worth noticing that larger values of $\text{BR}(\chi_2^0 \rightarrow \chi_1^0 \tau \tau)$ could be found for smaller $M_{1/2}$, since $\chi_2^0 \rightarrow \chi_1^0 \tilde{\tau}_1 \rightarrow \chi_1^0 \tau \tau$ becomes one of the few kinematically opened decay channels due to heavier LH sleptons. Nevertheless, no edges would be observable in this regime. Although the processes $\chi_2^0 \rightarrow \chi_1^0 \ell \ell$ and $\chi_2^0 \rightarrow \chi_1^0 \tau \tau$ are mostly dominated by the exchange of intermediate left- and right-handed real sleptons, there are other channels leading to the same final states, e.g. via the direct decay of the χ_2^0 into an LSP and the lightest Higgs boson or the Z . Throughout the experimentally viable $m_0 - M_{1/2}$ parameter space, the $\text{BR}(\chi_2^0 \rightarrow \chi_1^0 Z \rightarrow \chi_1^0 \tau \tau (\ell \ell))$ never exceeds the level of 0.03%, while the $\text{BR}(\chi_2^0 \rightarrow \chi_1^0 h)$ is at most $\mathcal{O}(12\%)$ inside the “standard window”, growing to 25% when softer outgoing leptons are allowed (solid blue bands). In turn, this induces a contribution to $\text{BR}(\chi_2^0 \rightarrow \chi_1^0 \tau \tau)$ ranging from 1.3% to 3%.

On the right panel of Fig. 1, we illustrate the parameter space for larger values of $\tan \beta$ (and a heavier spectrum). Having a substantially heavier gaugino and squark spectra when compared to that of the sleptons implies that the available phase space for χ_2^0 decays is much enlarged so that one can have sizable $\text{BR}(\chi_2^0 \rightarrow \chi_1^0 \tau \tau)$. However, the region strictly corresponding to the requirements of a “standard window” is somehow smaller, despite having the increased LR mixing compensated by heavier gauginos. As in the case of lower $\tan \beta$, intermediate h and Z states only marginally contribute to the final BRs. Finally, as expected from the significantly heavier SUSY

spectrum, the production of at least one χ_2^0 at the LHC has a cross section that now varies between 5×10^{-4} pb and 0.01 pb.

From Fig. 1, we extract two points in mSUGRA parameter space that we will use in the analysis of the slepton mass splittings (especially when studying the SUSY seesaw). Thus, points P3 and P4 (superimposed on the left and right panels, respectively) are points which in addition to complying with observational and experimental constraints, and being inside the corresponding “standard window”, also have sizable $\text{BR}(\chi_2^0 \rightarrow \chi_1^0 \ell \ell)$ and $\text{BR}(\chi_2^0 \rightarrow \chi_1^0 \tau \tau)$.

Other analyses of different regimes in mSUGRA parameter space have led us to identify two additional points P1 and P2 (with $A_0 = 0$ and 1 TeV, respectively), whose features complement points P3 and P4. To these points we further add two LHC benchmark points: P5-HM1 (from CMS [61]) and P6-SU1 ⁴ (from ATLAS [62]). This allows to establish a connection with the already conducted simulations and to study the flavour prospects at high energy. The most important features of these six points (mSUGRA parameters, spectra, production cross sections and BRs) are summarised in Tables 2-6.

Point	m_0 (GeV)	$M_{1/2}$ (GeV)	A_0 (TeV)	$\tan \beta$
P1	110	528	0	10
P2	110	471	1	10
P3	137	435	-1	10
P4	490	1161	0	40
P5-HM1 [61]	180	850	0	10
P6-SU1 [62]	70	350	0	10

Table 2: mSUGRA benchmark points selected for the LFV analysis: m_0 , $M_{1/2}$ (in GeV) and A_0 (in TeV), as well as $\tan \beta$. For all points we take $\mu > 0$. Points P5-HM1 and P6-SU1 are LHC CMS- and ATLAS-proposed benchmark points.

After summarising the mSUGRA coordinates of each point in Table 2, we present part of the corresponding SUSY spectrum on Table 3. Among the six points we find distinct hierarchies for the slepton sector, which will have an impact regarding the di-lepton mass distributions: (a) $m_{\tilde{\tau}_2} \gtrsim m_{\tilde{\ell}_L}$; (b) $m_{\tilde{\ell}_L} \gtrsim m_{\tilde{\tau}_2}$.

For instance, points P1 and P6-SU1 are examples of (a) while all the others fall in (b). The hierarchy in the right-handed sleptons is always $m_{\tilde{\ell}_R} \gtrsim m_{\tilde{\tau}_1}$, the stau being the NLSP. A common feature to all these proposed points (and an indirect consequence of the “standard window”) is that the correct relic density of the LSP is always obtained from $\tilde{\tau}_1 - \chi_1^0$ co-annihilation, as already noticed in [56, 57, 66]. We also notice that P2 and P6-SU1 lead to a value of $m_h \sim 111$ GeV using the SPHENO code (which is still in agreement with data if one allows for a theoretical error of ± 3 GeV [99]).

Regarding the prospects for production at the LHC, we present in Table 4 the NLO production cross sections in fb (obtained using PROSPINO2.1 [95]) for c.o.m. energies of $\sqrt{s} = 7$ TeV and 14 TeV. We separately display the production of at least one and exactly two χ_2^0 states. For illustrative purposes, we also detail in Table 5 the production cross section for at least one χ_2^0 , identifying the dominant production modes: direct χ_2^0 production, from squark decay, or from $\tilde{g}\tilde{g}$ (see Section 2).

⁴Although the P6-SU1 benchmark point does not fully fulfil the “standard window” requirements, we nevertheless consider it in our analysis, to study the flavour prospects of one of the ATLAS benchmark points.

Point	$m_{\chi_2^0}$	$m_{\chi_1^0}$	$m_{\tilde{\ell}_L}$	$m_{\tilde{\ell}_R}$	$m_{\tilde{\tau}_2}$	$m_{\tilde{\tau}_1}$	$< m_{\tilde{q}} >$	m_h
P1	410	217	374	231	375	224	1064	115.1
P2	356	191	338	212	335	198	963	111.4
P3	342	179	327	218	325	186	877	117.6
P4	938	499	911	653	877	499	2189	121.6
P5-HM1	676	358	595	368	594	360	1641	118.6
P6-SU1	262	140	251	156	254	147	733	111.8

Table 3: Part of the neutralino and slepton spectra for the benchmark points, as well as the average squark mass (in GeV). For completeness we include m_h as obtained from SPHENO.

Point	$\sigma(pp \rightarrow \tilde{\chi}_2^0)$ (fb)		$\sigma(pp \rightarrow \tilde{\chi}_2^0 \tilde{\chi}_2^0)$ (fb)	
	7 TeV	14 TeV	7 TeV	14 TeV
P1	17.5	278.7	1.0	19.1
P2	38.8	513.9	2.2	32.6
P3	60.6	806.9	3.8	52.1
P4	0.04	1.87	~ 0.00	0.13
P5-HM1	0.57	16.50	0.02	1.24
P6-SU1	239.0	2485.8	15.1	158.0

Table 4: Production cross sections for at least one χ_2^0 , $\sigma(pp \rightarrow \tilde{\chi}_2^0)$ (in fb), and exactly two χ_2^0 , $\sigma(pp \rightarrow \tilde{\chi}_2^0 \tilde{\chi}_2^0)$ (in fb), for the benchmark points, with $\sqrt{s} = 7$ TeV and 14 TeV.

Primary prod. mode	\sqrt{s} (TeV)	σ (fb) for the production of at least one $\tilde{\chi}_2^0$					
		P1	P2	P3	P4	P5-HM1	P6-SU1
“Direct” – $\sum_X \tilde{\chi}_2^0 X$	7	11.1	23.1	28.8	0.04	0.53	101.8
	14	69.0	124.4	154.5	1.11	6.50	447.8
“Squarks” – $\sum_Y \tilde{q}_L Y$	7	6.3	15.3	31.0	~ 0.00	0.04	129.6
	14	194.2	356.4	602.5	0.75	9.70	1758.3
$\tilde{g}\tilde{g}$	7	0.1	0.4	0.8	~ 0.00	~ 0.00	7.6
	14	15.5	33.1	49.9	0.01	0.30	279.7

Table 5: Primary production modes and corresponding cross sections for at least one χ_2^0 (in fb) for the benchmark points, for $\sqrt{s} = 7$ TeV and 14 TeV.

Finally, in Table 6 we summarise the information regarding χ_2^0 decays into a di-lepton final state. In each case we present the specific $\text{BR}(\chi_2^0 \rightarrow \tilde{\ell}_X^i \ell_i \rightarrow \ell_i \ell_i)$, corresponding to the contribution of a given intermediate $\tilde{\ell}_X^i$ (X denoting L, R) and the total sum over $\tilde{\ell}_X^i$ states.

The decay chains considered in this study, with charged leptons in the final state and missing energy from the escaping χ_1^0 , ensure that a large signal to background ratio is likely to be obtained. Notice that we will not address background estimation in the present analysis. For the points P5-HM1 and P6-SU1, estimations of the corresponding backgrounds can be found in Refs. [61, 62],

$\ell_i \ell_i$	\tilde{l}_X^i	BR($\chi_2^0 \rightarrow \tilde{l}_X^i l_i \rightarrow l_i l_i \chi_1^0$) (%)					
		P1	P2	P3	P4	P5-HM1	P6-SU1
$\tau\tau$	$\sum_{\tilde{l}}$	15.2	19.2	30.2	1.7	9.4	25.6
	$\tilde{\tau}_2$	7.9	7.6	4.0	1.7	9.4	2.4
	$\tilde{\tau}_1$	7.3	11.6	26.2	—	—	23.2
$\mu\mu$	$\sum_{\tilde{l}}$	12.6	8.7	6.1	3.1	15.2	6.5
	$\tilde{\mu}_L$	12.2	7.3	5.8	3.0	15.1	4.6
	$\tilde{\mu}_R$	0.4	1.4	0.3	0.1	6.5×10^{-2}	1.9
ee	$\sum_{\tilde{l}}$	12.5	8.7	6.0	3.0	15.3	6.5
	\tilde{e}_L	12.2	7.3	5.8	3.0	15.2	4.6
	\tilde{e}_R	0.3	1.4	0.2	3.2×10^{-2}	5.7×10^{-2}	1.9

Table 6: Branching ratios BR($\chi_2^0 \rightarrow \tilde{l}_X^i l_i \rightarrow l_i l_i \chi_1^0$) (in %) for a given di-lepton final state, isolating specific intermediate sleptons and summing over all exchanged (slepton) states.

respectively. Since at least one of the sleptons will always be lighter than the χ_2^0 , the distribution of the di-lepton invariant mass will be (double-) triangular with an endpoint given by Eq. (2.6) of Section 2.

In Figs. 2, we illustrate the di-muon invariant mass ($m_{\mu\mu}$) versus the BR($\chi_2^0 \rightarrow \mu\mu\chi_1^0$) for the mSUGRA points proposed in Table 2. We also display the expected number of events for $\sqrt{s} = 7$ TeV and 14 TeV and corresponding expected integrated luminosities of $\mathcal{L} = 1 \text{ fb}^{-1}$ and $\mathcal{L} = 100 \text{ fb}^{-1}$. In general, in our analysis, we will only study di-muon (di-electron) mass distributions. It is expected that the edges of di-muon mass distributions will be successfully reconstructed to an edge splitting resolution of around 1 GeV [59]. Although di-tau mass distributions are equally rich in the information they might convey on the edges, the experimental reconstruction of the decay chains can be more complicated: if decaying hadronically, the taus can still be identified, but the associated signal is plagued by an important SM background so that the reconstruction of its momentum can be comparatively more difficult.

As expected from the spectrum of the benchmark points (in particular from the slepton hierarchy), points P2, P3 and P6-SU1 have a double triangular distribution for the invariant di-muon mass. This is confirmed by the upper panel of Fig. 2, where two edges are visible in the different distributions, each corresponding to the intermediate left- and right-handed smuons in the chain. We summarise the numerical values of the kinematical edges in Table 7. The lowest edge of P1 (corresponding to $\tilde{\mu}_R$) is hardly visible, while that of P2 appears superimposed on the Z peak. The same distribution shape is present for points P4 and P5-HM1. However, in the latter the lowest edge (around 130 GeV) is almost invisible to the naked eye and the values of the edges $m_{\mu\mu}(\tilde{\mu}_{L,R})$ are in agreement with those obtained using Eq. (2.6).

In all points (upper and lower panels) the Z peak is visible, although in some cases, such as P1 and P5-HM1, the relative height of the peak (as given by the corresponding BR) is very small compared to its width. The peak of the lightest Higgs boson is only visible for some of the points - P2, and P6-SU1 - since for the others the width is tiny when compared to the corresponding height. In general, the expected number of events renders these processes visible only for a high centre of mass energy (i.e. $\sqrt{s} \approx 14$ TeV), as can be seen from the secondary y-axes on the right. Notice, however, that a proper study of the background has to be taken into account.

Although we will not display it here, a comparison of di-electron and di-muon distributions for different benchmark points would confirm the superposition of the kinematical edges of both

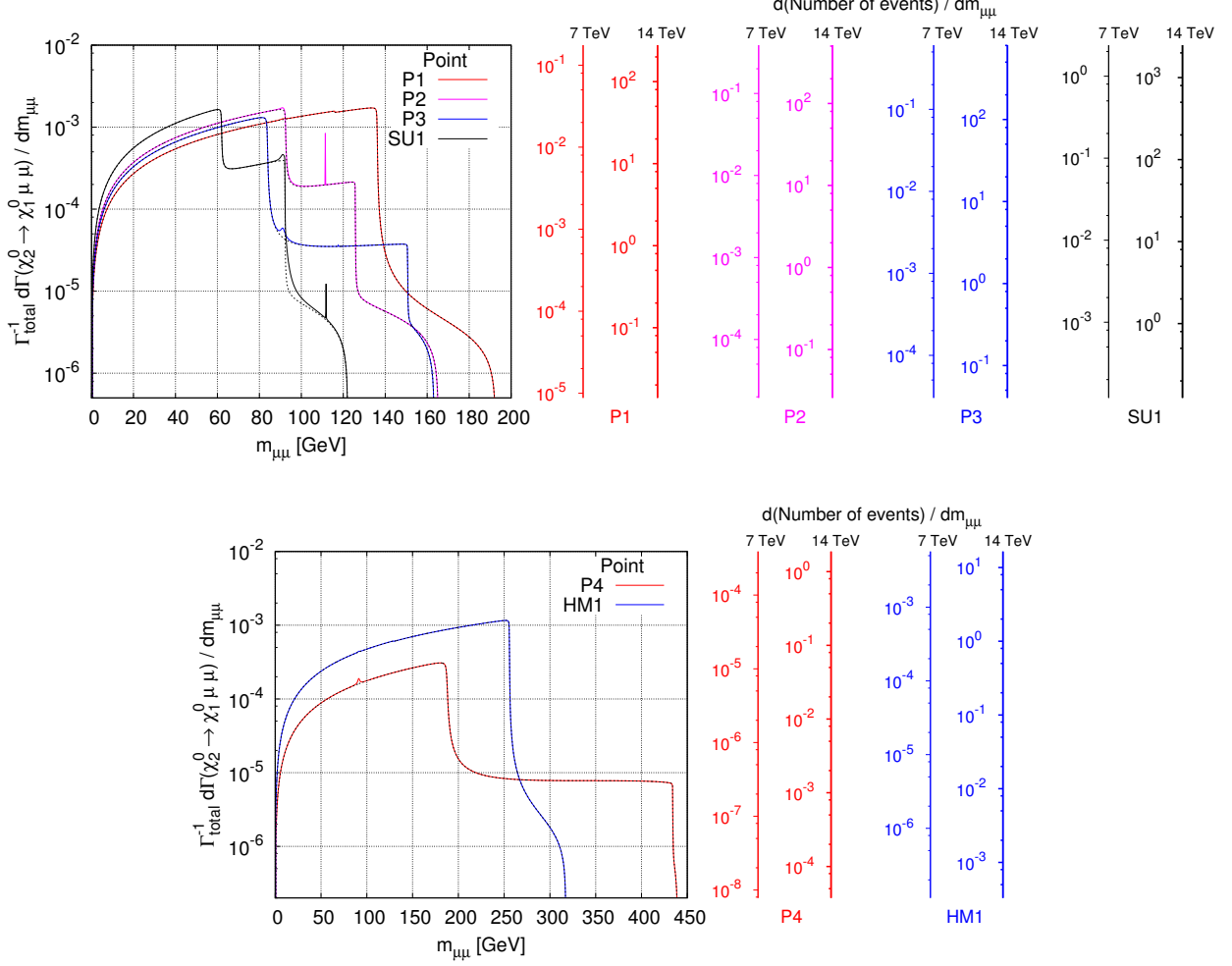


Figure 2: Di-lepton invariant mass ($m_{\mu\mu}$) versus $\text{BR}(\chi_2^0 \rightarrow \mu\mu\chi_1^0)$ for the benchmark points (Table 2). Upper panel: P1 (red), P2 (magenta), P3 (blue) and P6-SU1 (black); lower panel: P4 (red) and P5-HM1 (blue). Secondary-right y-axes denote the corresponding expected number of events for $\sqrt{s} = 7$ TeV and 14 TeV, with $\mathcal{L} = 1 \text{ fb}^{-1}$ and $\mathcal{L} = 100 \text{ fb}^{-1}$, respectively.

distributions - see exact values in Table 7 -, the only significant difference between them being the disappearance of the Higgs boson peaks.

5.2 Slepton mass splittings and $\text{BR}(\chi_2^0 \rightarrow \chi_1^0 l_i l_i)$ in the cMSSM

As mentioned in Section 2, one expects that the LHC will measure the kinematical edges of the di-lepton distributions with a precision of $\mathcal{O}(0.1\%)$. Although it has been claimed [68] that a $\tilde{e} - \tilde{\mu}$ relative mass difference as small as 10^{-4} could be measurable, in the discussion of our numerical results we will always adopt a conservative view, assuming maximal sensitivities of $\mathcal{O}(0.1\%)$ for $\Delta m_{\tilde{e}}/m_{\tilde{e}}(\tilde{e}, \tilde{\mu})$ and $\mathcal{O}(1\%)$ for $\Delta m_{\tilde{e}}/m_{\tilde{e}}(\tilde{\mu}, \tilde{\tau})$.

We begin the numerical analysis of slepton mass splittings by a brief overview of the cMSSM case (no flavour mixing in the lepton and slepton sectors).

\tilde{l}_X	$m_{ll}(\tilde{l}_X)$ (GeV)					
	P1	P2	P3	P4	P5-HM1	P6-SU1
\tilde{e}_R	116.1	125.9	150.8	434.3	129.2	92.3
\tilde{e}_L	136.2	92.5	83.8	187.2	255.7	62.0
$\tilde{\mu}_R$	116.0	125.7	150.7	434.2	129.0	92.2
$\tilde{\mu}_L$	136.2	92.5	83.8	187.5	255.7	62.0
$\tilde{\tau}_1$	82.6	77.5	78.4	16.2	56.0	67.7
$\tilde{\tau}_2$	134.4	98.0	87.9	274.4	256.4	54.2

Table 7: $m_{ll}(\tilde{l}_X)$ (GeV) where l is any of the charged leptons and X stands for left- and right-handed sleptons (all families).

In Fig. 3 we display the correlation between the BR of the neutralino cascade decay, $\text{BR}(\chi_2^0 \rightarrow \tilde{\ell}_{L,R} \ell \rightarrow \chi_1^0 \ell \ell)$ and the different slepton mass differences. In particular, we present the numerical results for the mass splittings $\tilde{e}_{L,R} - \tilde{\mu}_{L,R}$ and $\tilde{\mu}_{L,R} - \tilde{\tau}_{2,1}$, where the heaviest/lightest staus are dominated by the left-/right-handed component. Here, as throughout the remaining analysis, we normalise the slepton mass splittings to the corresponding average slepton masses (cf. Eq. (2.8)). Fixing $\tan \beta = 10$ and taking $\mu > 0$, we have scanned the remaining mSUGRA parameters as follows: $300 \text{ GeV} \leq M_{1/2} \leq 1.2 \text{ TeV}$, $-1 \text{ TeV} \leq A_0 \leq 1 \text{ TeV}$, m_0 being determined in each point by the requirements of a “standard window” (leading to $50 \text{ GeV} \lesssim m_0 \lesssim 550 \text{ GeV}$). In this case, and for simplicity, we have relaxed the requirement of compatibility with the WMAP bound of Eq. (5.1). To illustrate the mass splittings associated with the proposed benchmark points (see Table 2), we superimpose the corresponding predictions on the different panels.

As stated in Section 4, in the absence of flavour violation, the mass degeneracy between the first two slepton families is only lifted by tiny RGE-running and LR mixing effects. Since both are proportional to the corresponding Yukawa couplings, the $\tilde{e}_{L,R} - \tilde{\mu}_{L,R}$ mass differences are expected to be very small (see Eq. (4.1)). This can be observed in Fig. 3, where one confirms that both $\Delta m_{\tilde{\ell}}/m_{\tilde{\ell}}(\tilde{e}_L, \tilde{\mu}_L)$ and $\Delta m_{\tilde{\ell}}/m_{\tilde{\ell}}(\tilde{e}_R, \tilde{\mu}_R)$ lie in the range $10^{-7} - 10^{-3}$. Both LR mixing and RGE-induced effects are more important for the stau sector, so that the splittings $\Delta m_{\tilde{\ell}}/m_{\tilde{\ell}}(\tilde{\ell}_L, \tilde{\tau}_2)$ and $\Delta m_{\tilde{\ell}}/m_{\tilde{\ell}}(\tilde{\ell}_R, \tilde{\tau}_1)$ are somewhat larger, typically above 10^{-3} . Mass splittings involving third generation sleptons strongly depend on $\tan \beta$: as an example, for $\tan \beta = 40$, with A_0 being varied as in Figs. 3 and $m_0, M_{1/2}$ randomly varied as to fulfil the standard window requirement – which for this strong $\tan \beta$ regime corresponds to $900 \text{ GeV} \leq M_{1/2} \leq 2 \text{ TeV}$, and $380 \text{ GeV} \lesssim m_0 \lesssim 1 \text{ TeV}$ –, we find $3\% \leq \frac{\Delta m_{\tilde{\ell}}}{m_{\tilde{\ell}}}(\tilde{\mu}_L, \tilde{\tau}_2) \leq 6.5\%$, as can be read from the right panel of Fig. 4. Nevertheless, it should be stressed that increasing $\tan \beta$ (both in the cMSSM and in its right-handed neutrino extensions) lowers the lightest stau mass, so that in the large $\tan \beta$ regime χ_2^0 predominantly decays via an intermediated $\tilde{\tau}_1$ ($\sim \tilde{\tau}_R$), with $\text{BR}(\chi_2^0 \rightarrow \tilde{\tau}_R \tau) \sim 1$. Fig. 3 also summarises the prospects of the different benchmark points regarding production at the LHC (notice that since the spectrum of P5-HM1 kinematically forbids $\tilde{\tau}_1 \rightarrow \chi_1^0 \tau$ decays, this point is absent from the lower right panel).

From the comparison of each of the upper panels of Figs. 3 to the corresponding lower one, it can also be observed that in the cMSSM the ratio of the $\tilde{\mu} - \tilde{\tau}$ and $\tilde{e} - \tilde{\mu}$ mass splittings indeed goes as $\Delta m(\tilde{\mu}_{L,R}, \tilde{\tau}_{2,1})/\Delta m(\tilde{e}_{L,R}, \tilde{\mu}_{L,R}) \sim (m_\tau^2/m_\mu^2)$ (see Eq. (4.2)). This can be further confirmed in Figs. 4, where we display $\tilde{\mu}_L - \tilde{\tau}_2$ versus $\tilde{e}_L - \tilde{\mu}_L$ mass differences for two values of $\tan \beta$. The full line denotes the m_τ^2/m_μ^2 slope. For larger $\tan \beta$ (as displayed on the right panel of Fig. 4)

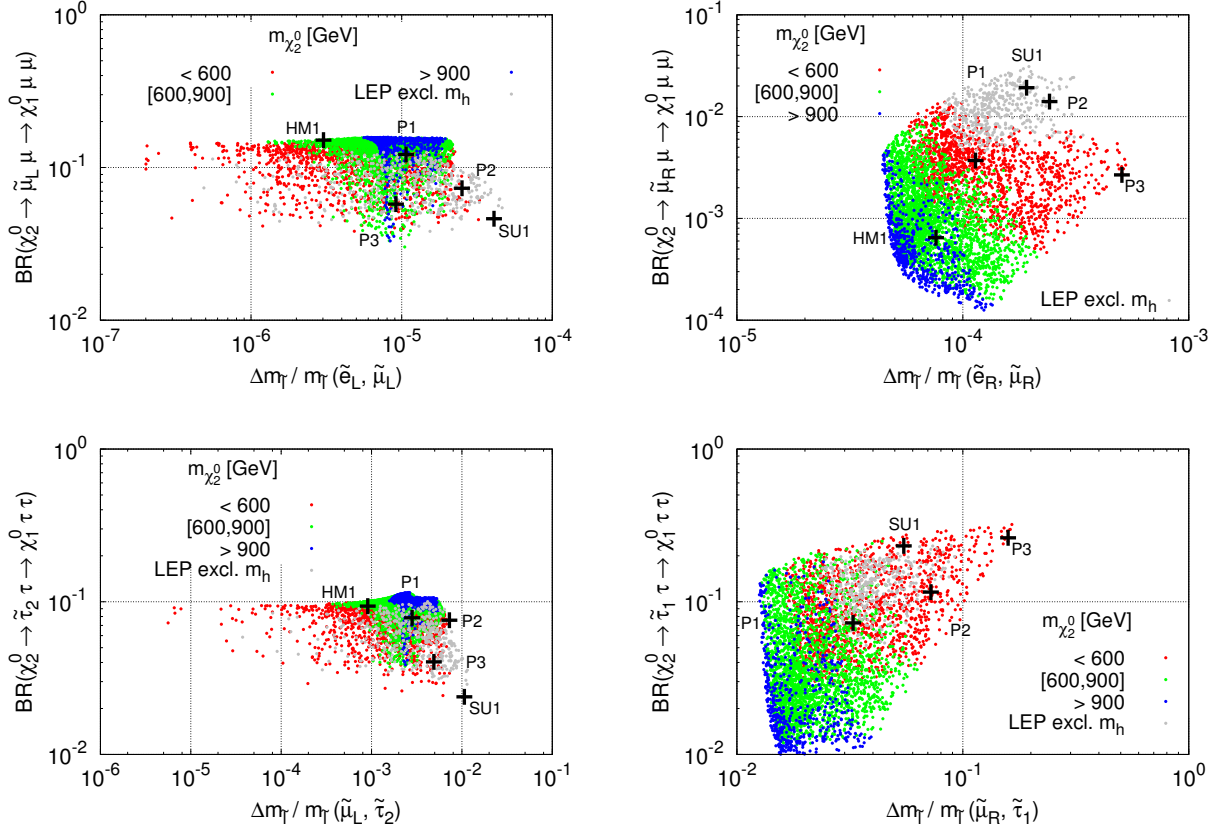


Figure 3: $\text{BR}(\chi_2^0 \rightarrow \tilde{l}_{L,R} l_i \rightarrow \chi_1^0 l_i l_i)$ as a function of $\Delta m_{\tilde{l}}/m_{\tilde{l}}$ for the cMSSM. Upper panels: $\Delta m_{\tilde{l}}/m_{\tilde{l}}(\tilde{e}_{L,R}, \tilde{\mu}_{L,R})$; lower panels: $\Delta m_{\tilde{l}}/m_{\tilde{l}}(\tilde{\mu}_{L,R}, \tilde{\tau}_{2,1})$. We take $\tan\beta = 10$, $\mu > 0$, and scan over $-1 \text{ TeV} \leq A_0 \leq 1 \text{ TeV}$, $300 \text{ GeV} \leq M_{1/2} \leq 1.2 \text{ TeV}$, m_0 determined as to account for the “standard window” ($50 \text{ GeV} \lesssim m_0 \lesssim 550 \text{ GeV}$). The different coloured regions illustrate regimes for the decaying neutralino mass. Gray points correspond to cases in which $m_h \lesssim 114 \text{ GeV}$. Crosses denote some of the benchmark points defined in Table 2.

the increased LR mixing effects for the staus induce a deviation to the simple approximation of Eq. (4.2).

In Figs. 5, we display a comprehensive scan of the $\tilde{\mu}_L - \tilde{\tau}_2$ mass difference in the cMSSM (the corresponding predictions for $\tilde{e}_L - \tilde{\mu}_L$ can be inferred from the previous discussion of Fig. 4). For three different values of the trilinear soft term ($A_0 = -1, 0, 1 \text{ TeV}$), we scan the mSUGRA parameter space to ensure an optimal survey of the volumes complying with the “standard window” requirement. We present the resulting mass splitting (in percentage) as a function of $\tan\beta$, identifying also distinct regimes for the χ_2^0 mass (and hence $M_{1/2}$, implicitly understood from the GUT relation $m_{\chi_2^0} \approx 0.8M_{1/2}$). For completeness, we also display regions corresponding to a relaxation of the energy of the outgoing leptons ($0 < m_{\chi_2^0} - m_{\tilde{l}_{L,R}} < 10 \text{ GeV}$). Finally, we provide complementary information about the corresponding ranges for the lightest Higgs boson mass, which can severely constrain the explored parameter space, especially in the low $\tan\beta$ and $A_0 \gtrsim 0$ regimes.

The most important conclusion to be drawn from Fig. 5 is that in the cMSSM $\tilde{\mu}_L - \tilde{\tau}_2$ mass

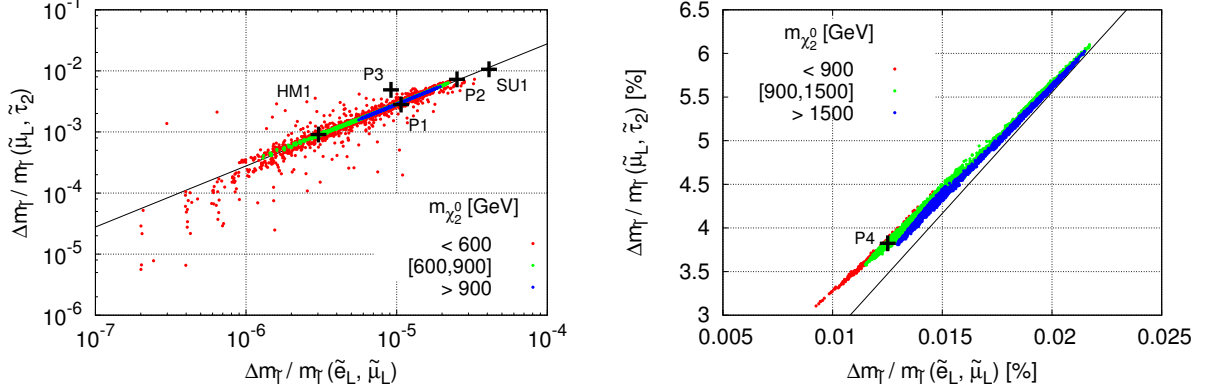


Figure 4: Mass differences $\tilde{\mu}_L - \tilde{\tau}_2$ versus $\tilde{e}_L - \tilde{\mu}_L$ (both normalised to an average slepton mass) for the cMSSM. On the left $\tan\beta = 10$, while on the right $\tan\beta = 40$ (notice that in this case the mass differences are given in %). In the left panel, scan and colour code as in Fig. 3, while in the right panel ($\tan\beta = 40$) we scan over $900 \text{ GeV} \leq M_{1/2} \leq 2 \text{ TeV}$ with m_0 determined as to account for the “standard window” ($380 \text{ GeV} \lesssim m_0 \lesssim 1 \text{ TeV}$), and A_0 varied as in Fig. 3. Crosses denote some of the benchmark points defined in Table 2.

splittings are at most $\mathcal{O}(7\%)$ (if $|A_0| \lesssim 1 \text{ TeV}$), and this occurs for regimes of very large $\tan\beta$. With increasing $\tan\beta$, the lowest vertex of the region complying with the “standard window” constraints is pushed towards larger values of both m_0 and $M_{1/2}$ (as can be seen from the displacement of the triangular-shape central regions in Figs. 1). This in turn implies that regions in mSUGRA parameter space associated with the largest values of the $\tilde{\mu}_L - \tilde{\tau}_2$ mass splittings will have poor prospects for production at the LHC (smaller cross sections), rendering them likely unobservable.

For intermediate regimes of $\tan\beta$, one expects $\Delta m_{\tilde{\ell}}/m_{\tilde{\ell}}(\tilde{\mu}_L, \tilde{\tau}_2)$ to lie in the range 2% - 5%, the latter corresponding to large (and negative) A_0 . This A_0 regime increases LR mixing in the stau sector, thus augmenting the cMSSM mass difference between the left-handed smuons and the heaviest (dominantly left-handed) stau.

Following the discussion of Section 4 concerning the correct definition of mass splittings for QDFC sleptons, we present here the “effective” (according to Eqs. (4.9, 4.10)) and “real” $\tilde{e}_L - \tilde{\mu}_L$ mass differences. Since in the cMSSM the sleptons have a well-defined flavour content, “real” and “effective” approaches coincide to a very good extent as can be seen from Fig. 6. Hereafter, and when addressing seesaw-induced slepton flavour mixings, we will always use the “effective” mass splitting for the first two slepton generations.

5.3 Slepton mass splittings in the type-I SUSY seesaw

As seen in the previous subsection, in the absence of flavour violation in the lepton sector, the mass splittings between the sleptons of the first two families are extremely small. The situation changes if interactions that violate lepton flavour are switched on: either schemes where the SUSY-breaking parameters for the sleptons are flavour violating (or at least non-universal) or mechanisms that account for both neutrino masses and lepton mixings, could induce significantly larger slepton mass splittings, large enough to be observed at the LHC. If flavour violating interactions in the slepton sector are indeed present, then other LFV processes are likely to occur: in addition to radiative and three body decays, lepton flavour can also be directly violated in sparticle decays,

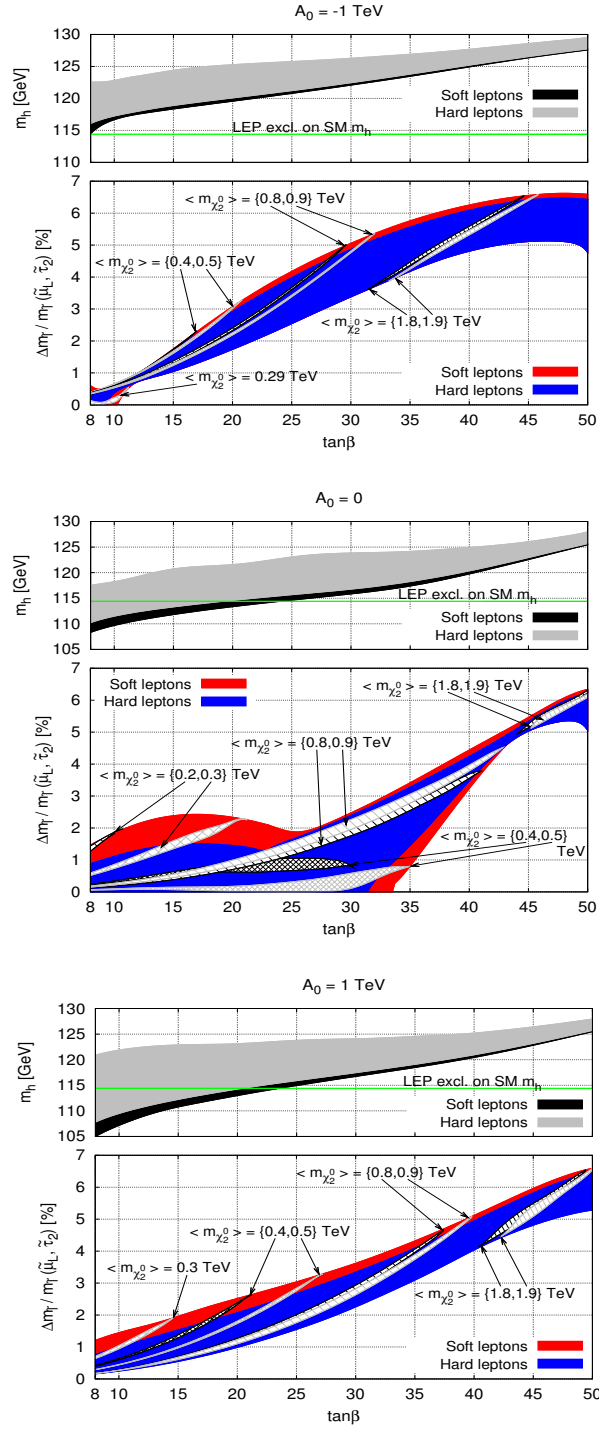


Figure 5: Mass difference $\tilde{\mu}_L - \tilde{\tau}_2$ (normalised to the average $\tilde{\mu}_L, \tilde{\tau}_2$ masses) in the cMSSM as a function of $\tan\beta$, for different values of A_0 (from top to bottom, $A_0 = -1, 0, 1$ TeV). The subplots above each panel denote the corresponding variation of m_h . The different solid regions correspond to hard (blue, gray) or soft (red, black) leptons in the final state. Inset are bands corresponding to different regimes for $m_{\chi_2^0}$ (in TeV).

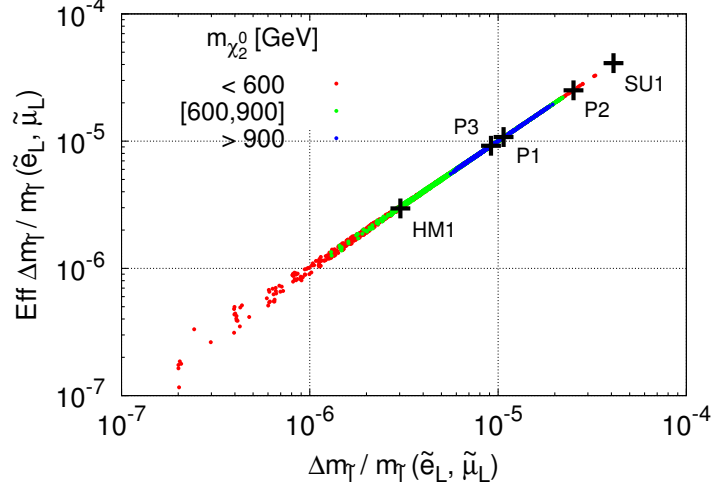


Figure 6: “Effective” parametrization of $\tilde{e}_L - \tilde{\mu}_L$ mass difference versus the “real” $\tilde{e}_L - \tilde{\mu}_L$ mass difference. Scan and colour code as in Fig. 3 (taking $\tan \beta = 10$). Crosses denote some of the benchmark points defined in Table 2.

e.g. $\chi_2^0 \rightarrow \tilde{\ell}_i \ell_j$.

Recent studies [66] have addressed the complementarity of high- and low-energy LFV adopting an effective approach. Here we will consider the framework of the type-I SUSY seesaw, studying the implications of having a unique source of flavour violation: the neutrino Yukawa couplings. Parametrizing Y^ν according to Eq. (3.13), flavour violation can arise both from the observed low-energy neutrino mixing pattern, or from mixings involving the (heavy) right-handed neutrino sector. Even though very little data is available to efficiently constrain each Y_{ij}^ν , there are several experimental bounds and theoretical arguments that should be taken into consideration:

- data on light neutrino mass-squared differences and leptonic mixing angles (cf. Eqs. (3.11, 3.12));
- bounds on LFV BRs and CRs (see Table 1), as well as lepton EDMs;
- perturbativity of the Yukawa couplings, $|Y_{ij}^\nu|^2 < 4\pi$;
- under the hypothesis that the BAU is explained via a mechanism of thermal leptogenesis, the requirement of a sufficiently large CP asymmetry (while avoiding the gravitino problem) leads to bounds on M_{N_1} and to constraints on combinations of the complex R matrix angles θ_i .

Aside from the perturbativity bounds, the most important constraints on the seesaw parameters will arise from the non-observation of LFV processes: since both flavour violating BRs and slepton mass splittings originate from the same unique source (Y^ν), compatibility with current bounds, in particular on $\text{BR}(\mu \rightarrow e\gamma)$ and $\text{BR}(\tau \rightarrow \mu\gamma)$, may preclude sizable values for the slepton mass splittings. This is in contrast with other scenarios of (effective) flavour violation in the slepton sector [66].

We begin by considering a minimal implementation of the SUSY seesaw, where flavour violation arises solely from the U^{MNS} mixing angles. This corresponds to taking $R = 1$ (i.e. $\theta_i = 0$) in the

Casas-Ibarra parametrization of Eq. (3.13), and translates into a “conservative” limit for flavour violation: apart from possible cancellations, and for a fixed seesaw scale (i.e. M_N), this limit provides in general a lower bound for the amount of LFV. (Notice however that leptogenesis is not viable in this case.) In the subsequent numerical analysis we will consider first strict normal hierarchies for both heavy and light neutrinos, commenting at a later stage on the effect of different mass schemes.

As can be inferred from the analytical discussion in Section 4 (based on the LLog approximation), $\Delta m_{\tilde{\ell}}/m_{\tilde{\ell}}$ are strongly dependent on the RH neutrino mass scale, M_N . In the limit $R = 1$, the overall magnitude of the flavour violating entries is dominantly driven by M_{N_3} (see Eq. (4.7)).

We begin by revisiting the correlation between the $\tilde{\mu}_L - \tilde{\tau}_2$ and $\tilde{e}_L - \tilde{\mu}_L$ slepton mass splittings. We conduct a similar scan over the mSUGRA parameters as in the previous subsections (see discussion leading to Fig. 3), considering a regime of low $\tan \beta = 10$, but now requiring compatibility with the WMAP bound on Ωh^2 (cf. Eq (5.1)). Here we take very small values of the reactor angle θ_{13} , also setting the CPV Dirac phase $\delta = 0$. The impact of θ_{13} will be addressed at a later stage.

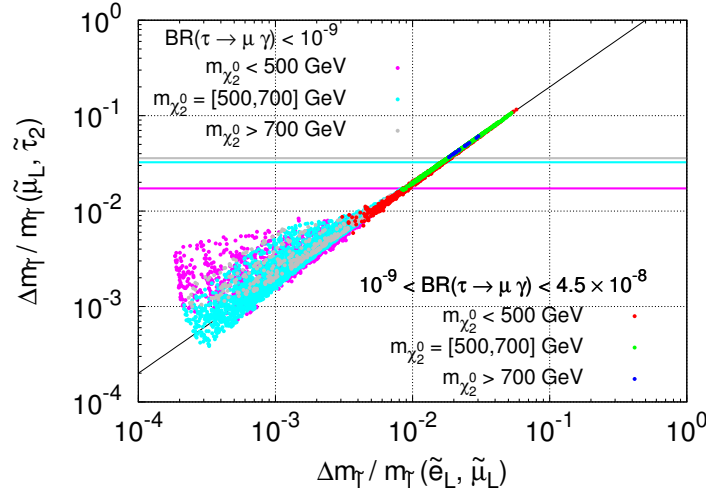


Figure 7: Mass differences $\tilde{\mu}_L - \tilde{\tau}_2$ versus $\tilde{e}_L - \tilde{\mu}_L$ (both normalised to an average slepton mass) in the type-I SUSY seesaw. Leading to the scan, we set $\tan \beta = 10$, and randomly vary the remaining mSUGRA parameters (with $|A_0| \lesssim 1$ TeV, satisfying the “standard window” constraint and requiring consistency with the dark matter and Higgs boson mass bounds). For the seesaw parameters we have taken $R = 1$, $\theta_{13} = 0.1^\circ$ (with $\delta = \varphi_{1,2} = 0$), and $M_{N_1} = 10^{10}$ GeV, $M_{N_2} = 10^{11}$ GeV, varying $10^{13} \lesssim M_{N_3} \lesssim 10^{15}$ GeV. All points shown comply with present bounds on LFV observables. We highlight in a different colour scheme points whose associated prediction for $\text{BR}(\tau \rightarrow \mu \gamma)$ lies in the interval delimited by current experimental bounds and future sensitivities (red, green, blue), corresponding to $m_{\chi_2^0}$ regimes. The magenta / cyan / gray lines denote the maximal value of $\Delta m_{\tilde{\ell}}/m_{\tilde{\ell}}(\tilde{\mu}_L, \tilde{\tau}_2)$ attainable for the magenta / cyan / gray points.

The effect of implementing a type-I seesaw for the slepton mass splittings is clearly visible in Fig. 7. It becomes even more striking noticing that this is the $R = 1$ seesaw version of the cMSSM case shown in the left panel of Fig. 4. Firstly, one observes that both $\tilde{\mu}_L - \tilde{\tau}_2$ and $\tilde{e}_L - \tilde{\mu}_L$ mass splittings become much larger, with values respectively up to 10% and 6%, well within the sensitivity range of the LHC. Recall that in the cMSSM case one typically had values $\mathcal{O}(10^{-3}, 10^{-5})$.

Furthermore, notice that the points whose $\text{BR}(\tau \rightarrow \mu\gamma)$ is in the sensitivity range of future experiments are in general associated to observable $\Delta m_{\tilde{\ell}}/m_{\tilde{\ell}}$, especially for $m_{\chi_2^0} > 500$ GeV. (The maximum value of the $\tilde{\mu}_L - \tilde{\tau}_2$ splitting for points whose $\text{BR}(\tau \rightarrow \mu\gamma)$ lies beyond experimental capabilities is marked by horizontal lines, with a colour code matching the corresponding spectrum colour code.) One can also observe an important deviation from the correlated behaviour of both mass splittings (see Eq. (4.6)), symbolically depicted by the full dark line, with a slope given by $|m_{\tilde{\mu}_L} - m_{\tilde{\tau}_2}|/|m_{\tilde{e}_L} - m_{\tilde{\mu}_L}| \approx 2$. This deviation towards the pure mSUGRA limit of $m_{\tilde{\tau}}^2/m_{\tilde{\mu}}^2$ (see Eq. (4.2)) occurs especially for points associated to both smaller mass splittings and smaller $\text{BR}(\tau \rightarrow \mu\gamma)$, starting at an intermediate seesaw scale of about $M_{N_3} \lesssim 2 \times 10^{13}$ GeV for small $|A_0|$ and approaching the mSUGRA limit for $M_{N_3} \lesssim 10^{10}$ GeV. For these regions in parameter space, even for comparatively smaller flavour violating entries, the seesaw induces corrections to flavour conserving LR terms, which in turn imply larger $\tilde{\mu}_L - \tilde{\tau}_2$ splitting when compared to $\tilde{e}_L - \tilde{\mu}_L$.

In Figs. 8 we display the variation of $\tilde{e}_L - \tilde{\mu}_L$ and $\tilde{\mu}_L - \tilde{\tau}_2$ mass differences as a function of A_0 , showing also the comparison with the cMSSM case. First of all, notice that both mass splittings are substantially larger, and for most of the A_0 interval considered, well within the expected sensitivity of the LHC. Recall however that the overall enhancement in $\Delta m_{\tilde{\ell}}/m_{\tilde{\ell}}$ is a consequence of having taken very large values of M_{N_3} , close to the perturbativity limit of the neutrino Yukawa couplings (especially Y_{32}^ν and Y_{33}^ν). Nevertheless, the rôle of A_0 in the SUSY seesaw is clearly manifest in Figs. 8, and especially in the comparison of the former with the $\tan\beta = 10$ band of Figs. 5 (where discrete values of A_0 were taken). While in the cMSSM the effect of A_0 was manifest through LR mixing (and via m_h constraints on the parameter space), in the seesaw case the dominant impact of A_0 on the mass splittings occurs via the RGE-induced contributions to the LL block (and LR , to a smaller extent) of the slepton mass matrix, as given in Eqs. (3.19). In other words, the dominant contribution to $\Delta m_{\tilde{\ell}}/m_{\tilde{\ell}}$ now clearly arises from the second term on the right-hand side of Eq. (4.3). This is substantiated by the approximate symmetric dependence of $\Delta m_{\tilde{\ell}}/m_{\tilde{\ell}}$ on A_0 . As expected, the regions of large positive A_0 (where small LR mixing effects in the squark sector reduce the supersymmetric radiative contributions to the Higgs boson mass) are disfavoured due to conflict with the LEP bounds on m_h . For very large negative values of A_0 , the RGE-induced amount of flavour violation is such that points associated with the largest mass splittings have corresponding predictions to $\text{BR}(\tau \rightarrow \mu\gamma)$ already excluded by experiment.

In Fig. 8 (as in all seesaw cases), we have displayed the “effective” $\tilde{e}_L - \tilde{\mu}_L$ mass difference, as justified by the discussion in Section 4. We recall that for the cMSSM, and as emphasised by Fig. 6, both approaches coincided. However when FV interactions are switched on, one should use the “effective” mass splitting. This can be confirmed in Fig. 9, where we compare “real” and “effective” $\Delta m_{\tilde{\ell}}/m_{\tilde{\ell}}$ as a function of A_0 . Leading to this figure, we have chosen the mSUGRA point P1, and allowed for variations of the trilinear coupling, $|A_0| \leq 1.2$ TeV (recall that for P1, $A_0 = 0$). Regarding the seesaw parameters, we have taken $R = 1$, $\theta_{13} = 0.1^\circ$, and considered three distinct right-handed neutrino spectra for illustrative purposes.

For a comparatively light seesaw scale (i.e. $M_{N_3} \sim \mathcal{O}(10^{13})$ GeV) minimising the amount of flavour violation, and small $|A_0|$, which minimises (diagonal) non-universality effects for the first two generations (see Eqs. (3.17, 3.18)), one verifies that both approaches nearly coincide. As the seesaw effects become more important, and flavour mixing increases, one clearly verifies that “effective” mass difference provides the phenomenologically reliable $\tilde{e}_L - \tilde{\mu}_L$ splittings.

Notice that the ratio “effective”/“real” mass splitting is always $\gtrsim 1/2$. For small values of $|A_0|$ and/or low seesaw scales we have a ratio of ~ 1 . For increasing $|A_0|$, approaching the turning point $m_{\tilde{\tau}_2} > m_{\tilde{\mu}_L} \rightarrow m_{\tilde{\tau}_2} < m_{\tilde{\mu}_L}$ the “effective”/“real” mass splitting ratio approaches the $\sim 1/2$ limit (this also implies that, in this region in parameter space, taking the “real” splitting could lead to

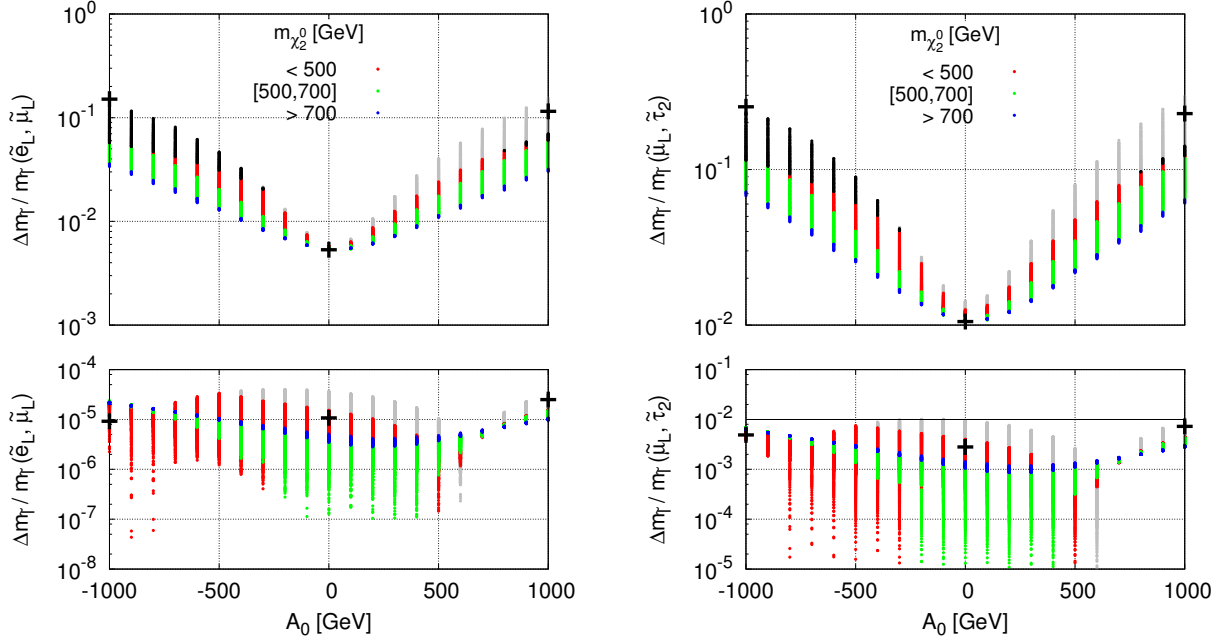


Figure 8: Mass differences $\tilde{e}_L - \tilde{\mu}_L$ (on the left) and $\tilde{\mu}_L - \tilde{\tau}_2$ (on the right) as a function of A_0 (in GeV). We have taken $\tan\beta = 10$, and scanned over m_0 and $M_{1/2}$ as satisfy the “standard window” and the dark matter constraints. The seesaw parameters have been set as $R = 1$, $\theta_{13} = 0.1^\circ$ (with $\delta = \varphi_{1,2} = 0$), and $M_{N_i} = \{10^{10}, 10^{11}, 10^{15}\}$ GeV. The colour code denotes different ranges for $m_{\chi_2^0}$ (black points denote violation of at least one experimental bound - in these cases $\text{BR}(\tau \rightarrow \mu\gamma)$ -, while gray correspond to $m_h < 114$ GeV). Crosses denote the benchmark points P1, P2 and P3 as defined in Table 2. The lower panels illustrate the corresponding cMSSM study (same mSUGRA parameters, with $Y_{ij}^\nu = 0$).

a considerable overestimation of $\Delta m_{\tilde{e}}/m_{\tilde{e}}$. For even higher values of $|A_0|$ and high seesaw scales the “effective”/“real” mass splitting ratio can be greater than 1 order of magnitude, however this typically corresponds to scenarios excluded by current bounds on LFV observables.

To better illustrate the evolution of the flavour content of a given slepton eigenstate in the presence of the seesaw (even for the conservative $R = 1$ case), we display on the left panel of Fig. 10 a simultaneous analysis of the variation of the flavour content of a slepton mass eigenstate, in particular of the τ/μ flavour ratio of the $\tilde{\mu}_L$ mass eigenstate as a function of M_{N_3} . We present this for the different mSUGRA points also showing the evolution of Y_{32}^ν on the upper axis.

For very low seesaw scales (i.e. $M_{N_3} \sim 10^{11}$ GeV), flavour and mass eigenstates coincide to a very good approximation. As M_{N_3} increases, and especially for points like P2 and P3 with large $|A_0|$ (enhancing the seesaw effects, see Eq. (4.7)) or points like P5-HM1 with $\left| (m_L^2)_{23} / [(m_L^2)_{33} - (m_L^2)_{22} + \delta_{LR}] \right| \gg 1$,

$$\delta_{LR} = m_\tau^2 \frac{(A_0 - \mu \tan\beta)^2}{(m_L^2)_{33} - (m_E^2)_{33} + M_Z^2 \cos 2\beta (-1/2 + 2 \sin^2 \theta_W)}, \quad (5.2)$$

i.e., with a resonant-type enhancement, $\mu - \tau$ mixing becomes maximal, and we are in the presence of truly QDFC sleptons. This is confirmed by the lower left panel.

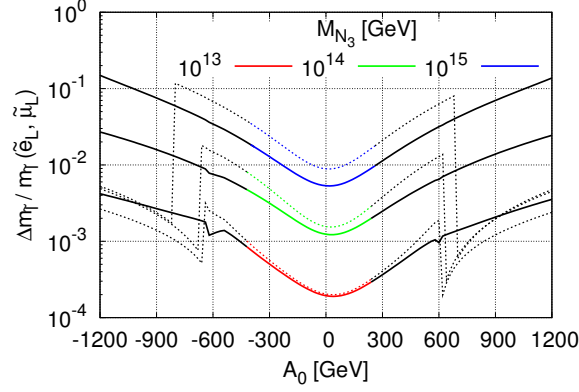


Figure 9: Comparison between “real” (dashed lines) and “effective” (full) slepton mass differences ($\tilde{e}_L - \tilde{\mu}_L$), normalised to the average $\tilde{e}_L, \tilde{\mu}_L$ mass, as a function of A_0 (in GeV). We have considered $R = 1$, $\theta_{13} = 0.1^\circ$, $M_{N_1} = 10^{10}$ GeV, $M_{N_2} = 10^{11}$ GeV, taking three distinct values for $M_{N_3} = 10^{13}$ GeV (red), $M_{N_3} = 10^{14}$ GeV (green) and $M_{N_3} = 10^{15}$ GeV (blue). The mSUGRA parameters have been set as for point P1 (except for $|A_0| \leq 1.2$ TeV). Black lines denote points excluded due to the violation of at least one experimental and/or observational constraint.

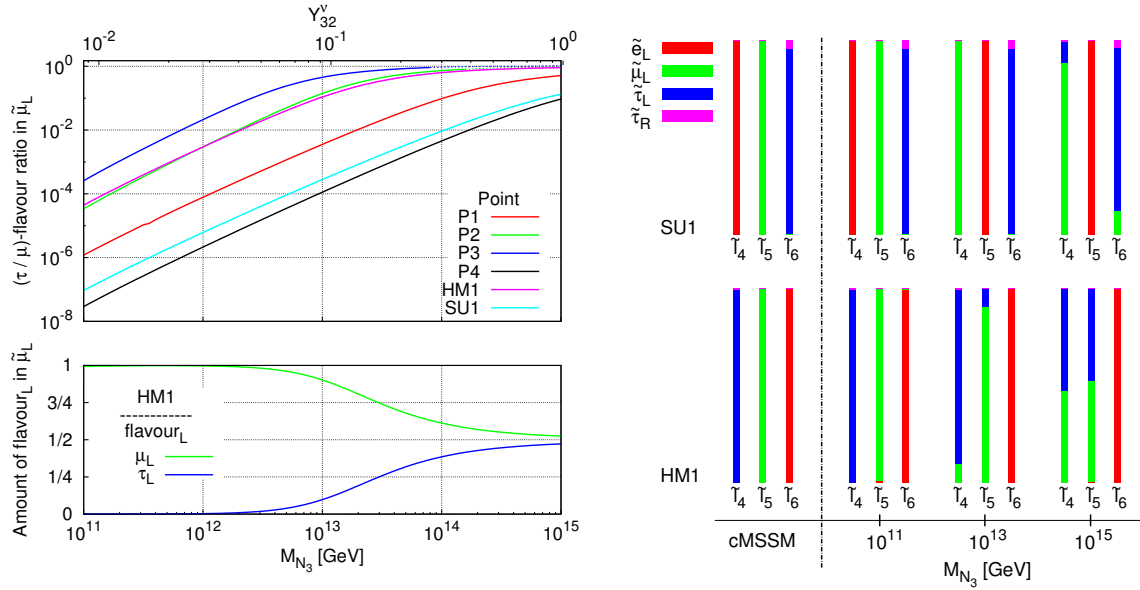


Figure 10: On the left, τ/μ flavour ratio in $\tilde{\mu}_L$ mass eigenstate as a function of M_{N_3} (in GeV). For the mSUGRA benchmark points of Table 2, we set $R = 1$, $\theta_{13} = 0.1^\circ$ (with $\delta = \varphi_{1,2} = 0$), and take $M_{N_1} = 10^{10}$ GeV, $M_{N_2} = 10^{11}$ GeV. On the upper axis we display the values of Y_{32}^ν . The secondary panel illustrates $|R_{5\mu_L}^{\tilde{L}}|^2$ and $|R_{5\tau_L}^{\tilde{L}}|^2$ for the same M_{N_3} interval. On the right we depict the flavour content of the 3 heavier mass eigenstates: red - \tilde{e}_L , green - $\tilde{\mu}_L$, blue (magenta) - $\tilde{\tau}_{L(R)}$, for P5-HM1 and P6-SU1, illustrating both the cMSSM case (on the far left) and the type-I seesaw, for three values of M_{N_3} (with the remaining seesaw parameters as before).

On the right panel of Fig. 10, we symbolically represent (not to scale) the flavour composition of the three heaviest mass eigenstates for the points P5-HM1 and P6-SU1, both for the cMSSM and distinct seesaw scales. Notice that in the cMSSM limit the slepton hierarchy is quite different in each case. For P6-SU1, the seesaw immediately induces an overcross of the $\tilde{e} - \tilde{\mu}$ eigenstates (no mixing involved); only for very large M_{N_3} does one observe a small mixing of the $\tilde{\mu}_L - \tilde{\tau}_L$ components.

As expected from the left panel of Fig. 10, large mixings occur for a much lower seesaw scale in the case of P5-HM1, with a nearly maximal mixing for $M_{N_3} \sim 10^{15}$ GeV. This further provides an excellent illustration of a configuration with QDFC sleptons.

One of the (perhaps) most illustrative ways of exploring the impact of a type-I SUSY seesaw is to consider the correlated behaviour of mass splittings and flavour-violating decays. In Figs. 11, we present the $\tilde{e}_L - \tilde{\mu}_L$ and $\tilde{\mu}_L - \tilde{\tau}_2$ mass differences versus $\text{BR}(\tau \rightarrow \mu\gamma)$ and $\text{BR}(\mu \rightarrow e\gamma)$ (providing in this case additional information on the $\text{CR}(\mu - e, \text{Ti})$). The data displayed in these figures corresponds to $\tan\beta = 10$, with the remaining mSUGRA parameters being randomly varied ($|A_0| \lesssim 1$ TeV), satisfying the “standard window” and requiring consistency with the dark matter and Higgs boson mass bounds.

We have taken values of the right-handed neutrino spectrum (especially of M_{N_3}) to ensure that mass splittings are within experimental sensitivity range, and that one avoids conflicts with low-energy flavour bounds (which would exclude most of the points).

One of the most interesting results of Figs. 11 consists in the fact that almost the entire region in parameter space associated with a $\tilde{e}_L - \tilde{\mu}_L$ mass splitting $\sim \mathcal{O}(1\%)$ is also within the future sensitivity of low-energy facilities, especially for $\text{CR}(\mu - e, \text{Ti})$ (even without the expected upgrade to $\mathcal{O}(10^{-18})$ for PRISM/PRIME)⁵. Also, any $\tilde{e}_L - \tilde{\mu}_L$ mass splitting above 4% would also be associated with a $\mu \rightarrow e\gamma$ signal within MEG sensitivity. A similar situation (albeit not so striking) is observed for $\tilde{\mu}_L - \tilde{\tau}_2$ mass differences: as an example, mass splittings above 3%, 4% and 6% would be associated to low-energy signals of LFV within PRISM/PRIME, SuperB, and MEG reach, respectively.

As already observed before, points with a tiny $\tilde{\mu}_L - \tilde{\tau}_2$ mass splitting and small LFV BRs are distributed in a more disperse way (fuzzy dropping region) due to the fact that the corresponding mass splittings are mostly arising due to an enhanced LR mixing (large, negative values of A_0).

The most significant effect of considering larger values of θ_{13} would be to displace the depicted regions towards higher values of $\text{BR}(\mu \rightarrow e\gamma)$ implying that points with smaller mass splittings could be within MEG reach. A regime of larger $\tan\beta$ would increase the mass differences, as already seen in Figs. 5, but the associated “standard window” would require a heavier SUSY spectrum. Although the BRs do indeed augment with increasing $\tan\beta$ (see Eq. (3.21)), this would be balanced by the suppression effects of having heavier particles in the loop.

Figs. 11 have been obtained in a very conservative limit for the seesaw parameters, i.e. $\theta_i = 0$ ⁶, very small θ_{13} and hierarchical light and heavy neutrino spectra. Nevertheless one can immediately draw some preliminary conclusions regarding the implications of high- and low-energy LFV observables for the seesaw mechanism:

If the LHC measures a given mass splitting, predictions can be made regarding the associated LFV BRs (for an already reconstructed set of mSUGRA parameters). Comparison with current bounds (or possibly an already existing BR measurement) may allow to derive some hints on the underlying source of flavour violation: a measurement of a slepton mass splitting of a few percent,

⁵ $\Delta m_{\tilde{e}}/m_{\tilde{e}}(\tilde{e}_L, \tilde{\mu}_L) \sim \mathcal{O}(0.1\%)$ would still be associated to predictions for $\text{CR}(\mu - e, \text{Ti})$ within the sensitivity of the future upgrade, $\mathcal{O}(10^{-18})$.

⁶ As we will later see, non-zero values of θ_i imply in general larger predictions for the BRs and mass splittings.

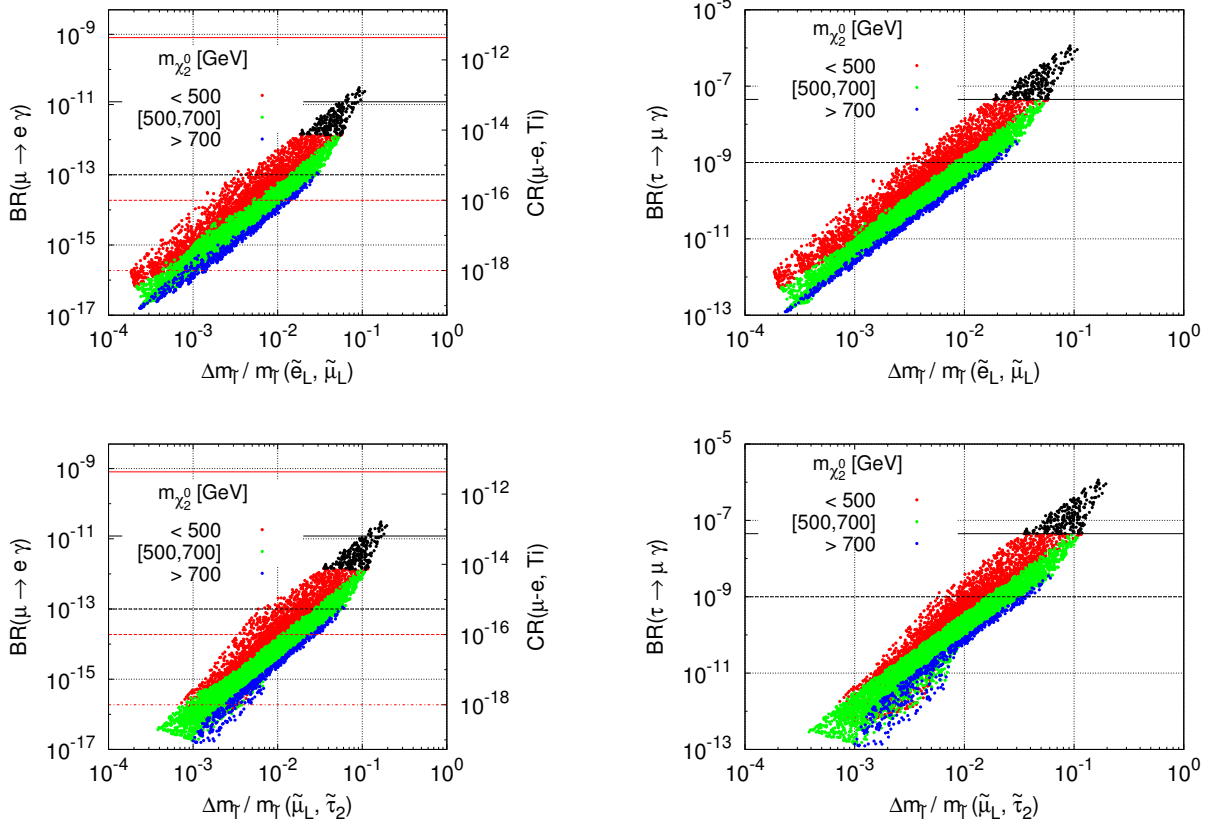


Figure 11: Upper left (right) panel: $\text{BR}(\mu \rightarrow e\gamma)$ ($\text{BR}(\tau \rightarrow \mu\gamma)$) on the left y-axis as a function of the mass difference $\tilde{e}_L - \tilde{\mu}_L$, normalised to the average $\tilde{e}_L, \tilde{\mu}_L$ mass. We display the corresponding predictions of $\text{CR}(\mu - e, \text{Ti})$ on the right y-axis. Horizontal lines denote the corresponding current bounds/future sensitivities. The lower panels correspond to the mass difference $\tilde{\mu}_L - \tilde{\tau}_2$, normalised to the average $\tilde{\mu}_L, \tilde{\tau}_2$ mass. Parameters varied as in Fig. 7. The colour code denotes different regimes of $m_{\chi_2^0}$ mass, and black points are associated with the violation of at least one experimental bound.

together with a measurement of a low-energy observable, for instance $\text{BR}(\mu \rightarrow e\gamma) \sim 10^{-12}$ at MEG (in agreement to what could be expected from the already reconstructed SUSY spectrum) would constitute two signals of LFV that could be simultaneously explained through one common origin - a type-I seesaw mechanism.

On the other hand, two conflicting situations can occur: (i) a measurement of a mass splitting associated to LFV decays experimentally excluded at present (black points in Figs. 11) or in a region already covered by the low-energy facilities at the time; (ii) observation of LFV low-energy signal, and (for an already reconstructed SUSY spectrum) approximate slepton mass universality. These scenarios would either suggest that non-universal slepton masses or low-energy LFV would stem from a mechanism other than such a simple realisation of a type-I seesaw (barring accidental cancellations or different neutrino mass schemes). The most simple explanation for the first scenario would be that the mechanism for SUSY breaking is slightly non-universal (albeit flavour conserving).

Although the reactor angle θ_{13} (and the Dirac phase δ) has no direct impact upon $\Delta m_{\tilde{e}}/m_{\tilde{e}}$, its rôle for some LFV transitions may preclude observable mass splittings: recall that $\Delta m_{\tilde{e}}/m_{\tilde{e}}$ is controlled by the dominant flavour violating entry of the slepton mass matrix, which is in general θ_{13} insensitive (only the τ - e and μ - e entries can have $\sin \theta_{13}$ as a global factor, while for τ - μ , $\sin \theta_{13}$ is a second order perturbation). However, flavour violating transitions involving the first generation (as is the case of $\mu(\tau) \rightarrow e\gamma$, $\mu - e$ in nuclei, etc) are very sensitive to θ_{13} [46]. Intermediate to large values of the Chooz angle, $\theta_{13} \sim 5^\circ - 12^\circ$, may lead to predictions for $\text{BR}(\mu \rightarrow e\gamma)$ (among others) already in conflict with current bounds. In Fig.12, we consider the impact of different values of the Chooz angle ($\theta_{13} = 0.1^\circ, 1^\circ, 5^\circ$ and 12°) for the slepton mass splittings and $\text{BR}(\mu \rightarrow e\gamma)$. From left to right, each set of points for a given mSUGRA benchmark is associated with increasing values of M_{N_3} .

Although (and as expected) θ_{13} indeed has a very small impact for the mass splittings, a joint measurement of flavour violation at the LHC and at a $\mu \rightarrow e\gamma$ dedicated facility (for a given reconstructed SUSY spectrum) strongly depends on the value of this angle. This is readily seen from Figs. 12, and as an example let us notice that for P3-like spectra a $\tilde{e}_L - \tilde{\mu}_L$ MS, in agreement with $\text{BR}(\mu \rightarrow e\gamma)$ bounds, is only possible for very small $\theta_{13} \lesssim 1^\circ$. Conversely, any hope of a joint signal at the LHC and at MEG for HM1-like points requires $\theta_{13} \gtrsim 1^\circ$ (recall that for M_{N_3} much larger than 10^{15} GeV, the Yukawa couplings become non-perturbative).

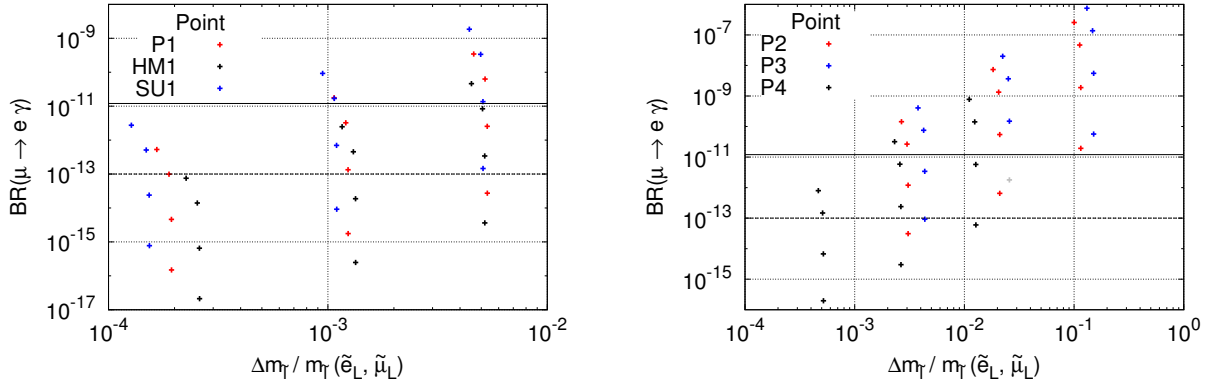


Figure 12: Mass difference $\tilde{e}_L - \tilde{\mu}_L$, normalised to the average $\tilde{e}_L, \tilde{\mu}_L$ mass, versus $\text{BR}(\mu \rightarrow e\gamma)$, for the benchmark points (Table 2) and for distinct values of $\theta_{13} = 0.1^\circ, 1^\circ, 5^\circ, 12^\circ$ (corresponding to increasing values of the BR). The remaining seesaw parameters were set as $R = 1$, with $M_{N_1} = 10^{10}$ GeV, $M_{N_2} = 10^{11}$ GeV and $M_{N_3} = \{10^{13}, 10^{14}, 10^{15}\}$ GeV. Gray points are those associated with the violation of $\text{BR}(\tau \rightarrow \mu\gamma)$ and non-violation of $\text{BR}(\mu \rightarrow e\gamma)$.

Before addressing the impact of the additional mixing involving the right-handed neutrinos (i.e. $\theta_i \neq 0$), let us consider how the conclusions so far derived hold for a different hierarchy in the heavy neutrino sector. In Fig. 13, we study the case of degenerate right-handed neutrinos, displaying the mass differences $\tilde{e}_L - \tilde{\mu}_L$ and $\tilde{\mu}_L - \tilde{\tau}_2$ versus $\text{BR}(\tau \rightarrow \mu\gamma)$ and $\text{BR}(\mu \rightarrow e\gamma)$ (also providing information on $\text{CR}(\mu - e, \text{Ti})$).

The results shown in Fig. 13 should be compared to those of Fig. 11 (notice that apart from M_{N_i} , all the other parameters have been identically varied with the exception of θ_{13} which we took as $\theta_{13} = 0.1^\circ$ in the hierarchical case and $\theta_{13} = 0.1^\circ, 1^\circ, 5^\circ$ for the degenerate case. However the comparison in the lower panel of Fig. 13 is made for the same $\theta_{13} = 0.1^\circ$).

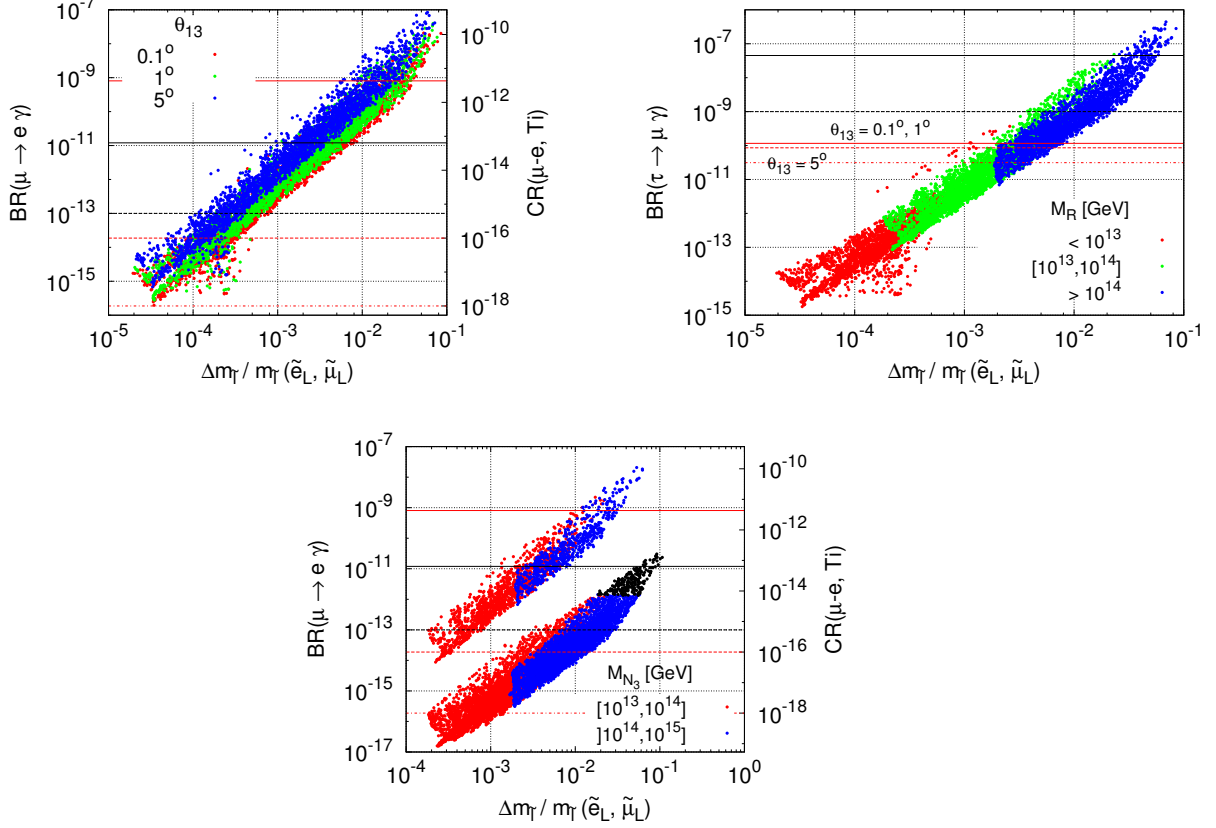


Figure 13: Degenerate right-handed neutrino case. Upper left (right) panel: $\text{BR}(\mu \rightarrow e\gamma)$ ($\text{BR}(\tau \rightarrow \mu\gamma)$) on the left y-axis as a function of the mass difference $\tilde{e}_L - \tilde{\mu}_L$, normalised to the average $\tilde{e}_L, \tilde{\mu}_L$ mass. We display the corresponding predictions of $\text{CR}(\mu - e, \text{Ti})$ on the right y-axis. Horizontal lines denote the corresponding current bounds/future sensitivities and regimes of θ_{13} (in the upper right panel). Leading to the scan, we set $\tan\beta = 10$, and the remaining mSUGRA parameters were randomly varied (with $|A_0| \lesssim 1$ TeV, satisfying the “standard window” constraint and requiring consistency with the dark matter and Higgs boson mass bounds). For the seesaw parameters we have taken $R = 1$, $\theta_{13} = 0.1^\circ, 1^\circ, 5^\circ$ (with $\delta = \varphi_{1,2} = 0$), and $M_{N_1} = M_{N_2} = M_{N_3} = M_R$ being varied as $10^{12} \text{ GeV} \lesssim M_R \lesssim 10^{15} \text{ GeV}$. In the upper left (right) panel colour code denotes different regimes of θ_{13} (M_R). Lower panel: comparison of degenerate (region with higher BR) and hierarchical (region with lower BR) spectrum. Same scan as before, but now taking only $\theta_{13} = 0.1^\circ$ and $10^{13} \text{ GeV} \lesssim M_R \lesssim 10^{15} \text{ GeV}$. For the hierarchical case, same scan as in Fig. 11. Colour code denotes different regimes of M_{N_3} (or M_R for the degenerate case) and black points are associated with the violation of at least one experimental bound.

As seen from the direct comparison of the high- and low-energy flavour violation prospects, potential measurements (and even negative searches) can hint towards the RH neutrino hierarchy, in the case $R = 1$. This is especially true in the limit of very small θ_{13} : if a sizable mass splitting $\tilde{e}_L - \tilde{\mu}_L \sim \mathcal{O}(10^{-2})$ is measured at the LHC, then a hierarchical spectrum appears to be the only candidate to explain such a signal. If a $\Delta m_{\tilde{\ell}}/m_{\tilde{\ell}}(\tilde{e}_L, \tilde{\mu}_L)$ between 10^{-3} and 10^{-2} is reconstructed, and a $\mu \rightarrow e\gamma$ decay is observed, then both hierarchies are hard to disentangle based

on observation. For the same mass splitting range, $\text{CR}(\mu - e, \text{Ti})$ within reach of PRISM/PRIME (and a potential upgrade), would strongly favour the hierarchical spectrum. Finally, should the LHC be able to measure $\Delta m_{\tilde{\ell}}/m_{\tilde{\ell}}(\tilde{e}_L, \tilde{\mu}_L) \sim \mathcal{O}(10^{-4})$, an observation of $\mu \rightarrow e\gamma$ could be due to either RH spectrum (although in this case larger values of θ_{13} would be required to accommodate the hierarchical hypothesis).

To conclude the study of the conservative limit of $R = 1$ in the type-I SUSY seesaw, we conduct a distinct analysis, explicitly focusing on the dependence of the mass splittings on different mSUGRA parameters. For fixed $\tan \beta = 10$, a scan is performed over m_0 and $M_{1/2}$, taking several discrete values of A_0 (always complying with the “standard window” requirements). We fix all seesaw parameters other than M_{N_3} , which is varied as to ensure that each point has $\text{BR}(\mu \rightarrow e\gamma)$ and $\text{BR}(\tau \rightarrow \mu\gamma)$ in agreement with current experimental bounds. The results are shown in the left panel of Fig. 14, which clearly displays how a potentially measurable mass difference (in agreement with the different low-energy LFV bounds) translates the interplay of A_0 and M_{N_3} . The two regimes (other than the nearly constant $\Delta m_{\tilde{\ell}}/m_{\tilde{\ell}}$ for $A_0 = 0$) reflect the different bounds which are effectively preventing larger values of $\Delta m_{\tilde{\ell}}/m_{\tilde{\ell}}$: for the ascending slope, the mass splittings are almost insensitive to the actual value of A_0 , since in this case the values of Y_{ij}^ν that saturate the current bounds on $\text{BR}(l_i \rightarrow l_j\gamma) - \text{BR}(\tau \rightarrow \mu\gamma)$ for the $\theta_{13} = 0.1^\circ$ regime considered – are attainable without violating the requirement of perturbative Yukawa couplings. On the right-handed (descending) part of each curve, the values of M_{N_3} are at the maximum value allowed by perturbative Yukawa couplings alone while $\text{BR}(l_i \rightarrow l_j\gamma)$ is below current bounds. In this latter case, A_0 is the discriminatory factor that enhances the $\propto Y^{\nu\dagger}LY^\nu$ radiative corrections to the soft slepton mass matrices, in turn constraining the maximal value of $\Delta m_{\tilde{\ell}}/m_{\tilde{\ell}}$ for a given A_0 . In each pair of lines, the one whose maximum mass splitting occurs for a lighter χ_2^0 corresponds to the positive value of A_0 . Larger values of $|A_0|$ would lead to an increase in the maximal values of $\Delta m_{\tilde{\ell}}/m_{\tilde{\ell}}$, which would also be associated with a heavier gaugino spectrum.

A similar study is conducted on the right panel of Fig. 14, taking discrete values of A_0 , and studying different combinations of $\tan \beta$ and θ_{13} . We notice that of all the SUSY seesaw parameters likely to be measurable, A_0 , $\tan \beta$, and θ_{13} , are those expected to be measured/reconstructed at a later stage. Just like in the previous figure, the two regimes for the slopes again denote the bounds for $\text{BR}(\ell_i \rightarrow \ell_j\gamma)$ (ascending), and $Y^\nu \sim 1$ (descending). The curves corresponding to $\tan \beta = 10$ and maximal θ_{13} present very low $\Delta m_{\tilde{\ell}}/m_{\tilde{\ell}}$: this is a direct consequence of having to take comparatively low values of the heaviest right-handed neutrino mass in order to comply with the $\text{BR}(\mu \rightarrow e\gamma)$ bound (easily saturated for $\theta_{13} = 5^\circ$).

From Figs. 14, it is clear that, even in the very conservative case of $R = 1$, without the reconstruction of the mSUGRA parameters and measurement of θ_{13} , very little can be said regarding the expected values of $\Delta m_{\tilde{\ell}}/m_{\tilde{\ell}}$, apart from some remarkable exceptions, which we proceed to discuss. Let us address the hypothetical measurements of $m_{\chi_2^0}$ and $\Delta m_{\tilde{\ell}}/m_{\tilde{\ell}}$ corresponding to three points highlighted in the right panel of Figs. 14 (α , β , γ). A measurement close to point γ would provide very little information regarding the underlying source of LFV: different choices of either M_{N_3} , $\tan \beta$ or θ_{13} could easily account for such an observation. The case denoted by β is already more interesting: although large values of $\Delta m_{\tilde{\ell}}/m_{\tilde{\ell}}$ (in association with a heavy χ_2^0) can be obtained for very large $|A_0|$, complying with the bound on the LSP relic density becomes increasingly more complicated in these regimes, so that a correct Ωh^2 might eventually preclude compatibility of a type-I SUSY seesaw with β . A set of measurements $\sim \alpha$ (and β to a certain extent) would certainly provide the most challenging scenario: such a mass splitting, in agreement with current bounds on low-energy LFV observables, and for such a light gaugino spectrum, cannot be accounted for by a type-I SUSY seesaw (in the $R = 1$ limit). Another mechanism of flavour

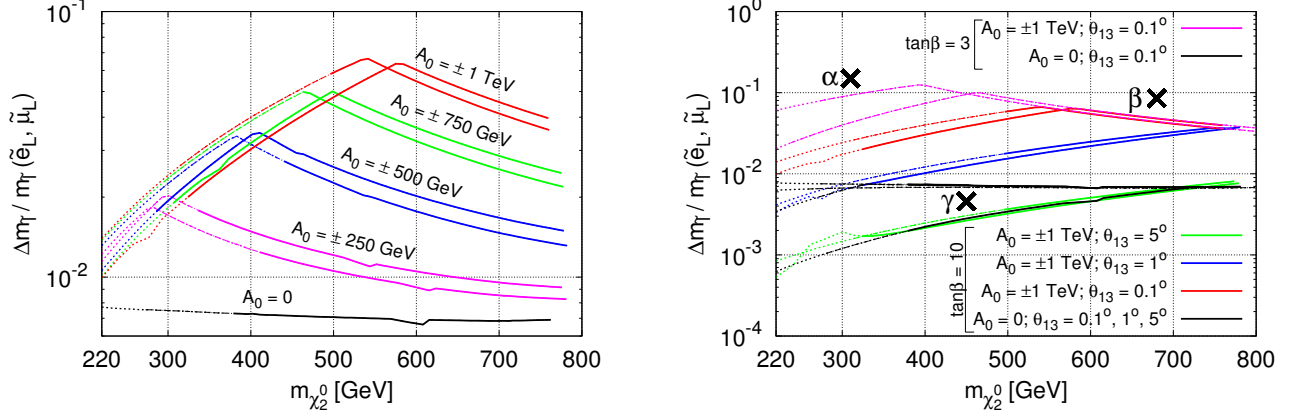


Figure 14: Mass difference $\tilde{e}_L - \tilde{\mu}_L$, normalised to the average $\tilde{e}_L, \tilde{\mu}_L$ mass, as a function of $m_{\chi_2^0}$ (in GeV). On the left we consider different values of $|A_0|$, setting $\tan \beta = 10$ and $\theta_{13} = 0.1^\circ$, while on the right we fix $A_0 = \{-1, 0, 1\}$ TeV, and take several choices for $\theta_{13} = 0.1^\circ, 1^\circ, 5^\circ$ with $\tan \beta = 10$ and $\theta_{13} = 0.1^\circ$ for $\tan \beta = 3$. We vary m_0 and $M_{1/2}$ in such a way that we satisfy the requirement of a viable Ωh^2 in the co-annihilation region. The seesaw parameters have been taken as $R = 1$, with hierarchical right-handed neutrinos, $M_{N_1} = 10^{10}$ GeV, $M_{N_2} = 10^{11}$ GeV, with M_{N_3} varied as to satisfy $\text{BR}(\mu \rightarrow e\gamma) \leq 1.2 \times 10^{-11}$ and $\text{BR}(\tau \rightarrow \mu\gamma) \leq 4.5 \times 10^{-8}$. Dotted lines denote points where the kinematical constraints are outside the “standard window” and dashed lines are for $m_h \leq 114.4$ GeV, while satisfying the “standard window” requirement. We have displayed three points α, β, γ used for the subsequent discussion in the text.

violation (or at least flavour non-universality) should be at work in this case, e.g. non-universal soft-breaking slepton masses. This will also be true for $\theta_i \neq 0$, as in this case the low-energy LFV observables would be enhanced making it even more difficult to account for a set of measurements $\sim \alpha$ and β , while respecting the current bounds on low-energy LFV observables.

We will now depart from the conservative (albeit singular) $R = 1$ case, allowing for additional sources of flavour violation through the θ_i angles. Given that the right-handed neutrino sector (both spectrum and mixings) is experimentally unreachable⁷, this translates into having parameters about which one has no direct information. As mentioned in Section 3, one can impose indirect constraints on the $\theta_i - M_{N_j}$ parameter space, choosing R -matrix angles and heavy neutrino hierarchies suggested by phenomenological arguments, such as generating the observed BAU from thermal leptogenesis and complying with lepton EDMs. For simplicity, and motivated by the analysis of the $R = 1$ limit, we have selected additional scenarios, that will play the rôle of seesaw “benchmark” points: three configurations of the heavy neutrino spectrum and reactor angle θ_{13} are summarised in Table 8 and can be applied to the different mSUGRA points (P1’, etc.). P⁽ⁿ⁾ denotes a case of nearly degenerate N_1 and N_2 (N_2 and N_3), while P^{'''} is the limit of a strongly hierarchical right-handed spectrum, with M_{N_3} close to its maximal value (as allowed by the perturbativity bound on Y^ν). We do not consider the case of degenerate RH neutrinos as the associated phenomenology will not differ significantly from the $R = 1$ case already discussed.

In order to summarise the results, we now display a comprehensive scan over the seesaw

⁷If the SUSY seesaw is indeed responsible for LFV observables within experimental sensitivity, as well as for the BAU via leptogenesis, then the seesaw scale lies in general well above the TeV range ($\sim 10^{10}$ GeV – 10^{15} GeV).

Point	M_{N_1} (GeV)	M_{N_2} (GeV)	M_{N_3} (GeV)	θ_{13}
P'	10^{10}	5×10^{10}	5×10^{13}	0.1°
P''	10^{10}	10^{12}	5×10^{12}	1°
P'''	10^{10}	10^{12}	10^{15}	0.1°

Table 8: Seesaw benchmark points. For the remaining parameters we have taken $R = 1$, and $\varphi_1 = \varphi_2 = \delta = 0$.

parameters, in particular over the complex angles of the R matrix. We consider mSUGRA benchmark point P1 with $M_{N_i} = \{10^{10}, 10^{11}, 10^{13}\}$ GeV, and randomly scan over $|\theta_i| \in [0, \pi]$ and $\arg \theta_i \in [-\pi, \pi]$. We also select four values of θ_1 and vary $\theta_{2,3}$ as favoured by leptogenesis [85] (see end of Section 3), and highlight these regions via a different colour code, for illustrative purposes only.

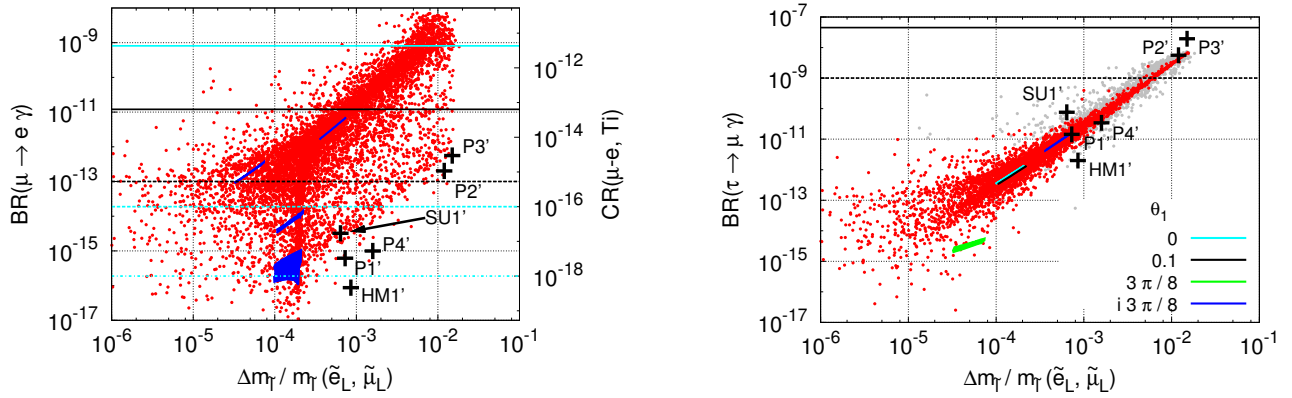


Figure 15: Left (right) panel $\text{BR}(\mu \rightarrow e\gamma)$ ($\text{BR}(\tau \rightarrow \mu\gamma)$) as a function of the mass difference $\tilde{e}_L - \tilde{\mu}_L$, normalised to the average $\tilde{e}_L, \tilde{\mu}_L$ mass, for seesaw variations of point P1. We display the corresponding predictions of $\text{CR}(\mu - e, \text{Ti})$ on the right secondary y-axis. Horizontal lines denote the corresponding current bounds/future sensitivities. We have taken $\theta_{13} = 0.1^\circ$, $M_{N_1} = 10^{10}$ GeV, $M_{N_2} = 10^{11}$ GeV, and $M_{N_3} = 10^{13}$ GeV, and the complex R matrix angles have been randomly varied as $|\theta_i| \in [0, \pi]$ and $\arg(\theta_i) \in [-\pi, \pi]$. The crosses correspond to the $R = 1$ case of the benchmark points P' (see Table 2 and 8). In each panel the four highlighted regions correspond to $\theta_1 = 0, 0.1, 3\pi/8$ and $i3\pi/8$, with $\theta_{2,3}$ scanned as favoured by leptogenesis (see text for discussion). In the left panel we show in solid blue the leptogenesis favoured regions for different values of $\theta_1 = 0, 0.1, 3\pi/8$ and $i3\pi/8$, from lower to higher $\text{BR}(\mu \rightarrow e\gamma)$. On the right panel these regions are identified in the inset.

The full realisation of a type-I seesaw leads to very rich scenarios (albeit less predictive) for flavour violation, as can be seen from Fig 15. Recall that for an mSUGRA configuration similar to P1 (see e.g. Fig. 12), the associated BR was $\mathcal{O}(10^{-16})$, with a mass splitting around 2×10^{-4} . Under a generic choice of θ_i , the associated amount of FV is extremely enhanced (even already excluded by current bounds in some cases). This confirms that, barring cancellations, the case $R = 1$ clearly constitutes a case of minimal flavour violation, inducing low values for the BRs and CR. Regarding the highlighted regions (corresponding to $\theta_{2,3}$ in the ranges given at the end of

Section 3), the distinct disconnected regions correspond, for increasing values of $\text{BR}(\mu \rightarrow e\gamma)$, to $\theta_1 = 0, 0.1, 3\pi/8$ and $i3\pi/8$. For a SUSY spectrum similar to P1, a type-I seesaw could easily account for slepton mass differences within the sensitivity of both the LHC and of low-energy flavour dedicated experiments (possibly associated to viable leptogenesis scenario).

For the other seesaw benchmark points, an identical scan would translate in scatter regions of comparable ranges, similarly positioned with respect to the different benchmark point.

In Fig. 16, we conduct a general scan over the θ_i parameter space, again displaying different low-energy LFV observables as a function of the $\tilde{e}_L - \tilde{\mu}_L$ mass difference. Given the amount of collider simulations conducted for the LHC benchmark points [61,62], we choose for this overview of the SUSY seesaw the LHC points P5-HM1 and P6-SU1. We randomly scan over $|\theta_i| \lesssim \pi$, and $\arg(\theta_i) \in [-\pi, \pi]$, taking $\theta_{13} = 0.1^\circ$, and choosing three representative values for M_{N_3} .

As can be seen from the first panel of Fig. 16, if a SUSY type-I seesaw is indeed at work, and θ_{13} has been constrained to be extremely small, a measurement of $\Delta m_{\tilde{e}}/m_{\tilde{e}}(\tilde{e}_L, \tilde{\mu}_L)$ between 0.1% and 1%, in association with a reconstructed sparticle spectrum similar to P5-HM1, would be accompanied (with a significant probability) by the observation of $\text{BR}(\mu \rightarrow e\gamma)$ at MEG. On the other hand, even for very large values of M_{N_3} , the constraints on the parameter space from $\text{BR}(\mu \rightarrow e\gamma)$ preclude the observation of a $\tau \rightarrow \mu\gamma$ transition for an HM1-like SUSY spectrum. From the comparison of both left and right panels, it is also manifest that the slepton mass splittings are predominantly generated from mixings involving the $\tau - \mu$ sector: this can be seen from the strongly correlated behaviour of $\Delta m_{\tilde{e}}/m_{\tilde{e}}(\tilde{e}_L, \tilde{\mu}_L)$ and $\text{BR}(\tau \rightarrow \mu\gamma)$, implying that both are governed by the term proportional to $(Y^{\nu\dagger}LY^\nu)_{23}$ (see Section 4). In this case, the three seesaw benchmark points appear almost superimposed on the $R = 1$ (i.e. $\theta_i = 0$) central diagonal region, and their corresponding $\Delta m_{\tilde{e}}/m_{\tilde{e}}$ and BRs follow the LLog dependency (i.e. $\text{BR} \propto M_{N_3}^2 \log^2 M_{N_3}$).

Although LHC production prospects have to be taken into account, when compared to P5-HM1, P6-SU1 offers a less promising framework for the observation of sizable mass splittings at the LHC (unless a precision of around 10^{-3} for $\Delta m_{\tilde{e}}/m_{\tilde{e}}(\tilde{e}_L, \tilde{\mu}_L)$ can indeed be achieved). In the latter case, it is expected that a determination of $\Delta m_{\tilde{e}}/m_{\tilde{e}}(\tilde{e}_L, \tilde{\mu}_L)$ be accompanied by evidence of LFV in muon decays. However the most interesting lepton flavour signature of P6-SU1 is related to its potential to induce large $\text{BR}(\tau \rightarrow \mu\gamma)$, within the future sensitivity of SuperB [11]: a measurement of $\Delta m_{\tilde{e}}/m_{\tilde{e}}(\tilde{e}_L, \tilde{\mu}_L) \sim 0.1\% - 1\%$ at the LHC would imply $\text{BR}(\tau \rightarrow \mu\gamma) \gtrsim 10^{-9}$, and would hint towards a heavy seesaw scale, $M_{N_3} \gtrsim 10^{13}$ GeV. For shortness, we do not present the analog of Fig. 16 for the mass difference $\tilde{\mu}_L - \tilde{\tau}_2$, as little new information is conveyed by these figures. Moreover, we have also verified that larger values of θ_{13} would only have the small effect of slightly augmenting the concentration of the points around the central region.

The analysis we have done for a few illustrative SUSY benchmark points can be reproduced for any other cMSSM realisation. In a hopefully not too distant future, when fundamental mSUGRA parameters will have been reconstructed, and a measurement of LFV observables ($\text{BR}(\tau \rightarrow \mu\gamma)$, and $\text{CR}(\mu - e)$, for instance) will have also been reported, one will then be able to predict the mass splittings associated to this (these) region(s) of the SUSY seesaw parameter space. Should an additional measurement of the slepton mass splittings correspond to the above prediction, one can say that the present seesaw realisation is in striking agreement with the data we will so far have collected. On the other hand, if the measurement of the mass splittings lies outside the predictions (as obtained by the SUSY seesaw, possibly in a leptogenesis motivated region), we will be led to the conclusion that one of the underlying hypothesis (either this seesaw realisation or a type-I seesaw as the dominant or even unique LFV source) has to be reconsidered, or even strongly disfavoured.

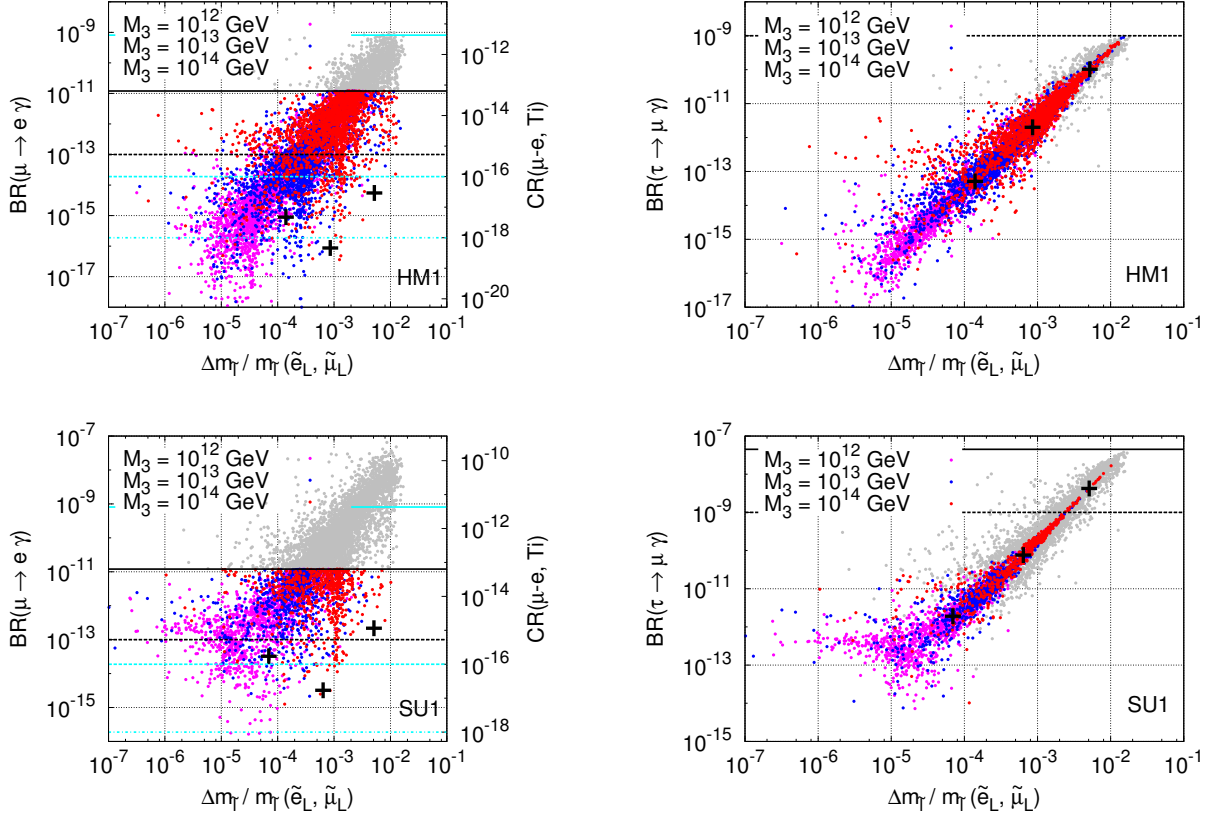


Figure 16: Upper left (right) panel: $\text{BR}(\mu \rightarrow e\gamma)$ ($\text{BR}(\tau \rightarrow \mu\gamma)$) on the left y-axis as a function of the mass difference $\tilde{e}_L - \tilde{\mu}_L$, normalised to the average $\tilde{e}_L, \tilde{\mu}_L$ mass, for seesaw variations of point P5-HM1. We display the corresponding predictions of $\text{CR}(\mu-e, \text{Ti})$ on the secondary right y-axis. Lower panels: same as above, but for point P6-SU1. Horizontal lines denote the corresponding current bounds/future sensitivities. The distinct coloured regions correspond to three different values of $M_{N_3} = \{10^{12}, 10^{13}, 10^{14}\}$ GeV. The remaining parameters were set as $M_{N_1} = 10^{10}$ GeV, $M_{N_2} = 10^{11}$ GeV, $\theta_{13} = 0.1^\circ$ and the complex R matrix angles have been randomly varied as $|\theta_i| \in [0, \pi]$, and $\arg(\theta_i) \in [-\pi, \pi]$. The crosses correspond to the different seesaw benchmark points: from smaller to larger mass splittings one has HM1'' (SU1''), HM1' (SU1'), HM1''' (SU1'''), for the upper (lower) panels.

5.4 Flavour violating neutralino decays: di-lepton distributions in the SUSY seesaw

To conclude our study of LFV at the LHC, we recondut the analysis of Section 4.2, but now in the framework of the SUSY seesaw. As mentioned before, models of supersymmetric LFV may be manifest in di-lepton distributions, either through the relative separation of the kinematical edges corresponding to \tilde{e}_L in m_{ee} and those of $\tilde{\mu}_L$ in $m_{\mu\mu}$ (implying that $m_{\tilde{e}_L} \neq m_{\tilde{\mu}_L}$), or via the appearance of new edges in a given di-lepton mass distribution.

In Fig. 17, we display the $\text{BR}(\chi_2^0 \rightarrow \mu\mu\chi_1^0)$ as a function of the di-muon invariant mass $m_{\mu\mu}$ for different SUSY seesaw points, comparing the distributions with those of the cMSSM (formerly shown in Fig. 2). For simplicity, we do not present here the peaks corresponding to the Z and h

intermediate states in $\chi_2^0 \rightarrow \ell\ell\chi_1^0$ decays. The values of the edges are presented in Table 9, and should be compared to those listed in Table 7 for the pure cMSSM case.

\tilde{l}_X	$m_{ll}(\tilde{l}_X)$ (GeV) for type-I SUSY seesaw					
	P1'''	P2'	P3'	P4'''	P5-HM1'''	P6-SU1'''
\tilde{e}_R	115.8	125.9	150.8	434.5	128.4	92.2
\tilde{e}_L	136.4	93.1	83.7	188.2	256.0	62.3
$\tilde{\mu}_R$	115.7	125.8	150.7	434.3	128.2	92.1
$\tilde{\mu}_L$	141.6	95.5	85.6	212.8	256.3	66.6
$\tilde{\tau}_1$	81.8	77.1	76.6	40.9	53.6	67.1
$\tilde{\tau}_2$	135.4	111.8	105.2	300.4	263.3	56.7

Table 9: $m_{ll}(\tilde{l}_X)$ (GeV) for type-I SUSY seesaw points (see Tables 2 and 8), where l is any of the charged leptons and X stands for left- and right-handed sleptons (all families).

As is manifest from Fig. 17, and readily confirmed from Table 9, the impact of the seesaw at the level of the di-muon mass distributions is quite spectacular, particularly in the appearance of a third edge in most of the benchmarks considered. With the exception of P1''', all other distributions exhibit now the edge corresponding to the presence of an intermediate $\tilde{\tau}_2$, implying that the decay occurs via $\chi_2^0 \rightarrow \tilde{\tau}_2\mu \rightarrow \mu\mu\chi_1^0$. For instance, for point P2', the $\text{BR}(\chi_2^0 \rightarrow \mu\mu\chi_1^0)$ via intermediate $\tilde{\mu}_L$, $\tilde{\mu}_R$ and $\tilde{\tau}_2$ are 2.6%, 1.1% and 1.6%, respectively.

In Fig. 18 we compare the di-muon with the di-electron distribution, for the previous seesaw benchmark points. We point here that unlike the smuon case the di-electron distribution does not change with respect to the cMSSM case. From this figure one further observes that selectron and smuon edges exhibit a clear separation. For a c.o.m. energy ~ 14 TeV at the LHC, and an integrated luminosity of 100 fb^{-1} , a few events should be indeed observable, implying that if present, these slepton mass splittings are likely to be measurable.

Comparing Table 9 and Table 7, one further verifies that in the type-I SUSY seesaw the mass splittings are indeed a LL sector phenomenon (notice that for both right-handed smuons and selectrons the edges remain identical up to ~ 0.1 GeV) and are essentially restricted to the $\tilde{\mu} - \tilde{\tau}$ sectors, since the edges corresponding to \tilde{e}_L also remain unaffected.

Interestingly, the fact that the SUSY seesaw leads to increased mass splittings only for the left-handed sleptons might provide another potential fingerprint for this mechanism of LFV. Compiling all the data collected throughout our numerical analysis, we have found that the maximal splitting between right-handed smuons and selectrons, in all the cases studied, is

$$\left. \frac{\Delta m_{\tilde{\ell}}}{m_{\tilde{\ell}}}(\tilde{\mu}_R, \tilde{e}_R) \right|_{\text{max}} \approx 0.09\%. \quad (5.3)$$

Recall that throughout the preceding subsections we have verified that within the SUSY seesaw $\Delta m_{\tilde{\ell}}/m_{\tilde{\ell}}(\tilde{\mu}_L, \tilde{e}_L)$ could easily reach values of a few %. Should the LHC measure mass splittings between right-handed sleptons of the first two families that are significantly above the 0.1% level, this could provide important indication to the fact that another mechanism of FV is at work (for instance, an effective parameterization of flavour violating effects in the lepton sector, as done in [66], induces similar mass splittings for both right- and left-handed sleptons). Among the many possibilities, a likely hypothesis would be the non-universality of the slepton soft-breaking terms.

Finally, we display the prospects for direct flavour violation in χ_2^0 decays: in addition to the possibility of having staus in the intermediate states, one can also have opposite-sign, different

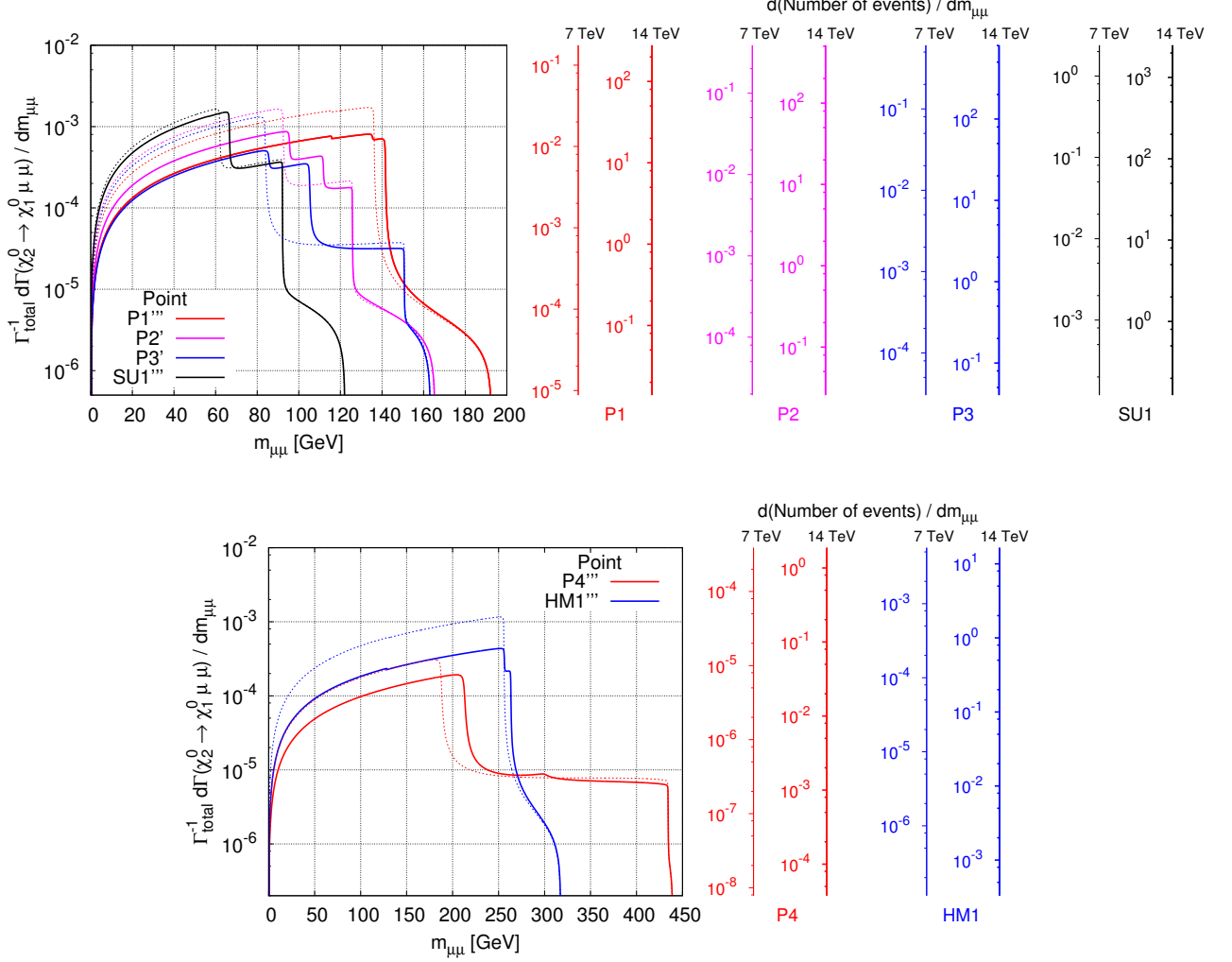


Figure 17: $\text{BR}(\chi_2^0 \rightarrow \mu\mu\chi_1^0)$ as a function of the di-muon invariant mass $m_{\mu\mu}$ (in GeV) for different SUSY seesaw points (see Tables 2 and 8). Upper panel: P1''' (red), P2' (pink), P3' (blue) and P6-SU1''' (black). Lower panel: P4''' (red) and P5-HM1''' (blue). Dotted (coloured) lines denote in both panels the curves for the corresponding cMSSM case. Secondary (right) y-axes denote the corresponding expected number of events for $\sqrt{s} = 7$ TeV and 14 TeV, respectively with $\mathcal{L} = 1 \text{ fb}^{-1}$ and $\mathcal{L} = 100 \text{ fb}^{-1}$.

flavour final state di-leptons. In particular, one can have $\chi_2^0 \rightarrow \mu\tau\chi_1^0$, with a non-negligible associated branching ratio, and the possibility of a few events for $\mathcal{L} = 100 \text{ fb}^{-1}$. This is shown in Fig. 19.

6 Conclusions

In this work we have studied lepton flavour violation in high- and low-energy observables in the framework of a type-I SUSY seesaw. If the seesaw is indeed responsible for both neutrino masses and leptonic mixings, and accounts for low-energy LFV observables within future sensitivity reach,

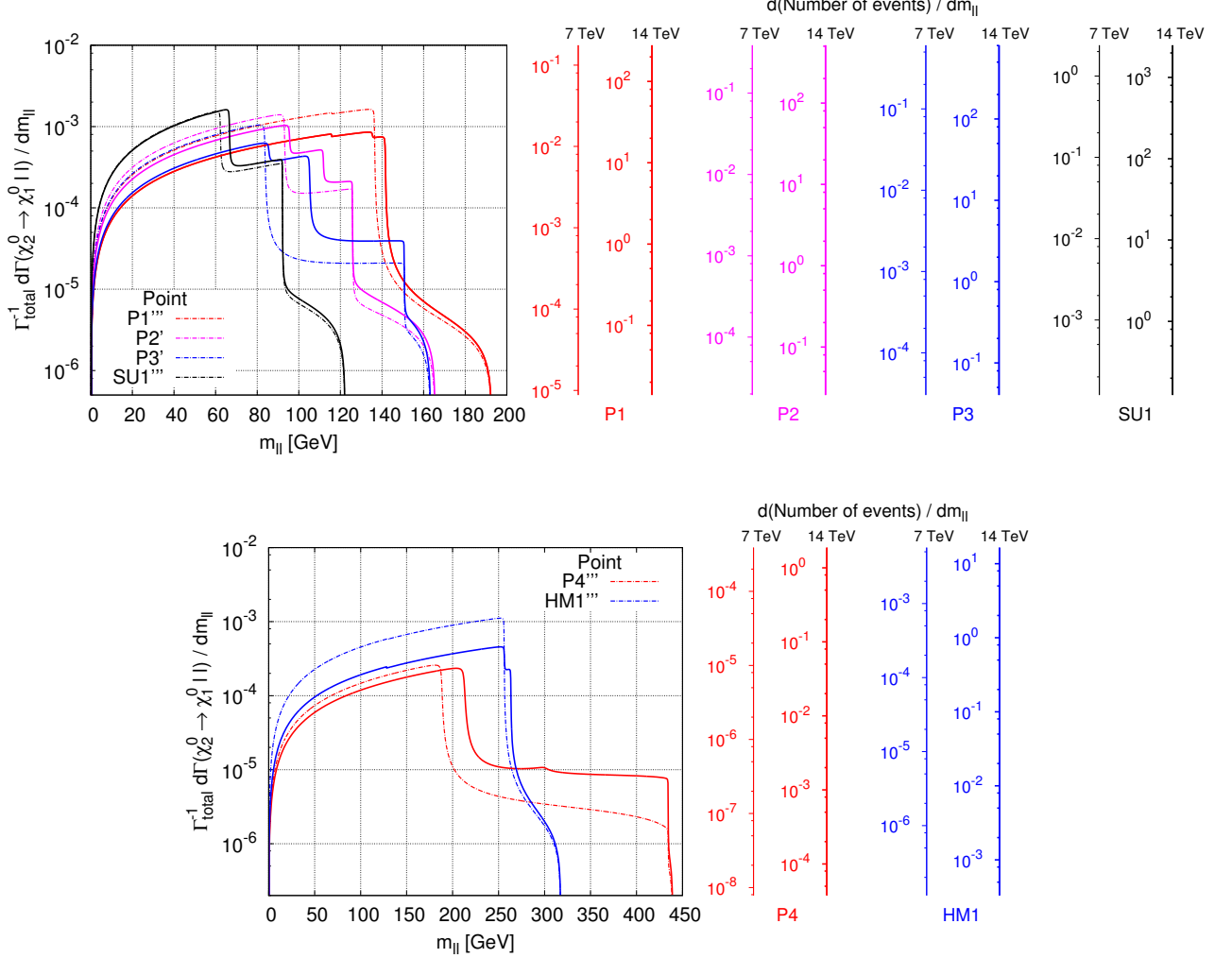


Figure 18: $\text{BR}(\chi_2^0 \rightarrow \ell\ell\chi_1^0)$ as a function of the di-lepton invariant mass $m_{\ell\ell}$ ($\ell = e, \mu$) (in GeV) for P1''' (red), P2' (pink), P3' (blue) and P6-SU1''' (black) (see Tables 2 and 8). Lower panel: P4''' (red) and P5-HM1''' (blue). Full (dashed) lines denote in both panels the curves for di-muon (di-electron) distributions. Secondary-right y-axes denote the corresponding expected number of events for $\sqrt{s} = 7$ TeV and 14 TeV, respectively with $\mathcal{L} = 1 \text{ fb}^{-1}$ and $\mathcal{L} = 100 \text{ fb}^{-1}$.

interesting slepton phenomena are expected to be observed at the LHC. Under the assumption of a unique source - the neutrino Yukawa couplings -, the interplay between these high- and low-energy LFV observables allows to derive some information about the seesaw parameters and, for specific configurations of the model, disfavour the type-I SUSY seesaw as being the unique source of LFV.

We began our analysis by considering the mSUGRA parameter space, looking for regions where the conditions for a successful reconstruction of the slepton masses can be met: the observation of a significant number of events of the type $\chi_2^0 \rightarrow \ell^\pm \ell^\mp \chi_1^0$ with sufficiently hard leptons in the final state implies that the mSUGRA parameters should follow specific relations. In general the most promising scenarios are encountered for low to intermediate $\tan \beta$ and a light sparticle spectrum.

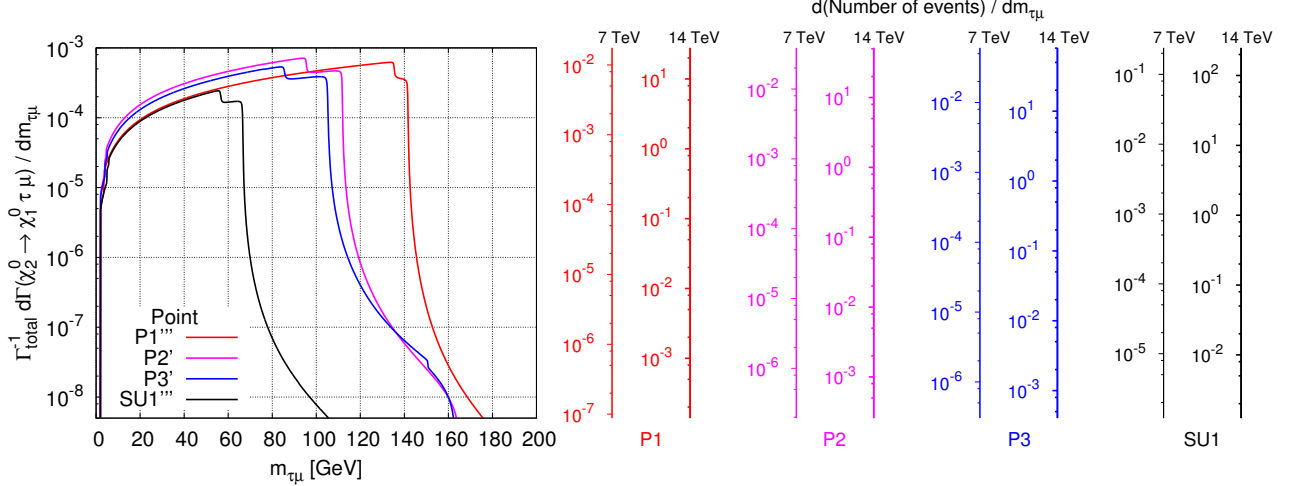


Figure 19: Flavour violating $\text{BR}(\chi_2^0 \rightarrow \mu\tau\chi_1^0)$ as a function of the di-lepton invariant mass $m_{\tau\mu}$ (in GeV) for the seesaw benchmark points P1''' (red), P2' (pink), P3' (blue) and P6-SU1''' (black) (see Tables 2 and 8). On the right y-axis, we also display the expected number of events for $\sqrt{s} = 7$ TeV (with $\mathcal{L} = 1 \text{ fb}^{-1}$) and $\sqrt{s} = 14$ TeV (for $\mathcal{L} = 100 \text{ fb}^{-1}$).

In these regions the correct relic density is always obtained via $\tilde{\tau}_1 - \chi_1^0$ co-annihilation. We have illustrated these features by considering different points in mSUGRA parameter space. Among them, and in order to address LHC prospects, we included in our analysis two LHC benchmark points: SU1 (ATLAS) and HM1 (CMS).

The analysis of the slepton mass splittings in the cMSSM (in the absence of flavour violation in the lepton sector) reveals that the expected values are very small due to the tiny LR mixing and RGE effects. Although marginally observable for the smuon-stau sector, the mass differences for the first two generations of mostly LH sleptons is at best of order of 0.03 %. At the LHC, the cMSSM smuon and selectron masses could be reconstructed from the (double) triangular di-lepton invariant mass distributions (in the best case scenario) with identical kinematical edges for both di-muon and di-electron mass distributions.

In the minimal implementation of a type-I SUSY seesaw ($R = 1$, i.e. not taking into account possible mixings in the right-handed neutrino sector), the slepton spectrum reflects the mixing introduced at low energies due to the non-trivial structure of the Yukawa couplings (given by the U^{MNS} leptonic mixing matrix). These effects are only manifest for the left-handed sector, potentially leading to maximal mixing between left-handed smuons and staus. This has motivated us to introduce the concept of quasi-degenerate flavour content sleptons and “effective” mass splittings. Especially for larger values of $|A_0|$, the mass splittings between the first two generations are significantly enhanced with respect to the pure cMSSM case. Even in this limit of $R = 1$, mass splittings of a few percent can be easily found, and have associated lepton flavour violating low-energy observables within reach of the future LFV experiments.

Regarding the seesaw parameters that are likely to be measured, the Chooz angle only has an indirect effect on the slepton mass differences, independently of the entries of the R matrix and the seesaw scale M_{N_3} . For larger values of θ_{13} slepton mass differences within LHC sensitivity have associated $\text{BR}(\mu \rightarrow e\gamma)$ already excluded by current experimental bounds.

Given the dimensionality of the full SUSY seesaw parameter space, we have selected a set of

benchmark points, in particular the LHC points SU1 and HM1, to carry the analysis of the general seesaw case (that is $R \neq 1$), considering different values of θ_{13} and distinct right-handed neutrino spectra. A measurement of a $\tilde{e}_L - \tilde{\mu}_L$ mass splitting between 0.1% and 1% for P5-HM1 implies that MEG should observe a $\mu \rightarrow e\gamma$ signal. Provided the seesaw is the unique source of LFV, no signal is expected to be observed by SuperB. The most interesting LFV signature of P6-SU1 is that, contrary to P5-HM1, a measurement of a mass splitting between left-handed selectrons and smuons would imply a $\text{BR}(\tau \rightarrow \mu\gamma)$ within SuperB reach. Furthermore, such observation would strongly hint towards a heavy seesaw scale $M_{N_3} \gtrsim 10^{13}$ GeV.

Despite the richness of the SUSY seesaw regarding the interplay of slepton mass splittings and low-energy flavour violation, the most spectacular result would be definitely manifest in the di-lepton mass distributions obtained at the LHC. In addition to the clear separation between the edges of di-muon and di-electron distributions (or equivalently, the observation of slepton mass splittings) one expects the appearance of an additional third kinematical edge for most of the benchmark points considered (which exhibited only two edges for the pure cMSSM case). The latter would signal flavour violation in χ_2^0 and/or $\tilde{\ell}$ decays.

Interestingly, irrespective of the specific seesaw configuration, the mass differences of right-handed sleptons are hardly sensitive to Y^ν -induced radiative effects (at leading order). Should the LHC observe mass splittings between right-handed sleptons of the first two families significantly above the per mille level, this would strongly hint towards the presence of another source of flavour violation (other than the seesaw).

It is important to stress that although a joint set of LFV observables might contribute to disfavour a type-I seesaw as the underlying mechanism of neutrino mass generation (and lepton flavour violation), one cannot exclude the possibility (however unlikely) that low-energy effects such as slepton mass splittings or flavour violating decays originate from a non-trivial structure of the SUSY soft breaking Lagrangian (the sleptonic part) at the GUT scale.

7 Acknowledgements

We are grateful to J. Orloff for many enlightening discussions. This work has been done partly under the ANR project CPV-LFV-LHC NT09-508531. The work of A. J. R. F. has been supported by *Fundação para a Ciência e a Tecnologia* through the fellowship SFRH/BD/64666/2009. A. J. R. F. and J. C. R. also acknowledge the financial support from the EU Network grant UNILHC PITN-GA-2009-237920 and from *Fundação para a Ciência e a Tecnologia* grants CFTP-FCT UNIT 777, CERN/FP/83503/2008 and PTDC/FIS/102120/2008. Finally, A. J. R. F., J. C. R. and A. M. T. are indebted to the LPT-Orsay for the hospitality, and for the funding from ANR.

References

- [1] Super-Kamiokande collaboration, S. Fukuda *et al.*, Phys. Lett. B **539** (2002) 179 [arXiv:hep-ex/0205075]; SNO collaboration, Q. R. Ahmad *et al.*, Phys. Rev. Lett. **89** (2002) 011301 [arXiv:nucl-ex/0204008]; KamLAND collaboration, K. Eguchi *et al.*, Phys. Rev. Lett. **90** (2003) 021802 [arXiv:hep-ex/0212021]; Super-Kamiokande collaboration, Y. Fukuda *et al.*, Phys. Rev. Lett. **81** (1998) 1562 [arXiv:hep-ex/9807003]; T. Kajita, New J. Phys. **6** (2004) 194; K2K collaboration, M. H. Ahn *et al.*, Phys. Rev. D **74** (2006) 072003 [arXiv:hep-ex/0606032]; MINOS collaboration, P. Adamson *et al.*, Phys. Rev. Lett. **101** (2008) 131802 [arXiv:0806.2237]; KamLAND collaboration, S. Abe *et al.*, Phys. Rev. Lett. **100** (2008) 221803 [arXiv:0801.4589].

- [2] M. Raidal *et al.*, Eur. Phys. J. C **57** (2008) 13 [arXiv:0801.1826 [hep-ph]] and references therein.
- [3] M. L. Brooks *et al.* [MEGA Collaboration], Phys. Rev. Lett. **83** (1999) 1521 [arXiv:hep-ex/9905013].
- [4] B. Aubert *et al.* [BABAR Collaboration], Phys. Rev. Lett. **96** (2006) 041801 [arXiv:hep-ex/0508012].
- [5] B. Aubert *et al.* [BABAR Collaboration], Phys. Rev. Lett. **95** (2005) 041802 [arXiv:hep-ex/0502032].
- [6] U. Bellgardt *et al.* [SINDRUM Collaboration], Nucl. Phys. B **299** (1988) 1.
- [7] B. Aubert *et al.* [BABAR Collaboration], Phys. Rev. Lett. **92** (2004) 121801 [arXiv:hep-ex/0312027].
- [8] A. G. Akeroyd *et al.* [SuperKEKB Physics Working Group], arXiv:hep-ex/0406071.
- [9] J. Aysto *et al.*, arXiv:hep-ph/0109217.
- [10] Y. Kuno, Nucl. Phys. Proc. Suppl. **149** (2005) 376.
- [11] M. Bona *et al.*, arXiv:0709.0451 [hep-ex].
- [12] O. A. Kiselev [MEG Collaboration], Nucl. Instrum. Meth. A **604** (2009) 304.
- [13] S. Ritt [MEG Collaboration], Nucl. Phys. Proc. Suppl. **162** (2006) 279.
- [14] The PRIME working group, unpublished; LOI to J-PARC 50-GeV PS, LOI-25, <http://psux1.kek.jp/jhf-np/LOIlist/LOIlist.html>
- [15] K. Hayasaka *et al.* [Belle Collaboration], Phys. Lett. B **666** (2008) 16 [arXiv:0705.0650 [hep-ex]].
- [16] G. Jungman, M. Kamionkowski and K. Griest, Phys. Rept. **267** (1996) 195 [arXiv:hep-ph/9506380].
- [17] G. Bertone, D. Hooper and J. Silk, Phys. Rept. **405** (2005) 279 [arXiv:hep-ph/0404175].
- [18] D. Larson *et al.*, arXiv:1001.4635 [astro-ph.CO].
- [19] P. Minkowski, Phys. Lett. B **67** (1977) 421; M. Gell-Mann, P. Ramond and R. Slansky, in *Complex Spinors and Unified Theories* eds. P. Van. Nieuwenhuizen and D. Z. Freedman, *Supergravity* (North-Holland, Amsterdam, 1979), p.315 [Print-80-0576 (CERN)]; T. Yanagida, in *Proceedings of the Workshop on the Unified Theory and the Baryon Number in the Universe*, eds. O. Sawada and A. Sugamoto (KEK, Tsukuba, 1979), p.95; S. L. Glashow, in *Quarks and Leptons*, eds. M. Lévy *et al.* (Plenum Press, New York, 1980), p.687; R. N. Mohapatra and G. Senjanović, Phys. Rev. Lett. **44** (1980) 912.
- [20] R. Barbieri, D. V. Nanopolous, G. Morchio and F. Strocchi, Phys. Lett. B **90** (1980) 91; R. E. Marshak and R. N. Mohapatra, *Invited talk given at Orbis Scientiae, Coral Gables, Fla., Jan. 14-17, 1980*, VPI-HEP-80/02; T. P. Cheng and L. F. Li, Phys. Rev. D **22** (1980) 2860; M. Magg and C. Wetterich, Phys. Lett. B **94** (1980) 61; G. Lazarides, Q. Shafi and C. Wetterich, Nucl. Phys. B **181** (1981) 287; J. Schechter and J. W. F. Valle, Phys. Rev. D **22** (1980) 2227; R. N. Mohapatra and G. Senjanović, Phys. Rev. D **23** (1981) 165.

- [21] E. Ma, Phys. Rev. Lett. **81** (1998) 1171 [arXiv:hep-ph/9805219]; R. Foot, H. Lew, X. G. He and G. C. Joshi, Z. Phys. C **44** (1989) 441.
- [22] F. Borzumati and A. Masiero, Phys. Rev. Lett. **57** (1986) 961.
- [23] L. J. Hall, V. A. Kostelecky and S. Raby, Nucl. Phys. B **267** (1986) 415.
- [24] J. F. Donoghue, H. P. Nilles and D. Wyler, Phys. Lett. B **128** (1983) 55.
- [25] T. Schwetz, M. Tortola and J. W. F. Valle, New J. Phys. **10** (2008) 113011 [arXiv:0808.2016].
- [26] M. C. Gonzalez-Garcia, M. Maltoni and J. Salvado, JHEP **1004** (2010) 056 [arXiv:1001.4524 [hep-ph]].
- [27] J. Hisano, T. Moroi, K. Tobe and M. Yamaguchi, Phys. Rev. D **53** (1996) 2442 [arXiv:hep-ph/9510309].
- [28] J. Hisano, T. Moroi, K. Tobe, M. Yamaguchi and T. Yanagida, Phys. Lett. B **357** (1995) 579 [arXiv:hep-ph/9501407].
- [29] J. Hisano and D. Nomura, Phys. Rev. D **59** (1999) 116005 [arXiv:hep-ph/9810479].
- [30] W. Buchmuller, D. Delepine and F. Vissani, Phys. Lett. B **459** (1999) 171 [arXiv:hep-ph/9904219].
- [31] Y. Kuno and Y. Okada, Rev. Mod. Phys. **73** (2001) 151 [arXiv:hep-ph/9909265].
- [32] J. A. Casas and A. Ibarra, Nucl. Phys. B **618** (2001) 171 [arXiv:hep-ph/0103065].
- [33] S. Lavignac, I. Masina and C. A. Savoy, Phys. Lett. B **520** (2001) 269 [arXiv:hep-ph/0106245].
- [34] X. J. Bi and Y. B. Dai, Phys. Rev. D **66** (2002) 076006 [arXiv:hep-ph/0112077].
- [35] J. R. Ellis, J. Hisano, M. Raidal and Y. Shimizu, Phys. Rev. D **66** (2002) 115013 [arXiv:hep-ph/0206110].
- [36] F. Deppisch, H. Pas, A. Redelbach, R. Ruckl and Y. Shimizu, Eur. Phys. J. C **28** (2003) 365 [arXiv:hep-ph/0206122].
- [37] T. Fukuyama, T. Kikuchi and N. Okada, Phys. Rev. D **68** (2003) 033012 [arXiv:hep-ph/0304190].
- [38] A. Brignole and A. Rossi, Nucl. Phys. B **701** (2004) 3 [arXiv:hep-ph/0404211].
- [39] A. Masiero, S. K. Vempati and O. Vives, New J. Phys. **6** (2004) 202 [arXiv:hep-ph/0407325].
- [40] T. Fukuyama, A. Ilakovac and T. Kikuchi, Eur. Phys. J. C **56** (2008) 125 [arXiv:hep-ph/0506295].
- [41] S. T. Petcov, W. Rodejohann, T. Shindou and Y. Takanishi, Nucl. Phys. B **739** (2006) 208 [arXiv:hep-ph/0510404].
- [42] E. Arganda and M. J. Herrero, Phys. Rev. D **73** (2006) 055003 [arXiv:hep-ph/0510405].
- [43] F. Deppisch, H. Pas, A. Redelbach and R. Ruckl, Phys. Rev. D **73** (2006) 033004 [arXiv:hep-ph/0511062].

- [44] C. E. Yaguna, Int. J. Mod. Phys. A **21** (2006) 1283 [arXiv:hep-ph/0502014].
- [45] L. Calibbi, A. Faccia, A. Masiero and S. K. Vempati, Phys. Rev. D **74** (2006) 116002 [arXiv:hep-ph/0605139].
- [46] S. Antusch, E. Arganda, M. J. Herrero and A. M. Teixeira, JHEP **0611** (2006) 090 [arXiv:hep-ph/0607263].
- [47] M. Hirsch, J. W. F. Valle, W. Porod, J. C. Romao and A. Villanova del Moral, Phys. Rev. D **78** (2008) 013006 [arXiv:0804.4072].
- [48] E. Arganda, M. J. Herrero and A. M. Teixeira, JHEP **0710** (2007) 104 [arXiv:0707.2955].
- [49] E. Arganda, M. J. Herrero and J. Portoles, JHEP **0806** (2008) 079 [arXiv:0803.2039 [hep-ph]].
- [50] Y. Okada, K. i. Okumura and Y. Shimizu, Phys. Rev. D **61** (2000) 094001 [arXiv:hep-ph/9906446].
- [51] J. R. Ellis, J. Hisano, S. Lola and M. Raidal, Nucl. Phys. B **621** (2002) 208 [arXiv:hep-ph/0109125].
- [52] J. R. Ellis, J. Hisano, M. Raidal and Y. Shimizu, Phys. Lett. B **528** (2002) 86 [arXiv:hep-ph/0111324].
- [53] I. Masina, Nucl. Phys. B **671** (2003) 432 [arXiv:hep-ph/0304299].
- [54] N. Arkani-Hamed, H. Cheng, J. L. Feng and L. J. Hall, Phys. Rev. Lett. **77** (1996) 1937 [arXiv:hep-ph/9603431].
- [55] I. Hinchliffe and F. E. Paige, Phys. Rev. D **63** (2001) 115006 [arXiv:hep-ph/0010086].
- [56] D. F. Carvalho, J. R. Ellis, M. E. Gomez, S. Lola and J. C. Romao, Phys. Lett. B **618** (2005) 162 [arXiv:hep-ph/0206148].
- [57] E. Carquin, J. Ellis, M. E. Gomez, S. Lola and J. Rodriguez-Quintero, JHEP **0905** (2009) 026 [arXiv:0812.4243].
- [58] F. E. Paige, *Determining SUSY particle masses at LHC, in the proceedings of 1996 DPF/DPB Summer Study on New Directions for High-Energy Physics (Snowmass 96)*, June 25–July 12, Snowmass, Colorado, U.S.A. (1996), arXiv:hep-ph/9609373.
- [59] I. Hinchliffe, F. E. Paige, M. D. Shapiro, J. Soderqvist and W. Yao, Phys. Rev. D **55** (1997) 5520 [arXiv:hep-ph/9610544].
- [60] H. Bachacou, I. Hinchliffe and F. E. Paige, Phys. Rev. D **62** (2000) 015009 [arXiv:hep-ph/9907518].
- [61] G. L. Bayatian et al [CMS Collaboration], J. Phys. G **34** (2007) 995.
- [62] W. W. Armstrong et al [ATLAS Collaboration], *ATLAS: Technical proposal for a general-purpose p p experiment at the Large Hadron Collider at CERN*, CERN-LHCC-94-43; G. Aad et al [The ATLAS Collaboration], *Expected Performance of the ATLAS Experiment - Detector, Trigger and Physics*, arXiv:0901.0512.

- [63] J. Hisano, M. M. Nojiri, Y. Shimizu and M. Tanaka, Phys. Rev. D **60** (1999) 055008 [arXiv:hep-ph/9808410].
- [64] G. A. Blair, W. Porod and P. M. Zerwas, Eur. Phys. J. C **27** (2003) 263 [arXiv:hep-ph/0210058].
- [65] M. R. Buckley and H. Murayama, Phys. Rev. Lett. **97** (2006) 231801 [arXiv:hep-ph/0606088].
- [66] A. J. Buras, L. Calibbi and P. Paradisi, JHEP **1009** (2010) 042 [arXiv:0912.1309].
- [67] W. Beenakker, R. Hopker, M. Spira and P. M. Zerwas, Nucl. Phys. B **492** (1997) 51 [arXiv:hep-ph/9610490].
- [68] B. C. Allanach, C. G. Lester, M. A. Parker and B. R. Webber, JHEP **0009** (2000) 004 [arXiv:hep-ph/0007009].
- [69] A. Bartl, K. Hidaka, K. Hohenwarter-Sodek, T. Kernreiter, W. Majerotto and W. Porod, Eur. Phys. J. C **46** (2006) 783 [arXiv:hep-ph/0510074].
- [70] B. C. Allanach, J. P. Conlon and C. G. Lester, Phys. Rev. D **77** (2008) 076006 [arXiv:0801.3666 [hep-ph]].
- [71] A. Abada, C. Biggio, F. Bonnet, M. B. Gavela and T. Hambye, JHEP **0712** (2007) 061 [arXiv:0707.4058 [hep-ph]].
- [72] B. Pontecorvo, Sov. Phys. JETP **6** (1957) 429 [Zh. Eksp. Teor. Fiz. **33** (1957) 549]; Z. Maki, M. Nakagawa and S. Sakata, Prog. Theor. Phys. **28** (1962) 870.
- [73] S. P. Martin, arXiv:hep-ph/9709356.
- [74] Y. Grossman and H. E. Haber, Phys. Rev. Lett. **78** (1997) 3438 [arXiv:hep-ph/9702421].
- [75] W. Porod, Comput. Phys. Commun. **153** (2003) 275 [arXiv:hep-ph/0301101].
- [76] R. Kitano, M. Koike and Y. Okada, Phys. Rev. D **66** (2002) 096002 [Erratum-ibid. D **76** (2007) 059902] [arXiv:hep-ph/0203110].
- [77] C. Amsler *et al.* [Particle Data Group], Phys. Lett. B **667** (2008) 1 (and partial update for 2010 edition).
- [78] D. Glenzinski, AIP Conf. Proc. **1222** (2010) 383.
- [79] Y. G. Cui *et al.* [COMET Collaboration], “Conceptual design report for experimental search for lepton flavor violating $\mu^- - e^-$ conversion at sensitivity of 10^{-16} with a slow-extracted bunched proton beam (COMET)”, KEK-2009-10.
- [80] D. DeMille, S. Bickman, P. Hamilton, Y. Jiang, V. Prasad, D. Kawall and R. Paolino, AIP Conf. Proc. **842** (2006) 759.
- [81] EDM collaboration, ”J-PARC Letter of Intent: Search for a Permanent Muon Electric Dipole Moment at the 10^{-24} e cm Level”, manuscript available from http://www.bnl.gov/EDM/papers/jparc_loi_030109.ps.
- [82] M. Fukugita and T. Yanagida, Phys. Lett. B **174** (1986) 45.

- [83] S. Davidson, E. Nardi and Y. Nir, Phys. Rept. **466** (2008) 105 [arXiv:0802.2962 [hep-ph]].
- [84] J. R. Ellis, J. E. Kim and D. V. Nanopoulos, Phys. Lett. B **145** (1984) 181.
- [85] S. Antusch and A. M. Teixeira, JCAP **0702** (2007) 024 [arXiv:hep-ph/0611232].
- [86] E. Nardi, Y. Nir, E. Roulet and J. Racker, JHEP **0601** (2006) 164 [arXiv:hep-ph/0601084].
- [87] A. Abada, S. Davidson, A. Ibarra, F. X. Josse-Michaux, M. Losada and A. Riotto, JHEP **0609** (2006) 010 [arXiv:hep-ph/0605281].
- [88] A. Abada, S. Davidson, F. X. Josse-Michaux, M. Losada and A. Riotto, JCAP **0604** (2006) 004 [arXiv:hep-ph/0601083].
- [89] S. Davidson, J. Garayoa, F. Palorini and N. Rius, JHEP **0809** (2008) 053 [arXiv:0806.2832 [hep-ph]].
- [90] J. R. Ellis and M. Raidal, Nucl. Phys. B **643** (2002) 229 [arXiv:hep-ph/0206174].
- [91] S. T. Petcov and T. Shindou, Phys. Rev. D **74** (2006) 073006 [arXiv:hep-ph/0605151].
- [92] F. R. Joaquim, I. Masina and A. Riotto, Int. J. Mod. Phys. A **22** (2007) 6253 [arXiv:hep-ph/0701270].
- [93] S. Blanchet, D. Marfatia and A. Mustafayev, arXiv:1006.2857 [hep-ph].
- [94] G. Belanger, F. Boudjema, A. Pukhov and A. Semenov, Comput. Phys. Commun. **180** (2009) 747 [arXiv:0803.2360 [hep-ph]].
- [95] W. Beenakker, R. Hopker and M. Spira, arXiv:hep-ph/9611232; W. Beenakker et al, Phys. Rev. Lett. **83** (1999) 3780 [arXiv:hep-ph/9906298]; see also Ref. [67].
- [96] T. Hahn, Comput. Phys. Commun. **168** (2005) 78 [arXiv:hep-ph/0404043].
- [97] R. Barate et al [LEP Working Group for Higgs boson searches Collaboration], Phys. Lett. B **565** (2003) 61 [arXiv:hep-ex/0306033].
- [98] R. Assmann, M. Ferro-Luzzi, M. Giovannozzi, W. Herr, J. Jowett, M. Lamont, E. Shaposhnikova, “LHC beam parameters for the physics run at 3.5 TEV”, LHC-OP-ES-0020, March 2010.
- [99] B. C. Allanach, A. Djouadi, J. L. Kneur, W. Porod and P. Slavich, JHEP **0409**, 044 (2004) [arXiv:hep-ph/0406166].